Utrecht University

Gold Catalysts for Direct Propene Oxide Synthesis

The effect of adding a second metal.

Bryan Justin Folmer BSc.

Master Thesis

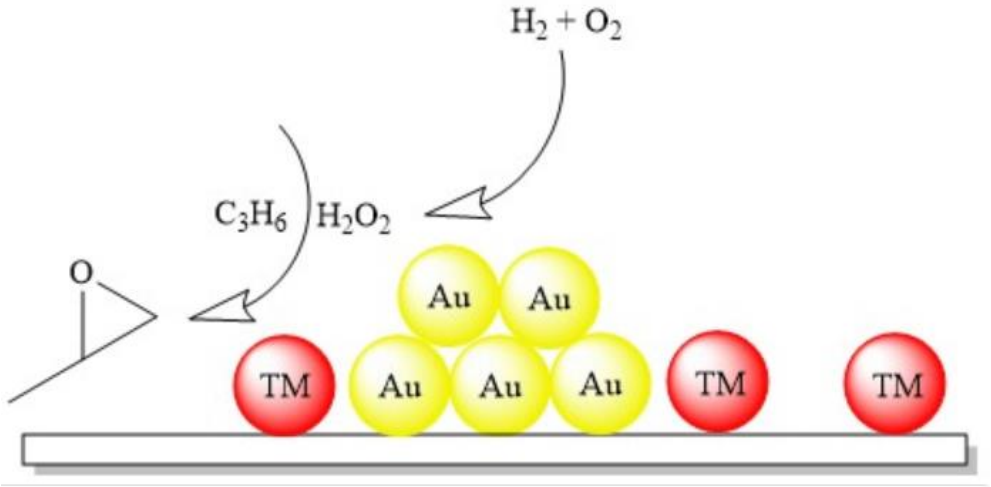

Daily Supervisor: E.J.J de Boed Msc.

First Examiner: Prof. Petra E. de Jongh
Second Examiner: Dr. P. Ngene

Inorganic Chemistry and Catalysis
Debye Institute for Nanomaterials Science
Utrecht University

15th of March 2021

Abstract:

Supported gold nanoparticles (AuNPs) have been studied extensively for the direct epoxidation of propene with H_2/O_2 mixtures to yield propene oxide, an intermediate required to fabricate polyesters. Au/TiO_2 catalysts achieve high selectivity, but catalyst deactivation and low hydrogen conversions are major limitations. In this research, we explore the possibility of achieving selective propene epoxidation with gold-based bifunctional catalysts. The gold-based catalysts consisted of gold nanoparticles and (transition)-metal complexes active in homogeneous propene oxidation. Afterward, the catalytic performance of gold-based bifunctional catalysts has been studied in the direct gas-phase oxidation of propene with H_2/O_2 mixtures. Analysis of the catalytic results proved that SiO_2 supported gold-based bifunctional catalysts are highly active but lack selectivity towards propene oxide primarily due to limited intimacy between both supported metals. Secondly, we studied the stability of monometallic Au/TiO_2 catalysts, which tend to deactivate quickly at 100°C due to the irreversible adsorption of propene oxide. Furthermore, we aimed to increase the catalytic performance by the formation of supported bimetallic nanoparticles on either TiO_2 or $Ti\text{-}SiO_2$. UV-Vis Spectroscopy, XRD and TEM were applied to study the structure of the bimetallic nanoparticles. However, these characterization techniques were insufficient to verify the structure of the supported bimetallic nanoparticles. We found that $Au/Ti\text{-}SiO_2$ was the best performing catalysts for the oxidation of propene. Bimetallic supported nanoparticles negatively affected the catalytic performance compared to monometallic supported catalyst due to excessive particle growth, competitive adsorption and the formation of individual nanoparticles.

Layman's summary:

This research presents our investigations and findings of catalysts for one particular chemical reaction. Catalysts are molecules or substances that facilitate a reaction to take place without being consumed themselves. Nearly all products we use daily are produced with a chemical reaction in the presence of a catalyst. Chemical reactions can occur without catalysts, but catalysts often make the entire production process easier and more efficient. A typical example used to describe catalysis is the sketch where the point of destination is located behind a mountain. Instead of spending much effort and energy climbing the mountain, people constructed tunnels to reach the destination faster and with much less effort.

There are various chemical reactions classified among groups, but this research involves oxidation. Oxidation involves adding or inserting oxygen (O_2) to a molecule or chemical substance and thereby creating one or more new chemical products. In this case, oxygen fulfills the function of "oxidant," the molecule which contains the oxygen molecule to be inserted into another molecule. There are many different oxidants available, for example, hydrogen peroxide (H_2O_2) since it also contains oxygen. The most common oxidation reaction is the combustion of fuel with molecular oxygen. The reaction products of this reaction are CO_2, water and energy in the form of heat. This indirectly explains why catalysts in oxidation reactions are pivotal. Simply adding oxygen or another oxidant might result in the combustion of molecules and carbon dioxide production, which is highly undesired in most production processes. With particular catalysts, we can direct the chemical reaction to the desired outcome. Nowadays, most oxidation catalysts are comprised of platinum, iron, manganese, molybdenum, and vanadium. One specific oxidation reaction favors an iron-based catalyst, molybdenum-based catalysts, or maybe a combination of both. To clarify, a catalyst can consist of several elements.

This research project focuses on propene oxidation to fabricate a molecule named propene oxide, using hydrogen peroxide (H_2O_2) as an oxidant. However, propene oxide's current industrial production processes are environmentally unfriendly, the catalyst deactivates relatively quickly or the catalyst lacks activity. The deactivation of a catalyst means that the catalyst suffers from a loss in performance over time and has to be replaced by a new, identical catalyst, which increases expenses and is a shortcoming. Therefore, this research strives to develop a new, environmentally friendly catalyst, which produces the desired product and does not deactivate.The new catalyst must possess two functions and therefore are called "Bifunctional catalysts". First of all, it must be able to produce hydrogen peroxide. Researchers have found that gold (Au) can produce hydrogen peroxide from a gaseous mixture of hydrogen (H_2) and oxygen (O_2), which is more environmentally friendly than using commercially available produced hydrogen peroxide. Secondly, the catalyst must be capable of inserting the oxygen into propene and successfully produce propene oxide. Gold is responsible for hydrogen peroxide formation but not for the insertion of oxygen into propene. Therefore, we need a second chemical element, such as vanadium and molybdenum. We aim to investigate what chemical element carries out the insertion step most efficiently.

To evaluate the performance of these catalysts, we performed catalytic tests. We exposed our designed catalysts, consisting of gold and other chemical elements, to a gaseous mixture of hydrogen, oxygen, and propene and analyzed the amount of propene oxide produced. Catalysts comprised of different chemical elements led to the production of all types of chemical products but propene oxide. We were only partially able to explain the production of these undesired products. Our research led to the discovery that our designed bifunctional catalysts did not improve the catalytic stability and propene oxide production in general.

Besides bifunctional catalysts, we investigated and analyzed the performance of mono- and bimetallic catalysts in the propene oxide production under similar reaction conditions. Bimetallic catalysts are catalysts which are comprised of two chemical elements, similar to bifunctional catalysts, but instead of separate chemical elements in close proximity, an alloyed structure is formed. Our research obtained results that showed monometallic catalysts were highly unstable, as often described in literature. On the other hand, bimetallic catalysts showed increased or similar activity, but decreased propene oxide production. We were able to presumably explain the experimental results.

Contents

1: Introduction **8**
2: Theory **11**
2.1: Production of Propene oxide **11**
2.1.1: Chlorohydrin production process 12
2.1.2: Hydroperoxide production process 13
2.2: Heterogeneously catalysed epoxidation of propene 16
2.2.1: Supported silver catalysts: ethene epoxidation vs propene epoxidation 16
2.2.2: Supported Ti-catalysts in propene epoxidation with H_2O_2 18
2.2.3: Supported Au/Ti-catalysts in propene epoxidation with H_2 and O_2 19
2.2.4: Influence of support 20
2.3: Supported bimetallic catalysts in propene epoxidation **22**
2.4: Transition-metal catalysed epoxidation reactions **25**
2.5: Characterization methods **27**
2.5.1: Transmission Electron Microscopy 27
2.5.2: Diffuse Reflectance UV-Vis Spectroscopy 27
2.5.3: X-Ray Diffraction 28
3: Aim & Scope of Research **29**
3.1: Bifunctional Au catalysts: preparation and characterization **29**
3.2: Bimetallic Au catalysts: preparation and characterization **30**
3.3: Catalytic testing **30**
4: Experimental Methods **31**
4.1: Chemicals and general considerations 31
4.2: Catalysts preparation 31
4.2.1: Synthesis of bifunctional Au catalysts 32
4.2.2: Synthesis of mono- and bimetallic Au catalysts 32
4.2.3: Synthesis of gold-titanium(IV)-silica based catalysts 33
4.3: Heat treatment of catalysts 33
4.4: Characterization of catalysts **33**
4.5: Catalytic tests **34**
5: Results and Discussion **35**
5.1: Bifunctional Gold Catalysts supported on a functionalized silica. **35**
5.1.1: Characterization of bifunctional catalysts 35
5.1.2: Hydrogen conversion 41
5.1.3: Bifunctional Au-M/APS-SiO2 catalysts in propene epoxidation. 43

5.1.4: Intermediate conclusion. 46
5.2: Gold-titania based catalysts **47**
5.2.1: Characterization of mono- and bimetallic catalysts 47
5.2.2: Catalytic tests of monometallic catalysts 51
5.2.3: Catalytic tests of bimetallic catalysts 56
5.2.4: Intermediate conclusion 57
5.3: Gold-titanium(IV)-silica based catalysts **58**
5.3.1: Characterization of bimetallic catalysts on Ti-SiO_2 58
5.3.2: Catalytic tests of bimetallic catalysts on Ti-SiO_2 60
6: Conclusion **64**
7: Outlook **65**
8: Acknowledgements. **66**
9: Bibliography **67**

1. Introduction.

The chemical industry fulfills the societal needs for food, water, energy, and all other types of secondary needs. However, the chemical industry and its size nowadays would not exist without catalysis. Catalysis is the heart of the chemical industry, since 80% of all chemical products manufactured involve at least one catalytic step in the production process [54]. Our society's reliance on catalysis is continuously rising due to increased consumption of petrochemical products, shrinking resources, and the increasing demand for improved sustainability. Thereby, catalysis is expected to play a pivotal role in maintaining an economically viable society and at the same time deal with sustainability concerns. In 2019, the monetary value of all catalysts produced equaled 33.9 billion USD and was estimated to grow by 4.4% annually [55]. The concept of catalysis is applied in most scientific areas, varying from inorganic and organic chemistry to bio-engineering. Catalysts themselves are classified into three groups, homogenous, heterogeneous, and biocatalysis. Biocatalysis involves enzymes and parts of living organisms to carry out chemical transformations and will not be mentioned in detail.

Homogeneous catalysis involves chemical transformations in which catalysts occupy the same phase as the mixture of reactants. The main advantage of homogeneous catalysts is their excellent selectivity [56,57]. The excellent selectivity of homogeneous catalysts results from the catalyst's identical chemical environment and the reaction mixture. Indirectly, their nature to carry out chemical transformations highly selective limits the possibility to cause any environmental harm. Since catalysts are used and not consumed in chemical transformations, the necessity to separate the reaction products from the spent catalysts is a significant disadvantage compared to heterogeneous catalysis. Despite the high selectivity and efficiency of homogeneous catalysts, the use of solvents or stoichiometric reagents often results in waste production. Due to ecological and societal developments, researchers are forced to come up with another solution.

Heterogeneous catalysis consists of solid-phase catalysts that react with liquid- or gaseous substrates. Catalytic transformations are carried out on the surface, in which the solid phase of a catalyst is used to adsorb reactants. Subsequently, the reactants diffuse to the active sites since an adsorption site may not be active. At the active sites, reactants are transformed into products and desorb from the catalytic surface. Over time, massive efforts are put into heterogeneous catalysis to make it a viable alternative for homogeneous catalysis because heterogeneous catalysts are commonly less selective. After all, the catalysts and reaction mixtures are in a different phase [57]. However, the separation of catalysts from the product is stream is less complicated and therefore a major advantage. Supported nanoparticles consisting of noble metals are proven to be effective catalysts in hydrogenation and oxidation reactions [10,56,57]. In the development of new catalysts, we strive to achieve high activity, selectivity, stability, and the ability to regenerate catalysts.

As stated, supported nanoparticles consisting of noble metals received interest in hydrogenation and oxidation reactions. Initially, (supported) metals such as Pt, Pd, and Rh are used in oxidation reactions since they can dissociatively absorb oxygen and strongly adsorb CO and atomic oxygen [59]. CO oxidation attracted considerable attention to reduce the pollution originating from the car industry and the synthesis of methanol. Haruta's group discovered that supported gold nanoparticles on metal oxides showed surprisingly high catalytic activity in CO oxidation [60,61]. Gold was long thought to be chemically inert because gold is resistant to oxidation and corrosion. However, sufficiently small and supported gold nanoparticles possess catalytic properties, which are not limited to CO oxidation [37,58,60,61]. These catalytic properties arose due to a change in the surface-volume ratio in comparison with bulk gold.

Furthermore, they concluded that the catalytic performance is highly dependent on the degree of dispersion of nanoparticles across the surface area provided by, the support gold-metal oxide interaction, and the structure of the gold catalysts [60,61]. Since CO oxidation is a surface-catalyzed reaction, the rate of CO2 formation enhances by providing a higher surface area. Many other aspects affect the electronic and physical properties and thereby directly influence the catalytic performance, such as the size of NPs. A couple of decades earlier, in 1973, Bond and Sermon discovered that dispersed gold nanoparticles supported on SiO_2 were catalytically active in the hydrogenation of alkenes [37], but especially the high selectivity of the Au-based catalysts. Their discovery showed the importance of Au-catalysis in particular reactions and raised interest in the chemistry industry.

Moreover, supported Au catalysts were studied in the selective hydrogenation of butadiene. As Haruta et al. concluded, the catalytic performance is strongly dependent on the metal-support interaction (i.e., type of support) in CO oxidation, so does the support play a pivotal role in the selective hydrogenation of butadiene. Masoud N. et al. found that Au/SiO_2 exhibited superior stability compared to Au/TiO_2 catalysts. The titania supported gold nanoparticles (3-4nm) suffered from deactivation through the deposition of carbonate species and thereby deactivated nearby active Au sites [89]. Furthermore, Masoud N. et al. investigated the thermal stability of gold nanoparticles. She concluded that AuNPs supported on non-reducible supports (SiO_2) were more stable than AuNPs supported on reducible supports such as TiO_2 [88]. The stability is highly desired because instability promotes particle growth and deactivates the catalyst.

Thirdly, gold-based catalysis is extensively studied throughout the years in the selective oxidation of propene to propene oxide [1,5,6,12]. Until now, the selective oxidation of propene to propene oxide is carried out with organic hydroxy species in the presence of homogeneous catalysts or heterogeneous titanium-silicate catalysts (TS-1) with hydrogen peroxide [13,92,105]. Propene oxide is a highly desired bulk chemical in the industry used as a reaction intermediate for various products such as propylene glycol and polyether polyols [1,4]. Although propene oxide's sustainable production is achieved with the titanium-silicate because the only by-product is water, the degree of sustainability and economic viability is increased when the hydrogen peroxide can be produced from a gaseous hydrogen and oxygen stream [7].

Supported gold nanoparticles possess another ability besides oxidation and hydrogenation, which is the formation of hydroperoxyl species from H_2/O_2 mixtures. It is found that supported gold nanoparticles on titania (Au/TiO_2) are highly selective in the oxidation of propene to propene oxide in combination with H2/O2 mixtures, in which the gold nanoparticles are responsible for the in-situ formation of hydroperoxy species, and the supports contains the active Ti-sites for the oxidation reaction [1,8,9]. Despite the high initial selectivity of Au/TiO_2 in the propene epoxidation reaction, it does quickly deactivate due to deposition of carbonate species or oligomerization of propene oxide on the surface [78,84]. Moreover, Au/TiO_2 catalysts exhibit low activity in the propene epoxidation reaction and are considered to prevent the commercialization of these heterogeneous catalysts.

Last of all, supported bimetallic nanoparticles on either titania or titanium-silicate have been widely studied regarding propene epoxidation [45,46,73,74,76]. For example, the East Chinese University has found that Au-Ag/TS-1 doubled the propene oxide formation rate with respect to monometallic Au/TS-1 [45]. The improved catalytic performance of bimetallic catalysts has been attributed to several aspects, such as increased dispersion or facilitating oxygen adsorption and thereby electron transfer [45]. However, it is dependent on the bimetallic catalyst composition. It has been generally agreed that the improved catalytic performance of bimetallic catalysts can be attributed to the alteration of active sites, either electronic or geometric effects [114].

This research strives to improve existing heterogeneous catalysts in the propene epoxidation with H_2/O_2 mixtures. Firstly, we explore the possibility of replacing the active Ti-sites with other transition metals that are active in homogeneous alkene epoxidation. Bifunctional catalysts have been prepared, consisting of supported gold nanoparticles and transition-metal complex on functionalized silica. Secondly, we study the catalytic performance of bimetallic gold nanoparticles (AuPd, AuAg, and AuCu) supported on TiO_2 or Ti-SiO_2 in the direct epoxidation of propene. We based the choice of support on the catalytic activity of bifunctional Au-Ti catalysts and because gold-titanium(IV) have been frequently studied in the literature [1,8,9,12].

2. Theory.

This chapter will discuss the theoretical background of propene oxidation. First of all, industrialized production processes of propene oxide are provided. Secondly, mechanisms of heterogeneous catalyzed propene oxidation are discussed, including both monometallic- and bimetallic catalysts. At last, research objectives and questions are formulated and experimental approaches are explained.

2.1. Production of propene oxide.

In 2016, the propene oxide market value was estimated at $13 billion USD and was forecasted that this particular market would increase to approximately $18 billion USD in 2022, equaling a production capacity of $12.5x10^3$ t/year [3]. The expectation of global market growth is caused by rising polyurethane demands in different market segments, for example automotive [4]. Propene oxide (PO), also known as propene oxide, is a highly desired bulk chemical used as a reaction intermediate for various products illustrated in Figure 1. Propene oxide primarily finds its application in the manufacturing of polyether polyols used in polyurethane production. Moreover, propene glycol and glycol ethers, used as solvents and necessary for polyester production, require propene oxide for its production [1].

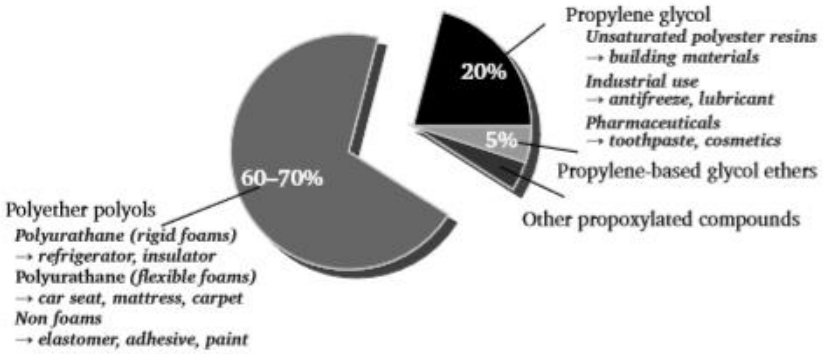

Figure 1: Numerous applications of propene oxide. Taken from ref. [2].

In 2020, five production routes for propene oxide production are commercialized [5,9,92]. The chlorohydrin process (CHPO) and the hydrogen peroxide (HPPO) are responsible for the majority of the propene oxide production [92]. Both commercialized processes are examples of an indirect process and must deal with environmental issues or co-product formation. An indirect production process resembles the necessity to produce an intermediate chemical that is eventually converted to the desired product. Recent developments in the technology of propene oxide production (new catalysts) slowly increase the PO production share of the HPPO at the expense of the chlorohydrin process [92]. Both production processes have a considerable environmental impact or footprint [7]. Potential opportunities are displayed and the authors conclude that the environmental impact can be minimized by new, selective production technologies [7]. Therefore, the development of an innovative, direct oxidation pathway for the production of PO is highly desired.

2.1.1. Chlorohydrin production process.

Propene oxidation involves the insertion of oxygen into the C=C bond of propene. The formation of propene oxide via the chlorohydrin process relies on the formation of a chlorohydrin intermediate. The chlorohydrin intermediate is produced by the addition of hypochlorous acid to propylene. Subsequently, the chlorohydrin is dehydrochlorinated by the addition of calcium hydroxide and propene oxide is formed. In 2008, the chlorohydrin route was responsible for 43.2% of propene oxide's worldwide production [91]. The chlorohydrin process is characterized by significant waste production. Every ton of propene oxide produced is associated with 2100 kg CaCl2 and 100 kilograms of 1,2-dichloropropane, which increases the cost/efforts for suitable wastewater treatment [92]. Over time, researchers and companies optimized the chlorohydrin process and developed a variant production way called the Lummus process. In this production pathway, tert-butylchloride reacts with water to form the propene chlorohydrin and tert-butanol. Secondly, the chlorohydrin is hydrolysed in the presence of caustic soda to form propene oxide. In comparison with the chlorohydrin process, the Lummus process limits the production of chlorinated hydrocarbons because the tert-butyl alcohol is recycled. On the contrary, the propene oxide formation rate is significantly lower. The final reaction step involves the chlorohydrin hydrolysis in the presence of caustic soda to form propene oxide [2]. The Lummus process limits chlorinated hydrocarbons' production with respect to the chlorohydrin process because the tert-butyl alcohol is recycled. On the contrary, propene oxide's formation rate is significantly reduced, since the formation of the propylene chlorohydrin intermediate is slower [2,92]

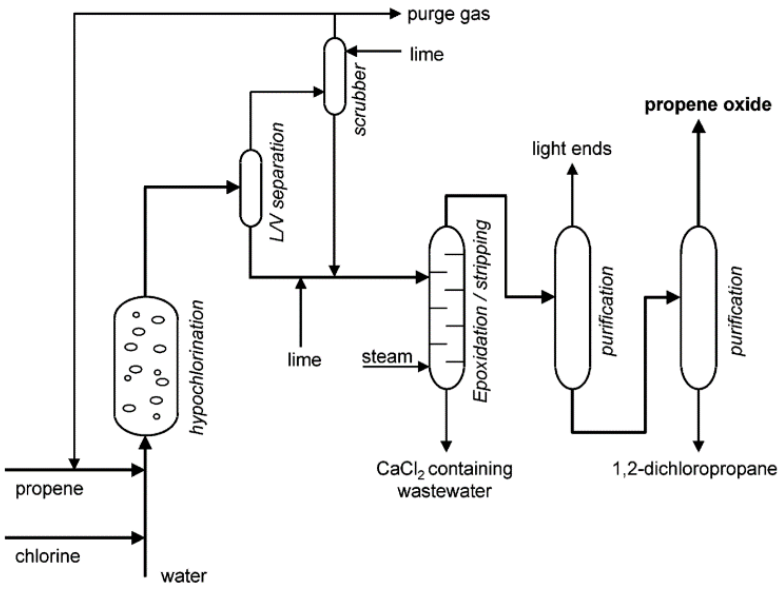

Figure 2: Schematic representation of the chlorohydrin process for the production of propene oxide. Taken from ref. [1].

2.1.2. Hydroperoxide production process.

Four different hydroperoxide production processes are commercialized. The hydroperoxide processes rely on the use of an alkyl-hydroperoxide as an oxidant to epoxidize propene. Two of these processes are called the styrene monomer propene oxide (SMPO) and the propene oxide tert-butyl alcohol (PO-TBA) process [1]. The SMPO process uses ethylbenzene as a reactant and consists of four consecutive reaction steps. The first step is the oxidation of ethylbenzene by molecular oxygen to ethylbenzene hydroperoxide (EBHP). This intermediate hydroperoxide reacts with propene to form propene oxide and methyl phenyl carbinol (MPC). Subsequently, MPC is dehydrogenated over alumina to styrene. A side product of this dehydrogenation reaction is methyl phenyl ketone, which can be converted to styrene by hydrogenation in the presence of a catalyst to MPC and led over alumina once again [91,92]. The propene oxide tert-butyl alcohol (PO-TBA) process relies on a similar mechanism. Firstly, isobutane is oxidized to tert-butyl hydroperoxide (TBHP). Subsequently, the hydroperoxide intermediate reacts with propene to produce propene oxide and the corresponding alcohol. Figure 3 shows a flow sheet of the PO/TBA process.

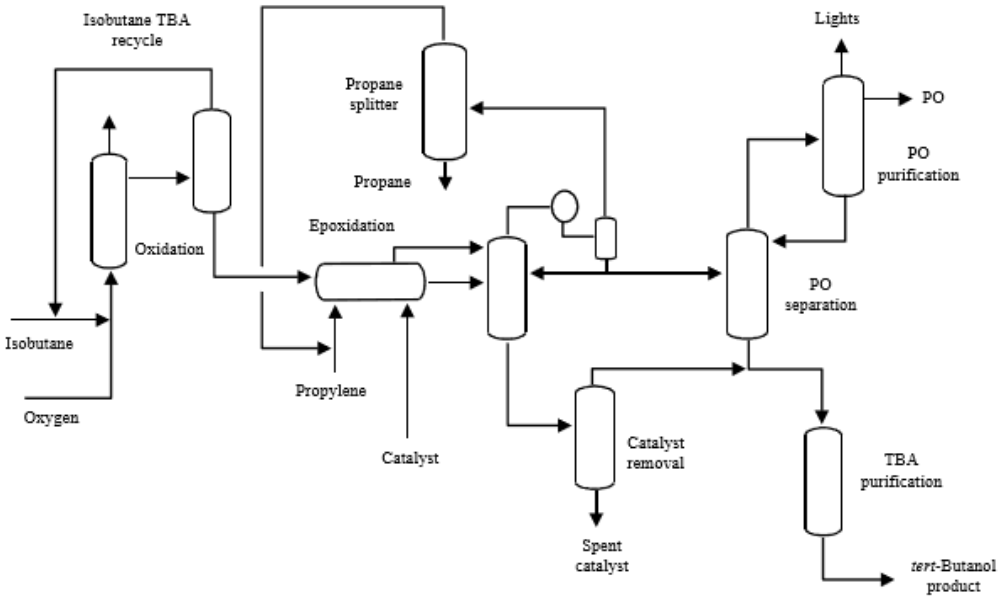

Figure 3: Flow sheet of the hydroperoxide process to PO and TBA. Taken from ref. [8].

The SMPO and the PO/TBA process shows selectivity >95% but suffer from low conversions [12]. Comparing these hydroperoxide production processes with the chlorohydrin process that shows selectivities between 90-95%, these hydroperoxide processes are environmentally more benign. On the contrary, there also multiple disadvantages that characterize the hydroperoxide production process. For example, the use of homogeneous catalysts is inevitable since the hydroperoxide is not electrophilic enough to attack the nucleophilic alkene [5]. Common homogeneous catalysts are molybdenum, vanadium, tungsten or rhenium complexes dependent on the type of hydroperoxide intermediate [103]. The need for catalyst separation besides product separation is a disadvantage compared to the chlorohydrin process. The separation can be performed by distillation, followed by evaporation to retrieve the spent catalyst. After the separation of propene oxide and the spent catalyst, the manufacturers are left with methyl phenyl carbinol (MPC) for the SMPO process and can be converted to styrene [91,92]. However, the global styrene market equaled approximately USD 50 billion in 2017 [30], but it is an entirely different market than PO. The PO-TBA process results in co-product formation of tert-butyl alcohol, which can be dehydrogenated to isobutene or converted to methyl-tert-butyl ether with methanol [1,103]

As stated, the PO/TBA and SMPO process utilizes homogeneous catalysts such as vanadium and molybdenum for the oxidation reaction of the hydroperoxide intermediate with propene [1,8]. Shell was able to optimize the SMPO process by the use of heterogeneous Ti-SiO_2 and eased the separation step [92].

The SMPO and PO/TBA are both examples of metal-catalyzed oxidation reactions facilitated by organic peroxides [10,11]. Since the SMPO and PO/TBA processes suffer from low conversions [12], innovative production pathways were desired. In 1991, a titanium-silicate catalyst (TS-1) was designed, which was active towards propene epoxidation at mild conditions with hydrogen peroxide and a methanol-water mixture as solvent, called the hydrogen peroxide production process (HPPO) [13]. The titanium-silicate catalyst was a modification of ZSM-5 with titanium incorporated in the framework. The pore size of ZSM-5 prevents the application of organic peroxides for the propene epoxidation [13]. In contrast to the chlorohydrin, PO-TBA, and SMPO process, the HPPO process consists of one reaction step: the epoxidation of propene. Furthermore, the primary by-product formed is water with negligible amounts of propylene glycol and methyl ethers [13]. In 2008, BASF and Dow and Solvay successfully commercialized the HPPO technology [92]. We further elaborate on supported Ti-catalysts in propene epoxidation in section 2.2.

Finally, the cumene hydroperoxide oxidation process developed by Sumitomo Chemical (CMHPO) is almost identical to the previously discussed hydroperoxide propene oxide production methods. In this process, cumene is oxidized to cumene hydroperoxide, which is subsequently used for the epoxidation of propene. The produced alcohol (by-product) is converted back to cumene by a hydrogenation reaction over a copper-chromium oxide catalyst [9]. After the propylene is removed from the stream, propylene oxide can be separated from cumene by a distillation process. The complete cumene hydroperoxide oxidation process is shown in Figure 4.

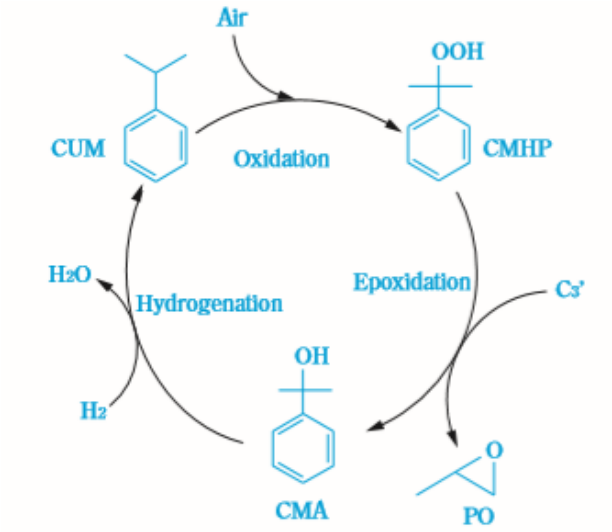

Figure 4: Schematic representation of the CMHPO production process. Taken from ref. [9].

The main characteristic of the cumene hydroperoxide oxidation process is the recyclable cumene as oxidant. Furthermore, the high activity of the titanium-silica catalyst and the overall stability of cumene allows for the commercialization of this production process by Sumitomo Chemicals [9]. Compared to the chlorohydrin and hydroperoxide process, the cumene hydroperoxide oxidation achieves higher selectivity thanks to the cumene cycle, making it more environmentally friendly while simultaneously achieving a similar propene oxide yield.

To conclude, table 1 provides an overview of the characteristics of each production processes. Among all propene oxide production processes, it can be concluded that HPPO has the most potential for the future.

Table 1: Comparison between different processes for propene oxide production. Adapted from ref. [105].

Production Process	***Chemicals***	***By-Products***	***Propene Oxide Sel. (%)***	****Catalyst***
Chlorohydrin	Propene, Chlorine, Water	Calciumchloride	87-90%	None
PO-TBA	Propene, Isobutane	Tert-butyl alcohol	95%	Tungsten, Molybdenum, Vanadium
SMPO	Propene, Ethylbenzene	Styrene	95%	Molybdenum
CMHPO	Propene, Cumene	Cumylalcohol	95%	None
HPPO	Propene, Hydrogen Peroxide	Water	>90%	Titanium-silicate

*(Transition)-*metals used in the propene epoxidation. Catalysts for the conversion/regeneration of by-products are not represented.*

2.2. Heterogeneously catalysed epoxidation of propene.

Selective propene oxide production with hydrogen peroxide over heterogeneous TS-1 stimulated further research in heterogeneous catalysts. Heterogeneous catalysis consists of solid-phase catalysts that react with liquid- or gaseous substrates. In contrast to homogeneous catalysts, the separation of heterogeneous catalysts is trouble-free. This chapter provides detailed information about supported (noble) metals on a support for propene epoxidation. First, we discuss heterogeneous catalysts used in ethene epoxidation and the difficulties in propene epoxidation. Secondly, we provide a more detailed analysis of supported Ti-catalysts in propene epoxidation. Thirdly, we discuss the in-situ production of hydroperoxide species over supported Au. In our search for new catalysts in selective propene epoxidation, we analyze the mechanisms of transition-metal alkene epoxidation.

2.2.1. Supported silver catalysts: ethene epoxidation vs propene epoxidation.

Current production processes of ethene oxide rely on direct oxidation of ethene, accomplished by reacting pure oxygen in the presence of an alpha-alumina supported silver catalyst. The epoxidation of ethene over silver catalysts in the presence has reached a selectivity of 86% [1]. Silver can dissociatively adsorb oxygen, and since the bonding is not too strong for higher metal loadings, epoxidation of ethene can occur.

However, epoxidation of propene with oxygen is not possible since there is a difference in reactivity of ethene and propene in epoxidation. Carter and Goddard have developed a detailed oxyradical mechanism for Ag-catalysed alkene epoxidation, by which the difference in reactivity for the oxidation of propene and ethene can be explained [15]. In the presence of molecular oxygen, the formation of an epoxide precursor intermediate is feasible. For the ethene epoxide precursor intermediate, there is only one reaction possible: the formation of ethene oxide. However, the propene oxide intermediate's reaction pathway has an alternative pathway since propene has an additional CH_3 compared to ethene, which can form an allylic intermediate. An allylic hydrogen atom in propene can be abstracted by the formed oxyradical, which is a more favorable pathway than propene oxide formation. Once the hydrogen atom abstraction from the propene oxide precursor occurs, it is kinetically favored to completely combust propene. Therefore, pure oxygen cannot be used for the epoxidation of propene. To conclude, the abstraction of hydrogen atoms by neighboring oxygen atoms facilitates the complete combustion of propene. Figure 5 shows the total oxidation of propene with oxygen as oxidant over supported silver catalysts.

Secondly, the difference in reactivity can also be attributed to the adsorbed oxygen species. It is assumed for ethylene that there is an interaction between an ethylene molecule and adsorbed oxygen [16]. For propylene, however, it is proposed that by Cant and Hall that the interaction between propylene and adsorbed oxygen forms a hydroperoxide. The hydroperoxide species quickly decompose to form an aldehyde because there is no intimacy with other adsorbed species [17]. Furthermore, there is a general assumption that propene oxide rapidly oxidizes towards carbon dioxide and water. The consecutive oxidation of propene oxide is much faster than for ethylene oxide. Nonetheless, Gorokhovatskii and Rubanik claimed that propene oxide is oxidized slower than propene [18].

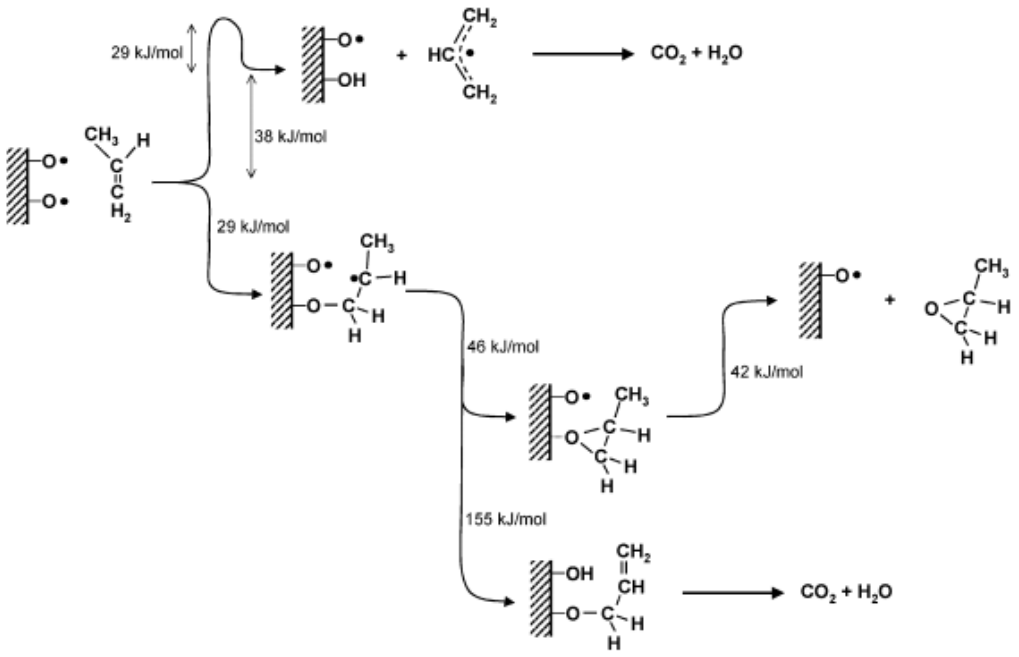

Figure 5: Schematic representation of the total oxidation of propene over Ag/TiO_2 catalysts using molecular oxygen. Taken from ref. [1].

2.2.2. Supported Ti-catalysts in propene epoxidation with H_2O_2

As previously stated, BASF and Dow and Solvay were able to commercialize the hydrogen peroxide production process using TS-1 catalysts with aqueous hydrogen peroxide as the oxidant [92]. Clerici et al. studied propylene oxide synthesis using propylene and hydrogen peroxide over TS-1 and assumed that these catalysts' performance could be attributed to several aspects [13]. In general, the solvents used in the hydroperoxide processes, such as alcohols, compete for the active sites. Clerici et al. assumed that the hydrophobic nature of TS-1 prefers the adsorption of less polar H_2O_2 and prevents water and methanol from any competition for active sites, achieving a propene oxide selectivity up to 95% [13]. The propylene epoxidation reaction mechanism relies on the formation of Ti-OOH [105,106]. The formation of Ti-OOH is possible by breaking the Ti-O-Si bonds, shown in Figure 6. Subsequently, the alcohol-water mixtures stabilize the Ti-OOH by co-adsorption. Small, electrophilic solvents are preferred because there are less steric constraints, and after the propene epoxidation easily and quickly diffuse out of the pore structure [109]. Thirdly, insertion of the peroxy oxygen atoms occurs in propene. In this situation, the peroxy oxygen atom is the most electrophilic and therefore reacts with the nucleophilic propene molecule [105,106]. Desorption of propene oxide is the last reaction step, and the Ti-O-Si is regenerated [105,106]. Moreover, titanium-silicates showed activity for epoxidation reactions of higher alkenes, for example a selectivity up to 97% for 1,2-epoxybutane [12]. However, the limitation of higher alkenes is due to the molecular size. Molecules or products must be able to diffuse out of the channels of TS-1.

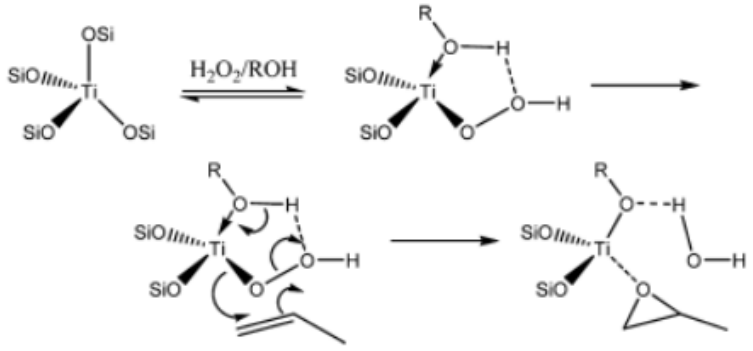

Figure 6: The reaction mechanism of propene epoxidation over TS-1 catalysts. Taken from ref. [105].

However, catalytic deactivation was observed and this was later attributed to the oligomerization of propene oxide, which blocked the zeolite micropores [104]. Several other titanium-containing supports were investigated in the propene epoxidation with hydrogen peroxide or alkyl hydroperoxides [107,108]. Ti-MCM-41, TiO_2-SiO_2 xerogel, and TiCl4- modified H-ZSM-5 zeolite were investigated by Chen et al. It was concluded that the shape/size selectivity of the silica support is pivotal for the catalytic performance in propene epoxidation with hydroperoxides [107]. For example, Ti-MCM-41 was subjected to catalytic tests and showed no activity towards propene oxide production. This was attributed to the mesoporosity of Ti-MCM-41 and therefore showed no shape selectivity.

On the contrary, TiO_2-SiO_2 xerogel contained too small pores to facilitate any propene epoxidation at all [107]. Furthermore, the hydrophobic nature of the Ti-containing catalysts was concluded to play a critical role [107]. Both TCM-41 and TiO_2-SiO_2 were characterized, and it was concluded that the more hydrophilic nature of these supports resulted in the competition of active sites between water and methanol with hydrogen peroxide [107].

2.2.3. Supported Au/Ti-catalysts in propene epoxidation with H_2/O_2

Gold was long thought to be chemically inert because it was resistant to corrosion/oxidation and did not (easily) react with other substances. As previously addressed, Bond and Sherman discovered that dispersed gold nanoparticles on SiO_2 were active in the hydrogenation of alkenes [37]. Furthermore, the discovery of the catalytic activity of supported gold nanoparticles in CO oxidation led to studies to understand the origin of this catalytic activity [60,61,94]. Decreasing the gold nanoparticle size led to a higher percentage of low-coordinated Au atoms, which have a stronger bonding of CO and O [94]. Stronger bonding lowers the adsorption energy of oxygen and thereby affects the catalytic activity. In general, (supported) nanoparticles greatly differ regarding their properties regarding the bulk material, since the high surface/volume ratio and the creation of quantum effects. In gold-catalyzed reactions, it is known that the catalytic activity of gold catalysts highly depends on the size of gold nanoparticles, the type of support, and the preparation method [20,21,94,95].

The application of supported gold nanoparticles is not limited to CO oxidation and the hydrogenation of alkenes. In 1998, Haruta's group discovered that supported gold particles in combination with metal catalysts show high catalytic activity and selectivity in propene oxidation [19]. This research showed that selective oxidation of propene is possible with H_2/O_2 mixtures in combination with supported gold nanoparticles on titania with a size between 2-5nm. However, Delgass argues that <2nm supported gold nanoparticles could significantly contribute to propene epoxidation, since they are hard to observe on TEM-images acquired of their gold-titanium silicate catalyst [6].

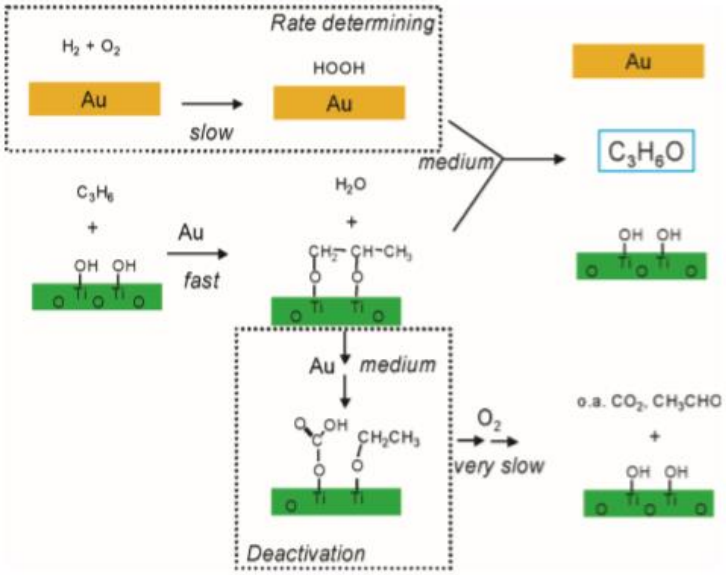

Figure 7: Schematic representation of propene oxidation reaction over of Au/TiO_2 catalysts. Taken from ref. [1,31,84].

The direct epoxidation of propene over supported gold nanoparticles on titania consists of three reaction sequences. First of all, a hydroperoxide is formed from molecular hydrogen and oxygen on gold nanoparticles' surface. Secondly, the hydroperoxide is spilled over to active titanium centers that result in a titanium-peroxo intermediate, the rate-determining step [1]. Subsequently, propene is adsorbed via an Eley-Rideal mechanism, which results in the production of bidentate propoxy species. Finally, the desorption of bidentate propoxy species allows for the reaction with the titanium-peroxo intermediate and propene oxide is produced [1,34,84]. The primary side reaction that is most likely to occur is the conversion of bidentate propoxy species by oxidation to carboxylates, catalyzed by active sites of titania next to gold nanoparticles by [19]. Therefore, the general assumption is that the propene oxidation takes place at the gold/titania interface. Multiple factors can influence the selectivity and activity of the

propene oxidation. Both the effects of different supports and size dependency have been investigated [20,21]. It is assumed that Au nanoparticles smaller than 2 nm will most likely hydrogenate propene to propane [19].

Since Haruta's group published their discoveries, major improvements have been made regarding Au/TiO_2 catalysts, achieving a selectivity up to 99% at low temperatures (80 °C) [26]. The side products primarily produced are propanal, ethanal, propane, and carbon dioxide [25]**.** Despite the high selectivities, Au/TiO_2 catalysts encounter stability issues in the selective oxidation of propene with H_2/O_2 mixtures. Mul. G. et al. performed an in Situ FT-IR study to understand Au/TiO_2 catalysts' deactivation within a few hours over stream. The spectroscopic results showed that the deactivation of 1wt% Au/TiO_2 catalysts was indeed caused by the formation of bidentate propoxy moieties on the active Ti sites, which was the result of irreversible adsorption of propene oxide [68]. Moreover, oligomerization of propene oxide on the acidic sites contributed to the deactivation of Au/TiO_2 catalysts [73]. Lastly, studies of the 1wt% $Au/TiO_2/SiO_2$ catalyst showed that the active Ti sites' occupation by propoxy species in propene oxidation was not present. However, propene oxide's irreversible adsorption was also observed on this catalyst, resulting in propanal and acetone formation.

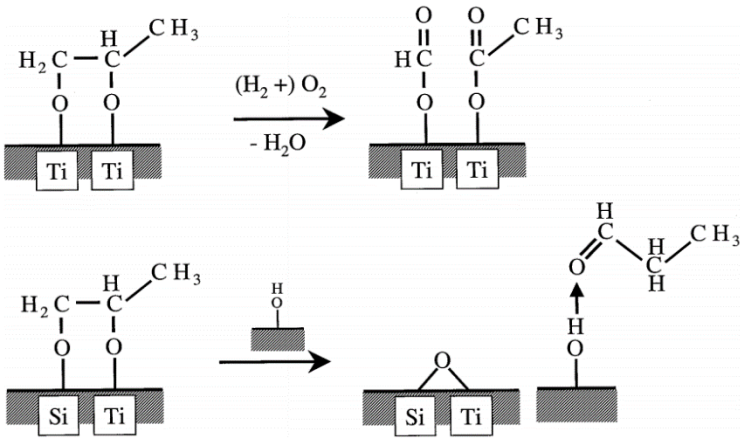

Figure 8: Formation of acetate from bidentate species and propanal formation over Au/TiO_2 and $Au/TiO_2/SiO_2$ catalysts. Taken from ref. [68].

2.2.4. Influence of support

In general, nanoparticles are immobilized on supports. The immobilization of nanoparticles on supports limits mobility and thereby prevents any sintering of nanoparticles [65]. Furthermore, supports like SiO_2 and Al_2O_3 can provide a large surface area. A large surface area allows for high dispersions of nanoparticles. The rate of a catalytic reaction is proportional to the amount of accessible active sites and therefore a high dispersion (in this case gold nanoparticles) is highly desired. Furthermore, highly dispersed gold nanoparticles across the support result in the formation of the highest amount of Au-Ti interfaces. The Au-Ti interfaces are necessary since the hydroperoxide must be spilled over from gold to active titanium centers and subsequently react with the desorbed bidentate propoxy species [1,34,84].

As addressed in the previous section, dispersed gold nanoparticles supported on titania selectively epoxidize propene to propene oxide but deactivate very quickly. Nijhuis et al. studied the performance of various other titanium-containing supports in propene epoxidation at low temperatures (<100°C) [102]. They found that dispersed supported gold nanoparticles with dispersed Ti-active sites resulted in more stable catalysts. Table 2 represents the catalytic performance of various titanium-containing support in the epoxidation of propene with H_2/O_2 mixtures.

Table 2: Direct Propene Epoxidation over Au nanoparticles supported on various titanium-containing supports; (10% H_2/10% O_2/10% C_3H_6), flow 33mL/min. Taken from ref. [102].

Catalyst	Reaction Temp. (K)	C_3H_6 Conversion (%)	PO Selectivity (%)	Activity ($mg_{propene}/g_{cat}/h$)
1wt% Au/TiO_2	323	0.8	>99	5.4
	343	1.3	>99	8.6
	363	0.5	20	3.3
1wt% Au/TS-1	343	0.3	>99	3.2
	373	0.5	>99	5.4
	398	0.8	>99	8.6
	448	1.5	78	16.1
1wt% Au on TiO_2 on SiO_2	373	1.0	>99	6.7
	398	1.5	80	10.0
	448	4.0	10	26.6
1wt% Au on SiO_2	No propene epoxidation activity			
1wt% Au on γ-Al_2O_3	No propene epoxidation activity			

These results show that titanium is pivotal for the epoxidation of propene to propene oxide, since supported gold nanoparticles on silica and alumina do now show any propene epoxidation activity. The improved stability of these catalysts can be described to the inhibition of oligomerization of propene oxide since the Ti-sites are highly dispersed [85,102]. However, a second consideration before these catalysts can be commercialized is that the hydrogen efficiency is relatively low [25]. One of the reasons that the hydrogen efficiency is low (~30%,) is the possible oxidation reaction of hydrogen to water, especially at higher temperatures [102]. An increase in hydrogen efficiency is highly desired for commercialization. At first, propene conversion was approximately 2% with a hydrogen efficiency of ~30%. In 2012, hydrogen efficiencies up to 50% were achieved with propene conversion of 6% while keeping a reasonable selectivity (88)% by supporting gold clusters on alkaline treated TS-1 [93].

The group of Haruta has performed research on the production of propene oxide with gold clusters and has reported that gold clusters (<2.0nm) can form peroxide species out of molecular oxygen and water [23]. Out of water and oxygen, a hydroxyl and hydroperoxyl radicals are generated. The formation of hydroperoxyl radical allows for the oxidation of propene in the presence of supported gold clusters **[**24]. A propene oxide selectivity of 50% is achieved with a propene conversion of approximately 1.0%. Recently, there have been significant improvements in gold-cluster catalysis, achieving propene oxide production with a selectivity of up to 80% **[**24]. The major flaw is that dissociated molecular oxygen attacks the allylic hydrogen atoms and causes acrolein formation. Comparing the performance of gold clusters with gold nanoparticles, the gold nanoparticles (>2.0nm) seem to hold more potential right now, since supported gold nanoparticles on titanium oxides achieve selectivities up to 99%. Therefore, this research aims for gold nanoparticle sizes between 2-5nm.

To elaborate further on the support influence, gold nanoparticles supported on γ-Al_2O_3 and SiO_2 did not show any propene epoxidation activity. However, it has been found that Al_2O_3 shows activity and selectivity in alkene epoxidation with hydrogen peroxide [35]. The reaction takes place on the alumina surface. Different types of alumina possess multiple (strong) Lewis acidic sites that can activate the hydrogen peroxide. On the contrary, heterogeneous alumina catalysts have their limitations.

First of all, a large excess of hydrogen peroxide is needed. Secondly, the yield of alumina-catalyzed epoxidation reactions is moderate, even in a large excess of catalysts [35].

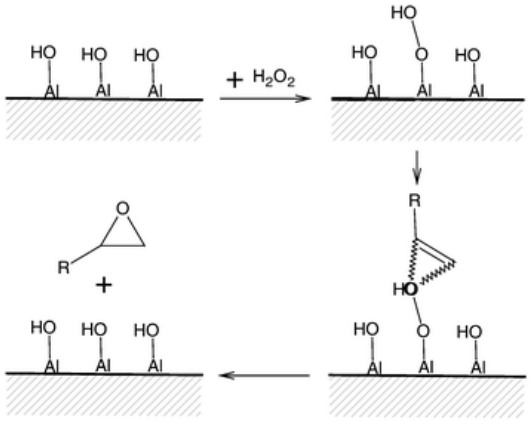

Figure 9: Mechanism for alumina catalysed alkene epoxidation. Taken from ref. [35].

2.3. Supported bimetallic catalysts in propene epoxidation.

Gold-titania catalysts hold a tremendous potential for the direct epoxidation of propene towards propene oxide. Unfortunately, as stated before, the activity and stability of these catalysts are still an issue. The reaction rate (formation of propene oxide) is determined by the rate of hydrogen peroxide formation, which is the rate-determining step since a peroxo-intermediate is formed [19]. The low hydrogen conversion (and thereby low efficiency) in direct propene epoxidation is one of the main reasons which prevent further industrial implementation of these gold-titania catalysts. Therefore, much research has been dedicated to improve hydrogen efficiency. For example, The East Chinese University has found that the introduction of bimetallic Au-Ag supported on titanium silicate improved the propene oxide formation rate significantly (2x times in mol%) [45].

Furthermore, the oxygen conversion is increased because synergy effects of Au-Ag facilitate the electron transfer between gold nanoparticles and molecular oxygen. Last, a hydrogen efficiency of 44% has been achieved, which is significantly higher than the usual 30% hydrogen efficiency for monometallic titanium silicates. Bimetallic nanoparticles (BNPs) are nanoparticles that consist of two different metals, for example in an alloy or core-shell form. BNPs were first commercialized in the 1960s, although since a decade interest in bimetallic nanoparticles started to rise [50]. In general, nanocatalysis focuses on achieving the highest selectivity and activity while minimizing the catalysts' deactivation. There are similarities between mono- and bimetallic nanoparticles in heterogeneous catalysis. Catalytic activity and selectivity in both cases are affected by the shape, size, choice of metal, and type of support. Bimetallic nanoparticles are often more stable and show higher activity than monometallic nanoparticles. Each different metal has unique electronic properties and catalytic properties can be altered more effectively with the introduction of a second metal.

Bimetallic catalysts are studied extensively to understand the origin of their unique catalytic properties. First of all, the bimetallic surface is altered by the formation of bonds between the metals. The alteration of the active sites of both metals originates from synergy effects. First of all, metal-metal interactions alter the electronic state/environment, known as the electronic effect. Secondly, a strain-effect is created since there are heteroatom bonds with different lengths compared to monometallic nanoparticles [72]. Both these effects contribute to the formation of unique active sites in bimetallic nanoparticles. In bimetallic catalysis, the electronic environment is pivotal since it describes the charge transfer [51,52], especially in oxidation reactions.

Numerous studies have been carried out regarding direct propene oxidation over supported bimetallic nanoparticles [45,46,73,74,76]. It was previously mentioned that Au-Ag/TS-1 enhanced the propene oxide formation rate by two times. They concluded that the introduction of Ag improved the dispersion of Au on the titanium silicate support. Furthermore, the supported bimetallic catalysts showed that oxygen adsorption and electron transfer is facilitated [45]. Another research group found that Ir-Au/TiO_2 showed higher activity than monometallic Au/TiO_2 [73]. Aguilar-Tapia A. et al. concluded that the enhanced activity, primarily at higher temperatures (>150°C), can be allocated to iridium and Au's synergy effects. Moreover, the gold nanoparticles prevented oxidation of iridium to the degree that benefits these supported bimetallic nanoparticles' activity in the direct oxidation of propene [73].

Besides AuAg supported bimetallic nanoparticles, supported AuPd and AuPt catalysts have also received considerable interest in propene oxidation. Hosseini M. et al. investigated the performance of core-shell and Pd-Au nanoparticles supported on TiO_2. They discovered that propene conversion is improved by both core-shell and alloy-based AuPd catalysts. The best-performing catalysts regarding activity were Pd(shell)-Au(core)/TiO_2, followed by Pd-Au(alloy)/TiO_2, both achieving a 100% propene conversion at 225 °C. On the contrary, Au/TiO_2 only achieves 100% propene conversion at a temperature above 325 °C. The excellent activity in these catalysts can be attributed to these catalysts' atomic distribution, facilitating oxygen adsorption [74]. Figure 10 shows the enhanced PO formation rate by supported bimetallic nanoparticles compared to monometallic supported Au/TS-1.

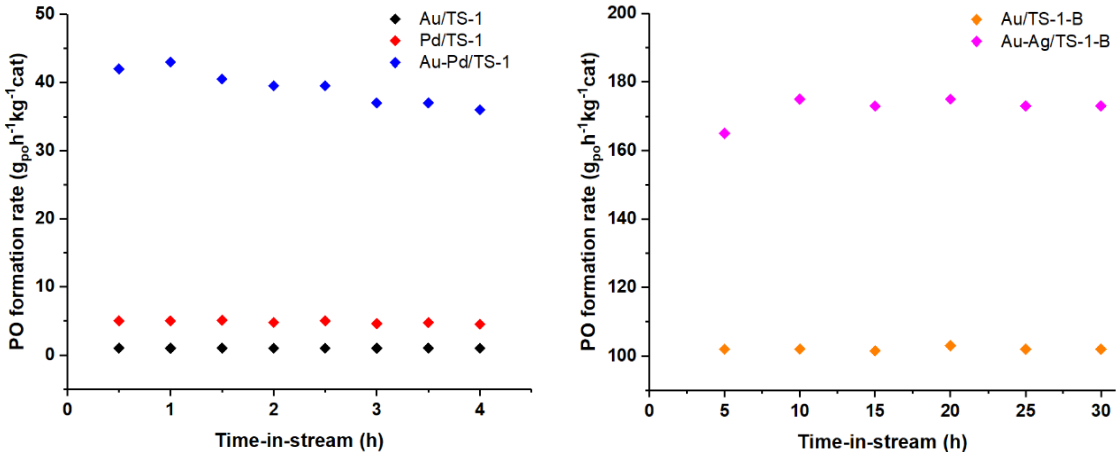

Figure 10: Enhanced PO formation rate by supported bimetallic nanoparticles in respect to monometallic supported Au/TS-1. A) Au_3Pd_1; B) $Au_{10}Ag_1$. Temperature = 200°C. Adapted from ref. [45,46].

Bimetallic nanoparticles AuPt and AuPd are clearly an improvement with respect to monometallic nanoparticles, but only regarding the catalytic activity. Since Pd and Pt-based catalysts are excellent hydrogenation catalysts, the enhanced catalytic activity in propene oxidation is associated with undesired hydrogenation of propene to propane. Literature often reports about these hydrogenation reactions in propene oxidation. For example, Pd-Au and Pt-Au (5:95 ratio) catalysts prepared by deposition-precipitation limits the production of propene oxide and stimulate propane formation (T = >100°C) [76]. However, the Pt-Au catalysts improved the H_2 and O_2 efficiency, since water formation is partially inhibited.

Secondly, Delft University of Technology researchers have found that the introduction of platinum to Au/TiO_2/SiO_2 catalysts improves activity and selectivity [46]. Therefore, it is plausible that the introduction of hydrogenative metals can improve hydrogen conversion and efficiency of gold-titania catalysts. On the contrary, both research groups found a volcano-shaped plot of the reaction rate for bimetallic nanoparticles. The addition of too much platinum results in more active sites (blocking Au active sites), thereby enabling propene's hydrogenation reaction to propane [46].

A high understanding of the chemical bonding between the catalytic surface and reactant is necessary to increase hydrogen efficiency by using bimetallic nanoparticles. A reacting molecule approaches the metal. The electrons of the adsorbate start to interact with the orbitals of the metal, which subsequently leads to the formation of bonding and antibonding orbitals [47]. One of the essential concepts concerning chemisorption is the Fermi level. The Fermi level is defined as an electron band's energy level, thereby indirectly determining the probability of being occupied [47]**.** Therefore, the orbitals below the Fermi level are filled with electrons. The position of the bonding/antibonding orbitals chemisorbed complexes primarily determines the strength of the chemical bond in relation to the Fermi level. A strong interaction between the metal and adsorbate results in strong bonding/antibonding orbital splitting. Thereby, the antibonding orbital is located above the Fermi level and is not likely to be filled. The strength of this interaction between the metal and adsorbate is proportional to the number of electrons occupying the d-orbitals in the transition metal. A transition metal with many electrons occupying the d-orbitals interacting with an adsorbate result in minimal orbital splitting. Then, both orbitals are located underneath the Fermi level (and occupied), which results in a weak bond. A weaker bond (higher binding energy) limits dissociative adsorption of adsorbates. The other way around, transition metals with half-filled d-orbitals results in powerful bonding. Then, the antibonding orbital is located above the Fermi level and unoccupied.

Secondly, the idea of introducing a second metal to create bimetallic particles affects chemisorption since the metal surface is modified. In theory, it is clear that the stronger the reactants are adsorbed, the more dissociation is facilitated because the activation energy is lowered [47]. For the in-situ production of H_2O_2, dissociative adsorption of H_2 and associative adsorption of O_2 is required. A trend is observed in the periodic table regarding atomic and dissociative adsorption. Smaller atoms with more electrons have a higher binding energy, since the d-orbital/band is highly occupied with electrons in a smaller area. Therefore, elements such as Pd, Pt, Ag, and Pd are studied extensively in direct propene epoxidation combined with gold because they restrict the dissociative adsorption of O_2.

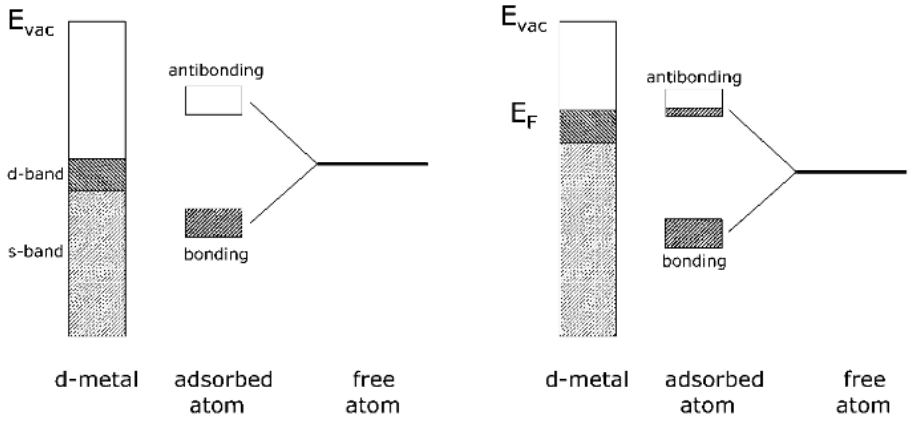

Figure 11: Energy diagram for the chemisorption of a single atom on the surface of a d-metal. In the left figure, the antibonding is located above the fermi level and thereby no electrons occupy the antibonding orbital. The figure on the right represents a partially filled antibonding orbital, which weakens the chemisorption bond. In the adsorption of an diatomic molecule (not presented here), the dissociative adsorption is limited. Taken from ref. [98].

Furthermore, introducing a second metal to supported monometallic catalysts affects the degree of dissociative adsorption and initial adsorption of the reactant on the metal surface. For example, the H_2 adsorption on gold nanoparticle surfaces is thermodynamically unfavorable. F.R. Lucci et al. have proven by DFT calculations that the activation barrier for the adsorption of H_2 on Au with the introduction of Pd monomers is lowered from 1,04 eV to 0.20 eV [71]. The level of H_2 and O_2 dissociation is thus related to the choice of metals for further increasing hydrogen conversion.

2.4. Transition-metal catalysed propene epoxidation.

From literature, it is known that other transition metals can be applied in alkene epoxidation with hydrogen peroxide as the oxygen donor [2,5,10,96]. Transition-metals can be divided into specific subclasses. Early transition metals are located from group 3 to group 7 within the periodic table, whereas late-transition metals are group 8 to 11 elements. These transition metals must fulfill specific requirements to be able to carry out an oxidation reaction.

First of all, the catalytic properties of transition metals are attributed to their ability to accept or donate electrons easily. Transition metals with partially filled d-orbitals lend themselves for the acceptance or donation of electrons, which is of extreme importance in reduction and oxidation reactions. Both of these type reactions involve electron transfer. In our research, we aim for alkene epoxidation, and therefore we need Lewis acidity to accept the electrons from the hydrogen peroxide. Lewis acidity is defined as any substance that can accept a pair of electrons [10].

This Lewis acidity is needed to remove the peroxidic oxygen charge and thereby facilitates the activation of the oxidant [5,96]. Furthermore, transition metals in alkene epoxidation must be stable in their highest oxidation state. As a result of this stability, the key intermediate M-OOH can be formed, indirectly required to activate the proximal oxygen. Besides this, transition metals oxidation state changes should not be favorable/easily performed. Easily accessible lower oxidation states lead to metal-catalyzed decomposition of the peroxide species via a redox mechanism [96]. Furthermore, the metal center is required to have a vacant coordination site for the adsorption of the alkene.

It is accepted that only early transition metals (ions), such as W(VI), Mo(VI), and RE(VII) operate by a Lewis acid mechanism [5]. Figure 12 shows the alkene epoxidation mechanism by early transition metals. A sequence of steps achieves the alkene epoxidation by Lewis acidity. The first reaction step is the formation of the critical M-OOH intermediate. The removal of charge from the O-O bond facilitates the dissociation of the oxidant and the activation of the proximal oxygen. Since alkenes are nucleophiles, the most electrophilic oxygen atom is inserted into the alkene, in this case, the proximal oxygen. The alkene coordinates by a Lewis Acid-Lewis Base interaction and not by back-bonding since no electrons occupy the d-orbitals in the metal's highest oxidation state. Last, the coordination of the alkene to the metal initiates the oxygen transfer [5].

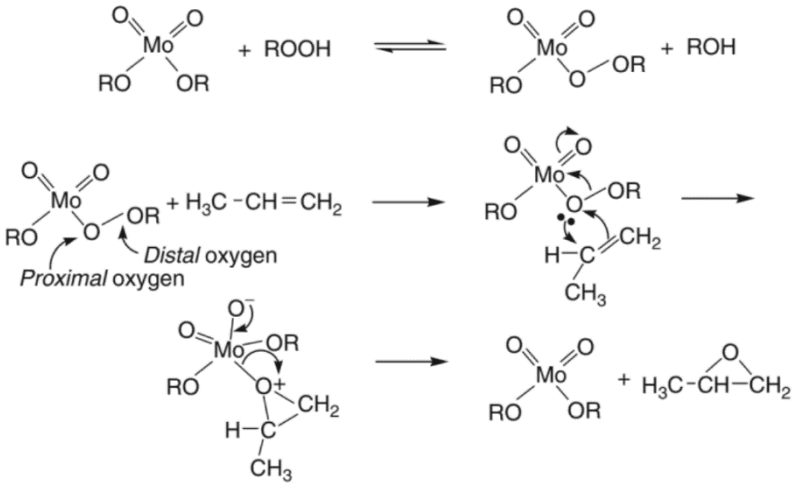

Figure 12: Lewis acid mechanism, molybdenum as the catalyst in the epoxidation of alkenes, with ROOH resembling H_2O_2 or an alkyl peroxide. Taken from ref. [5].

Thirdly, homogeneous complexes can also be applied in the epoxidation of alkenes in industrial processes. However, they operate via a different mechanism than early transition metals, called the redox mechanism. This mechanism is based on incorporating oxygen on the metal ion (metal-oxo species) and subsequently transferring it to the alkene. An example of the redox-mechanism is shown in Figure…. These late transition metals, such as Cr(III), Mn(III), and Fe(III) are firstly reduced. Low-valent early transition metals are reactive towards oxidation because high-valent states show higher stability. This redox-mechanism-driven epoxidation reaction is described as the long route in Figure 13, which uses molecular oxygen. Moreover, there is also a short route where hypochlorite (single oxygen atom donor) is used as an oxygen source for iron/manganese porphyrin catalysts. Once the oxygen is successfully dissociated, there is a decline in its oxidation state. This type of mechanism depends on the interaction of the alkene with the electrophilic peroxygens [2,5].

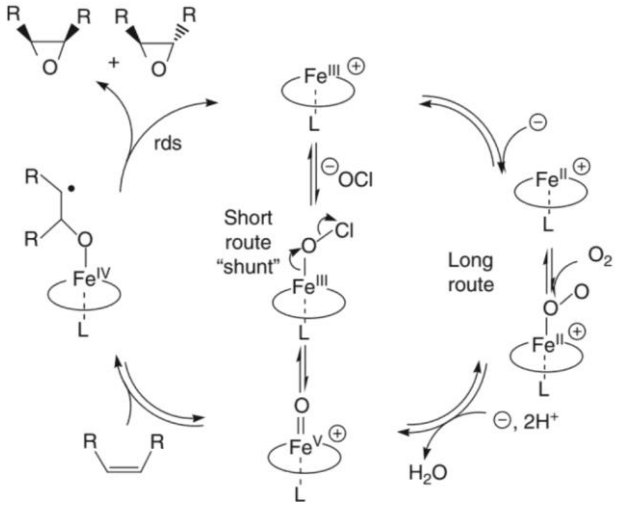

Figure 13: Epoxidation of alkenes by late-transition metals complexes (redox mechanism). Taken from ref. [5]

2.5. Characterization methods.

In this section, a brief description will be given about the experimental and analytical techniques that are applied throughout this research project.

2.5.1. Transmission Electron Microscopy.

Transmission electron microscopy (TEM) is an analytical technique used extensively in the field of material science. It allows for the characterization of catalysts consisting of supported (bi)metallic nanoparticles supported on various supports. An intense beam of electrons (120-200 kV) is shone at a sample and enables the creation of 2D-images by monitoring the interaction between electrons and the atoms on the support [95]. The contrast between two adjacent areas in a 2D-TEM image is generated by the thickness (i.e., density) and diffraction differences. More specifically, in this research only bright field TEM (BF-TEM) images are presented. BF-TEM images are generated by considering the unscattered dense electron beam as aperture. Scattering of the shone electron beam by nanoparticles results in darker areas. With the application of TEM, the average particle size and dispersion of nanoparticles can be determined and visualized with extremely high resolution.

2.5.2. Diffuse Reflectance UV-Vis Spectroscopy.

Nanoparticles of noble metals, particularly gold, silver, palladium, copper, and platinum have unique optical properties and intense colors. These nanoparticles show absorption bands in the UV-visible regime. UV-vis spectroscopy determines the extinction (absorption and scattering) of light by a sample and the maximum absorbance of a particular wavelength. Absorption bands of noble metals are generated by localized surface plasmon resonance (LSPR), which is defined as the collective oscillation of conduction electrons when (visible) light is shone on the sample. The principle of LSPR is represented in Figure 14A [70]. By the extent and amount of surface plasmon resonance, an estimation of the noble nanoparticles' size can be made. Gold nanoparticles exhibit absorption bands between 500-550nm, represented in Figure 14B. The LSPR spectrum is dependent on multiple aspects, with the most important one being size, besides composition. In terms of size, smaller nanoparticles result in spatial confinement and thereby restrict the motion of the conductive electrons. Therefore, the plasmon resonance will be stronger and spectrally narrower, resulting in a blue shift.

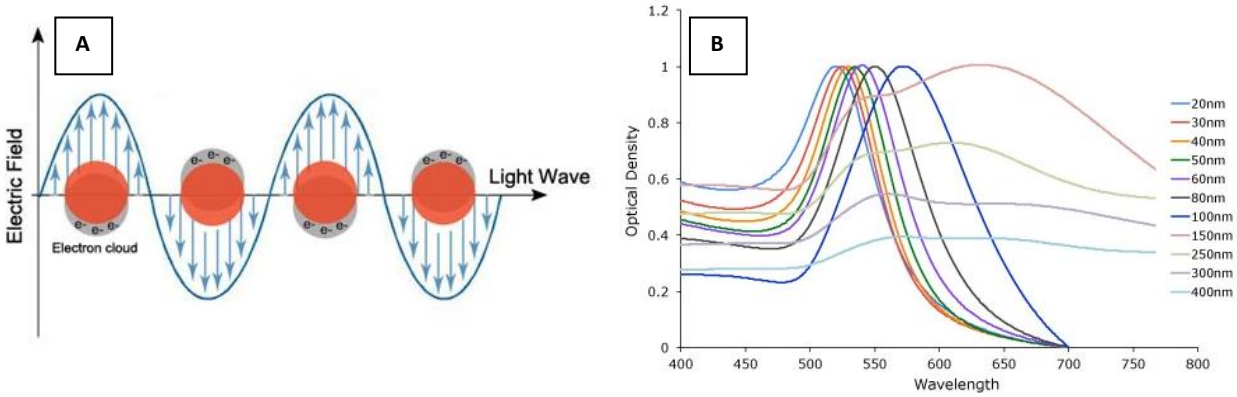

Figure 14: A) Basics of LSPR and the size dependent surface plasmon resonance of gold nanoparticles. B) The LSPR sprectrum dependency on size of nanoparticles. Taken from Ref. [70].

2.5.3. X-Ray Diffraction.

By X-ray diffraction (XRD), we can investigate the crystalline phases of the support and nanoparticles [94]. Thereby, XRD allows for the degree of dispersion of supported nanoparticles across the support. XRD relies on the elastic scattering of x-ray photons of a (crystalline) sample. Atomic planes of a crystalline sample will result in interference of x-ray beams, called constructive interference. Constructive interference only appears when Bragg's law is satisfied, $n\lambda = 2d\sin\theta$. This equation represents the relation between the wavelength of EM radiation, diffraction angles, and lattice spacing. The crystalline or amorphous solid catalyst must be scanned through various angles to obtain every diffraction direction. When there is a certain amount of crystallinity, the Debye-Sherrer formula allows us to estimate the crystallite size. The Bragg peaks in a XRD-pattern are broadened inversive proportional to the crystallite size.

$$D = \frac{0.9\lambda}{\beta cos\theta}$$

In which D resembles the average crystallite size, Full width half maximum (FWHM) of the diffractions peak is represented by β, the wavelength, typical 0.179nm for the cobalt source used and θ half the scattering angle.

3. Aim and scope of research.

Propene epoxidation with H_2/O_2 mixtures over Au/TiO_2 catalysts has been investigated extensively. Further research with other Ti-containing supports has led to a significant improvement of the catalytic performance. Moreover, supported bimetallic nanoparticles exhibit higher catalytic activity in comparison with their monometallic counterparts, which can be attributed to synergy effects [45,46,73]. However, monometallic and bimetallic catalysts suffer from either low reactant conversions or stability issues that prevent industrial implementation. As an alternative, homogeneous catalysis shows that alkene oxidation reactions can be carried out with transition-metals and main-group elements.

Therefore, this research project aims to investigate whether active Ti-sites in propene oxidation can be replaced by other transition metals in Au/Ti-catalysed propene oxidation with H_2/O_2 mixtures. Furthermore, this study strives to understand the effect on the catalytic performance by modifying supported gold nanoparticles to form bimetallic nanoparticles.

- How is Au-Ti catalyzed propene epoxidation influenced by replacing Ti with group 5-7 transition metals?
- What is the effect on the catalytic performance in propene epoxidation by making bimetallic AuM nanoparticles?

This section briefly discusses the required steps to answer the research questions. First of all, the choice of support is rationalized. SiO_2 provides high stability for highly dispersed gold nanoparticles [36,67]. Secondly, the method for the preparation of bifunctional catalysts is argued. After that, the catalytic performance was analysed and the catalyst with the best behavior was selected for further modification towards bimetallic nanoparticles. Subsequently, preparation methods for the synthesis of supported bimetallic nanoparticles are explained. At last, utilized characterization methods for the bifunctional and bimetallic catalysts are presented.

3.1. Bifunctional Au catalysts: preparation and characterization.

In this chapter, silica is used as the support since it provides high stability for highly dispersed gold nanoparticles [36,67]. The preparation of stable and highly dispersed gold nanoparticles is not feasible by deposition-precipitation or co-precipitation. Typically, small nanoparticles are obtained via deposition-precipitation. However, due to the low isoelectric point of silica and oxygen vacancies, supported gold nanoparticles on SiO_2 are highly unstable and aggregate upon heat treatment [36]. Furthermore, the deposition of the metal oxide on SiO_2 followed gold deposition is not successful. Unpublished results show that catalytically active elements (i.e., metal oxide) are removed from the silica surface during gold deposition.

Liu et al. have developed a procedure to adsorb thermally stable and highly dispersed gold nanoparticles on SiO_2 [36]. The silica surface is functionalized with amine-groups, which facilitated the adsorption of gold and the metal complex by strong electrostatic adsorption (SEA). SEA is a commonly applied procedure in the synthesis of supported metal nanoparticles dispersed across a (functionalized) silica support [36]. It relies on electrostatic interaction between a charged metal precursor complex and a charged support, which must be opposite and thereby results in an attractive interaction. The principle of SEA is shown in Figure 15. In the synthesis of our gold-based catalyst. the electronic interaction originates between the negatively charged gold precursor and positively charged sites in acidic solutions. Afterward, the adsorbed gold precursor is in-situ reduced by sodium borohydride to form gold nanoparticles.

Subsequently, ligand substitution, which indirectly relies on the Hard-soft acid and base theory, facilitated the adsorption of a second metal complex. The favorable metal precursor complexes were determined by rationalization and anchored with the remaining amine groups on the functionalized silica surface. After adsorption of the second metal complex, catalysts were reduced and calcined to remove the amine-groups from the support and ligands of the metal complex. The Au-M/APS-SiO_2 catalysts (i.e., bifunctional catalysts) were characterized with TEM to determine particle size and shape. Furthermore, DR UV-Vis was applied to determine if ligand substitution was successful. Transition-metal complexes are known to absorb light in the UV-Vis spectrum, caused by electronic d-d transitions, and are shown as unique absorbance band in the UV-Vis spectrum (200-800 nm). Finally, the catalysts were subjected to XRD and ICP-AES measurements to investigate the dispersion of the supported metal nanoparticles and acquire detailed information regarding the gold weight loadings.

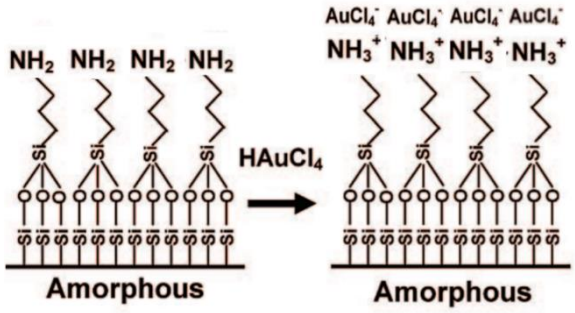

Figure 15: Simplistic overview of Strong Electrostatic Adsorption (SEA) of $HAuCl_4$ on APS-SiO_2. Adapted from [36].

3.2. Bimetallic Au catalysts: preparation and characterization.

Gold nanoparticles were modified to form bimetallic nanoparticles on the functionalized support with the best catalytic behavior in propene epoxidation according to literature. The monometallic and bimetallic nanoparticles were prepared by (sequential) deposition-precipitation, using either TiO_2 or Ti-SiO_2 as support. The deposition-precipitation method basically consists of two processes, precipitation and deposition. Precipitation is defined as the formation of a solid from a solution. Secondly, deposition is the process of anchoring the earlier formed precipitate to the support. This particular synthesis method relies on the interaction of the supports' functional groups (-OH) with the precursor ions in solution [48]. By slowly adding the precipitating agent, either urea or sodium hydroxide, the metal precursor solution's pH and support are increased. Higher pH values allow the formation of chloro-hydroxo gold species (when using tetrachloroauric acid as a precursor), which can interact with the titania support oxide [49]. Metallic gold particles are obtained after calcination. The size of these gold nanoparticles or bimetallic nanoparticles depends on several experimental conditions, such as pH value, reaction time, calcination conditions, and precursor concentrations [49]**.** The bimetallic catalysts are characterized by utilizing TEM, UV-VIS, ICP-AES, and XRD.

3.3. Catalytic testing.

The catalytic performance of gold-based catalysts in the gas -phase propene epoxidation is tested in a plug-flow reactor in the presence of $H_2/O_2/C_3H_6$ (10% vol. each) mixtures in helium (70% vol), usually at 200°C. This specific composition of the gas mixture is chosen since much research is carried out under this composition of gas mixtures [14,19,102]. Before catalytic testing, an in-situ reduction is carried out under a flow of H_2 and He. A detailed overview of all reaction conditions and flows are represented in section 4.5

4. Experimental methods.

This chapter will provide a detailed representation and explanation of the experimental procedures employed throughout this research project. Firstly, the synthesis of bifunctional catalysts (Au-M/APS-SiO_2) is explained. Secondly, the experimental methods for the synthesis supported bimetallic nanoparticles on TiO_2 (AuM/TiO_2) are displayed. Furthermore, in the subsequent section the characterization techniques for catalysts are briefly explained. At last, the applied heat treatments and settings for catalytic tests are represented.

4.1: Chemicals and general considerations.

In this research, all types of chemicals are used for the synthesis and catalytic tests. Table 3 provides an overview of all chemicals used throughout this project, including purity and suppliers.

Table 3: Information of the chemicals used in this research project.

Chemical	Chemical Formula	Supplier	Purity
Gold(III) chloride trihydrate	$HAuCl_4$	Sigma-Aldrich	>99.9%
Sodium Borohydride	$NaBH_4$	Sigma-Aldrich	>98.0%
Sodium hydroxide	NaOH	Sigma-Aldrich	97.0%
3-(aminopropyl)triethoxysilane	$C_9H_{23}NO_3Si$	Sigma-Aldrich	99.0%
Toluene	$C_6H_5CH_3$	Sigma-Aldrich	99.8%
Ethanol	C_2H_5OH	Sigma-Aldrich	>99.9%
Iron(III) trichloride hexahydrate.	$FeCl_3{}^*6H_2O$	Sigma-Aldrich	98.0%
Manganese(II) nitrate tetrahydrate	$Mn(NO_3)_2{}^*4H_2O$	Sigma-Aldrich	98.0%
Ammonium perrhenate	NH_4ReO_4	Sigma-Aldrich	>99.0%
Ammonium molybdate	$(NH_4)_6Mo_7O_{24}$	Merck	99.98%
Ammonium metatungstate	$H_{26}N_6O_6O_{40}W_{12}$	Merck	99.99%
Titanium(IV) butoxide	$Ti(OBU)_4$	Sigma-Aldrich	97.0%
Methylrheniumtrioxide	CH_3ReO_3	x	71.0-76.0% Re
Urea	CH_4N_2O	Sigma-Aldrich	99.0%
Silver nitrate	$AgNO_3$	Sigma-Aldrich	>99.0%
Palladium(II) nitrate dihydrate	$PdNO_3{}^*2H_2O$	Sigma-Aldrich	~40% Pd Basis
Copper nitrate dihydrate	$CuNO_3{}^*2H_2O$	Sigma-Aldrich	99.0%

Furthermore, various supports were used in this research. Silica (SiO_2) was provided by GRACE® (Davicat SI 1404, 7.4nm pores, 500m2/g, 0.9mL/g pore volume). Titania P25 (TiO_2) was purchased from Evonik Industries (80-90% anatase and 10-20% rutile) [101]. Secondly, Bis ethylene diamine gold (III) chloride ($Auen_2Cl_3$) and Ti-SiO_2 were synthesized by my supervisor and prepared using an adapted literature procedure [99,100]. Finally, all procedures involving gold were performed in the absence of light and glasswork was cleaned with aqua regia beforehand.

4.2. Catalyst preparation.

This chapter illustrates the experimental producers performed to synthesize bifunctional catalysts, mono- and bimetallic catalysts for the direct propene oxidation with H_2/O_2 mixtures. The bifunctional catalysts were prepared by strong electrostatic adsorption (SEA) of a gold precursor on an amine-functionalized silica surface, followed by ligand substitution of transition-metal complexes. Secondly, gold-titania based catalysts were synthesized by deposition-precipitation with urea. Subsequently, a series of AuM/TiO_2 were prepared by sequential deposition-precipitation with NaOH. At last, gold-titanium(IV)-silica-based catalysts were synthesized by deposition-precipitation with NaOH.

4.2.1. Synthesis of bifunctional catalysts.

The synthesis of Au-M/SiO_2 catalysts started with drying commercially available SiO_2 (Grace 1404, SBET 500 m^2/g, 7.4nm pores and pore volume 0.9mL/g) at 120°C under vacuum for a minimum of 12h. Secondly, the support (~6 g) was functionalized using aminopropyltriethoxysilane (APTES) according to a literature procedure [36]. Under an inert N_2 atmosphere, the dried support was dispersed in toluene (50mL). Subsequently, the amount of APTES required for complete functionalization of the support surface was added in excess (1 mL, three OH-groups per nm2). Afterward, the mixture was refluxed at 110°C for 16h in an inert N_2 atmosphere.

After the functionalized support was washed three times with ethanol (100mL) and dried in static air at 60 °C, the APS-SiO_2 was dispersed in miliQ H_2O (50 mL). For the deposition of 0.50 wt.% Au, an appropriate amount of $HAuCl_4$ solution was added dropwise under stirring (0.03M $HAuCl_4$, 5 mL) and continuously stirred for 1.5h at RT in the absence of light. Subsequently, 0.2M $NaBH_4$ (reducing agent) was quickly added under vigorous stirring (20 mL). After 20 minutes, the solid was retrieved by centrifugation and washed a minimum of 10 times by plenty of miliQ H_2O in between (100 mL) and dried in static air at 60 °C (24h).

1.0g of previously prepared Au/APS-SiO_2 was dispersed in 20 mL miliQ H_2O. Subsequently, the transition metal complex solution was added dropwise, corresponding to a 1:1 Au-M ratio. Stirring was continued for at least 48 hours until filtration of the supernatant through .45 µm filters did not show color. Thirdly, The precipitates were retrieved via vacuum filtration (glass filter, Büchner flask) and subsequently washed with plenty of miliQ H_2O (> 3 times, with 100 mL) with centrifugation in between. Afterward, the retrieved solid was dried in static air at 60°C. Several catalysts were reduced and calcined, while others were used as prepared.

4.2.2. Synthesis of mono- and bimetallic Au catalysts.

The Au/TiO_2 catalyst (0.10 wt.% Au) was prepared by deposition-precipitation with urea. Commercially available TiO_2 (45 m2/g, 8 g) was added to a 200 mL aqueous solution containing $HAuCl_4$ (0,021mM) and urea (0.42M). Subsequently, the reaction mixture was gradually heated to 80°C and stirred vigorously for 2h. The decomposition of the urea led increased the pH from ~3 to ~7.5. The solid catalyst was collected by centrifugation and washed ~5 times in between with an excess of miliQ H_2O (200 mL). 1.0g of previously prepared Au/TiO_2 was dispersed in 50 mL of miliQ water. Under stirring, a metal-precursor was added dropwise, corresponding to a 20:1 Au-M ratio. The pH was raised to ~9 by dropwise adding 0.5M NaOH solution (~20 drops) and stirred continuously for 2h in the absence of light. At last, the catalyst was retrieved by centrifugation and washed with an excess of miliQ H_2O in between (3 times, 100 mL) and dried overnight at 60°C in static air.

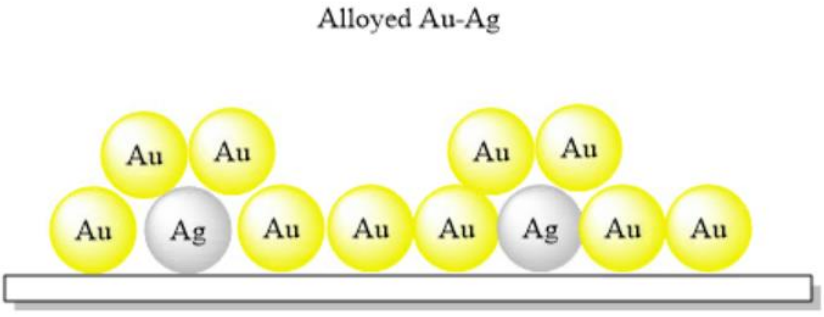

Figure 16: Representation of bimetallic nanoparticles supported on TiO_2.

4.2.3. Synthesis of gold-titanium(IV)-silica based catalysts.

The AuM/Ti-SiO_2 catalysts were prepared by deposition-precipitation with NaOH. By literature synthesized Ti-SiO_2 was dispersed in 100 mL miliQ H_2O. The gold precursor ($Auen_2Cl_3$) and metal precursor were added to the Ti-SiO_2 dispersion dropwise, in a molar ratio of 20:1 Au-M. Subsequently, by dropwise adding 0.5M NaOH the initial pH of ~3 was raised to ~9. The catalysts were recovered by centrifugation and washed with plenty of miliQ H_2O in between (3 times, 100 mL) and dried overnight in static air at 60°C.

4.3. Heat treatment of catalysts

After the synthesis of Au-M/APS-SiO_2 by strong electrostatic adsorption and ligand substitution, these synthesized catalysts are subjected to heat treatment to form supported nanoparticles and remove organic groups. Furthermore, the synthesized bimetallic catalysts supported on either TiO_2 or Ti-SiO_2 prepared by deposition-precipitation are also exposed to heat treatment. Table 4 provides a representation of all reduction and calcination steps applicable to each individual catalyst.

Table 4: Heat treatment applied to all synthesized catalysts. In general, reduction was performed under 20% H_2 in N_2 at 50 mL/min. Calcination was performed under 20% O_2 in N_2 at 50 mL/min.

Catalyst	Reduction Temperature (°C)	Reduction Length (min)	Calcination Temperature (°C)	Calcination Length (min)
Au-Fe/SiO_2	300	180	450	240
Au-Mn/SiO_2	300	180	450	240
Au-Re/SiO_2	300	180	450	240
Au-Mo/APS-SiO_2	X	X	X	X
Au-W/APS-SiO_2	X	X	X	X
Au-Ti/APS-SiO_2	X	X	X	X
Au-MTO/APS-SiO_2	X	X	X	X
Au/TiO_2	X	X	400	240
Au-Ag/TiO_2	X	X	400	240
Au-Cu/TiO_2	X	X	400	240
Au-Pd/TiO_2	X	X	400	240
*Au-Cu/Ti-SiO_2	300	180	400	240
*Au-Pd/Ti-SiO_2	300	180	400	240

**Reduction and calcination flows of 100 mL/min, 20% H_2 and 20% O_2, ramp 5°C/min.*

4.4. Characterization of catalysts.

TEM: Transmission electron microscopy (TEM) images were acquired using a FEI Technai T20 operating at 200 kV or a FEI Talos L120C operating at 120 kV. For particle size determination at least 100 separate particles were measured using ImageJ software to acquire a reasonable average particle size.

DR UV-Vis Spectroscopy: DR UV-Vis spectra were recorded by LAMBA 950S UV-vis spectrophotometer containing a 150 mm InGaAs integrating sphere. Absorption of the bifunctional, mono- and bimetallic catalysts were recorded in the 200-1000nm range, between 2 and 4nm resolution and a 1nm slit size. By the acquired UV-Vis spectra, the size and structure of the bifunctional catalysts (Au-M/SiO_2 or Au-M/APS-SiO_2) and bimetallic catalysts (AuM/TiO_2 or AuM/Ti-SiO_2) is analyzed.

XRD: X-ray diffraction (XRD) patterns were measured on a 2nd generation Bruker D2 phaser with a cobalt source (lambda = 0.179nm). 2 theta range: 20-80 for bifunctional catalysts and 20-90 for bimetallic catalysts with a matching timestep of 2.0s and step size of 0.04°.

ICP-AES: Inductively coupled plasma atomic emission spectroscopy, Gold loading of various catalysts were determined using ICP-AES at Utrecht University, Faculty of Geosciences.

TGA-MS: Thermogravimetric Analysis was applied to study the stability of supported AuNPs on titania, since coke formation is often observed. Furthermore, the removal of organic group during reduction and calcination of the Au-M/APS-SiO_2 can be confirmed. Firstly, the sample was dried at mild conditions (100 °C) under Ar. Subsequently, the spent catalyst was heated to 700 °C (ramp 5°C/min or 10°C/min) and afterward, the spent catalyst was cooled down to RT and heated once more to 700 °C (ramp 5°C/min).

4.5. Catalytic tests

The catalytic performance was connected to a Compact 4.0 gas chromatograph (GC). This particular gas chromatograph is connected to a thermal conductivity detector, equipped with a RT-Q-Bond (10m, 0.32mm in diameter) consists of a RT-Q-Bond (10m, 0.32mm in diameter). The reaction temperature was regulated by using a furnace and an internally controlled thermocouple. In a typical catalytic test, 300 mg of SiC (212-425 µm), 150 mg of catalyst (90-212 µm) were loaded into a plug flow reactor (quartz). The catalyst bed was kept in place by using quartz wool. Secondly, a pre-reduction (20% H2, 80% He) of the catalyst was performed to remove water and reduce formed metal oxide complexes (catalysts were stored in air). Detailed in-situ reduction conditions of all catalysts are given applicable to each catalyst when performance is provided. In general, the reaction conditions for propene oxidation were kept the same throughout all catalytic tests. The catalytic performance was tested at 200°C, a gas mixture of 10% vol O_2, H_2, C_3H_6 (2.5 mL/min each) and 70% He (17.5 mL/min) and thereby equaling a graded hour space velocity of 10000 mL/gcat/h. Any deviations are allocated in the result section.

5. Results and Discussion

This chapter presents the results obtained in propene epoxidation with H2/O2 mixtures of bifunctional, monometallic and bimetallic supported catalysts. Firstly, the prepared bifunctional catalysts were characterized by TEM, UV-Vis Spectroscopy, and XRD. Afterward, the catalytic performance of these bifunctional catalysts was investigated. Subsequently, the most active metal complex (titanium) was investigated further by synthesizing supported gold nanoparticles on titania, of which the stability and catalytic performance were described. Moreover, bimetallic nanoparticles on titania were synthesized and subjected to catalytic tests to investigate these bimetallic catalysts' catalytic performance compared with Au/TiO_2. The final part involves (bimetallic) gold-titanium(IV)-silica based catalysts that were characterized by XRD and TEM and subsequently subjected to catalytic tests. The catalytic performance was presented and discussed.

5.1. Bifunctional gold catalysts supported on a functionalized silica.

In order to study the possibility of replacing the active Ti-sites of supported Au/Ti-catalysts in propene epoxidation, catalysts were synthesized using a sequential adsorption principle. Firstly, Au was deposited on amine-functionalized silica by strong electrostatic adsorption, according to a literature procedure [36,89]. Secondly, a transition metal complex was adsorbed on the Au/APS- SiO_2 to provide the bifunctional Au-M/APS- SiO_2. The transition metal complexes were selected based on their ability to catalyse alkene epoxidation with peroxides, such as methyltrioxorhenium [115].

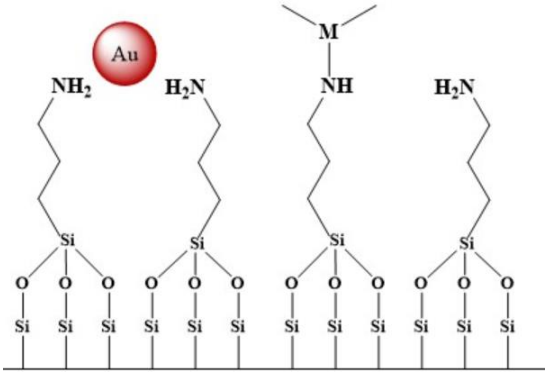

Figure 17: Representation of the bifunctional catalysts applied in the gas-propene epoxidation in this research before heat treatment..

5.1.1. Characterization of bifunctional catalysts.

The prepared bifunctional catalysts were characterized by TEM, ICP-AES, UV-Vis Spectroscopy, and XRD. Generally, supported gold nanoparticles on silica cannot directly be synthesized with usual preparation methods due to the low iso-electric point of the non-reducible silica. Typical preparation methods result in the formation of larger gold nanoparticles. Therefore, the subjected catalysts were subjected to XRD in order to determine the crystalline size and to verify if the amine-functionalization of silica was successful. Figure 18A represents the X-ray diffractograms (XRD) of gold nanoparticles supported on SiO_2 before and after calcination at 450 °C for 3 hours, providing us information about crystalline size and phases. The broad diffraction peak at approximately 25 degrees 2θ can be attributed to the amorphous silica support. Highly amorphous materials are recognized by broad diffraction peaks, considering that X-rays will be scattered in many directions. At higher angles, a low intensity but broad Bragg peak can be observed at an angle of 44.3. When the diffraction patterns of SiO_2 and Au/SiO_2 are compared, it is clear that the amorphous peak at 44.3 2θ can only be attributed to the gold nanoparticles, more specifically Au(200) planes [40]. The low intensity of the gold diffraction peak can be attributed

to two aspects, the degree of disorder and the relatively low weight percentage (0.5wt% theoretical). If the weight percentage is low, fewer phases are present and the contribution to the amount of scattering is less. Secondly, the acquired XRD-patterns of Au/APS-SiO_2 and Au/SiO_2 show a clear presence of the amorphous SiO_2 besides a minor broad peak at 44.3 degrees 2θ. The minor broad peak indicates that no large crystallites are formed on the external SiO_2 surface.

However, an estimation of the crystallite size is hardly possible. Since the peaks are broad and hardly visible, the distinction between background and scattering intensity from the crystallites is nearly impossible. The Debye-Sherrer equation cannot be applied to estimate the crystallite size and particle sizes are determined by TEM. Finally, the introduction of molybdenum to the Au/SiO_2, does not seem to change the characteristics of the silica and gold nanoparticles. Figure 18B represents the X-ray diffractograms of the bifunctional catalysts that contain the molybdenum complex. After calcination, we observe no crystalline MoO_3 phase that indicates a high dispersion of Mo(VI) on the catalyst surface. Furthermore, because we do not observe any large crystalline sizes and phases, we can conclude that the amine-functionalization of silica is successful.

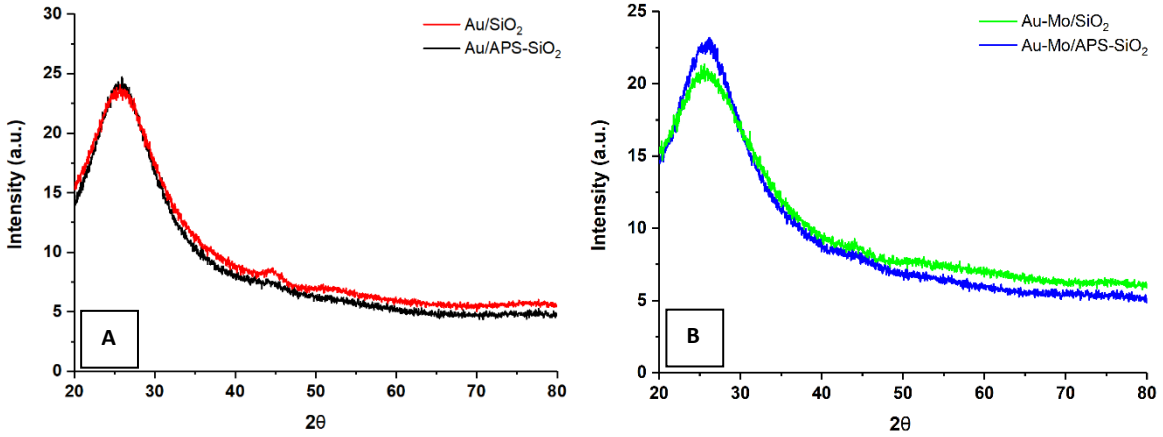

Figure 18:A) XRD diffractograms of Au/SiO_2, Au/APS-SiO_2, B)Au-Mo/SiO_2, Au-Mo/APS-SiO_2, pre/after heat treatment.

Noble metals, such as gold and silver, have specific optical properties known as localized surface plasmon resonance (LSPR). The LSPR is the collective oscillation of free conduction electrons induced by incident light. The size-dependent spectral shift for gold nanocrystals is related to the spatial confinement of the electrons. Smaller gold nanoparticles restrict the motion of conduction electrons and thereby, the LSPR is located at lower wavelengths. Nonetheless, the maximum absorbance at a specific wavelength provides only a rough estimation of the particle size since the SPR is affected by additional aspects such as shape and surface chemistry [39]. Besides, the average particle size affects the wavelength of maximum absorbance. Figure 19 shows the LSPR of different batches of Au/SiO_2. The UV-vis absorbance of the Au/APS-SiO_2 and Au/SiO_2 show a characteristic absorbance peak between 500-520 nm, which is caused by the localized surface plasmon resonance of gold nanoparticles. Furthermore, absorbance peaks at 400 nm can be allocated to the interband absorbance of gold nanoparticles [110]. Finally, the effect of heat treatment on the gold supported nanoparticles is investigated by analysing the LSPR. If Au/APS-SiO_2 (batch 1) is compared with Au/SiO_2 (batch 1), a red spectral shift to higher wavelengths (495 nm vs. 510nm) is observed. Since a red shift is observed, it is assumed that heat treatment plays a role i.e., causing particle growth, which is thoroughly investigated by TEM and emphasized later on.

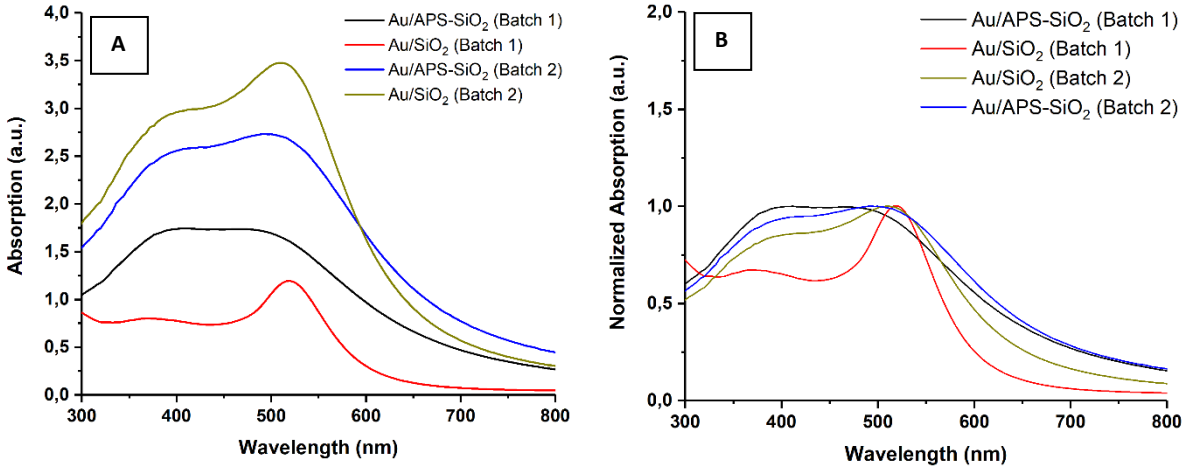

Figure 19: UV-Vis absorption spectra of monometallic (functionalized) supported gold catalysts, Au/SiO_2 and Au/APS-SiO_2, with Figure A) being absolute absorption intensity and B) Normalized absorption. All UV-vis absorption spectra are Kubelka-Munk corrected.

Secondly, UV visible spectroscopy is applied to investigate the adsorption of transition metal complexes. If ligand substitution is successful, additional bands appear relative to the Au/Silica UV-spectrum. The absorbance bands from transition metal complexes originate from ligand-metal charge transfer (LMCT). LMCT involves the transfer of electrons from the highest MO orbital with a ligand character to the metal-like MO and is observed in the electromagnetic spectrum. The absorption wavelength depends on several factors such as the size of the crystal field splitting, nature and geometry of the ligands, and the metal's oxidation state. Both Au-W/APS-SiO_2 and Au-Mo/APS-SiO_2 show unique appearing peaks in Figure 20, not present in the UV-Vis absorption spectra of monometallic supported Au/ SiO_2 or Au/APS-SiO_2. The absorbance bands originating from the Au-Mo/APS-SiO_2 correspond with earlier observed Mo(VI) complexes such as ammonium molybdate [116]. The presence of these peaks verifies that ligand substitution and the transition metal complex is successfully adsorbed on the functionalized silica support.

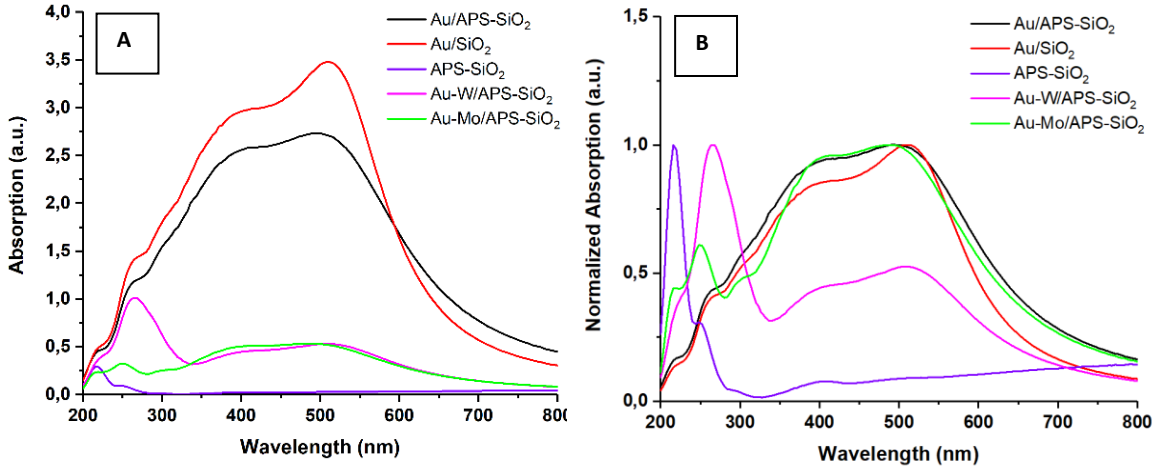

*Figure 20: UV-Vis absorption spectra of monometallic and bifunctional catalysts. Figure A: being absolute absorption intensity and B: Normalized absorption. *Bifunctional catalysts are not heat treated, ligands are attached to transition-metal complex.*

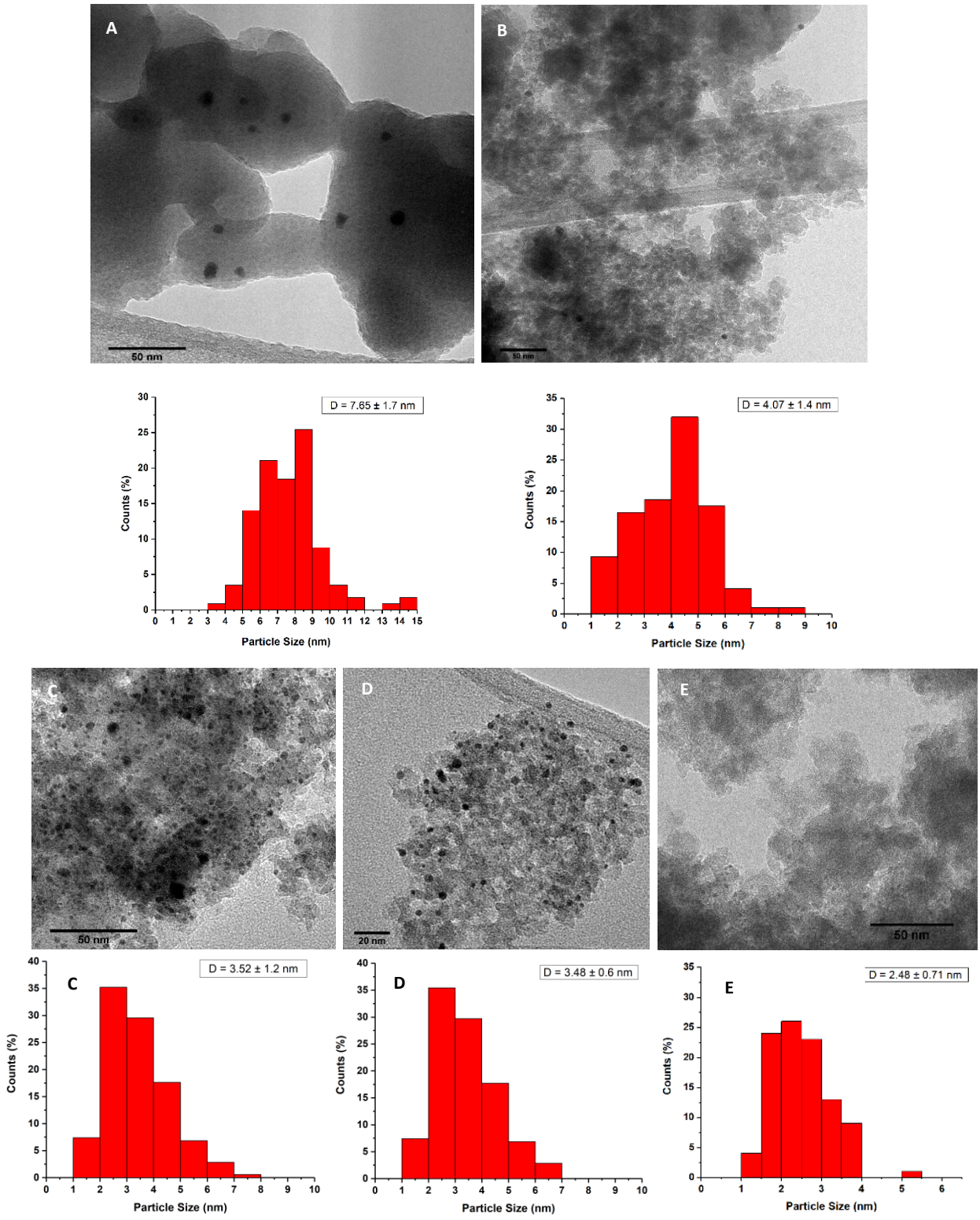

Figure 21: Transmission Electron Microscopy Images of monometallic/bifunctional supported catalysts with; A) Au(1)-Mn/Silica, B) Au(2)-Mo/Silica, C) Au(3)/APS-Silica, D) Au(3)/Silica, E) Au(4)/APS-SiO_2. The numbers indicate which batch of Au-APS/SiO_2 is utilized.

Table 5: Characterization overview of several monometallic/bifunctional catalyzed, prepared from different Au/APS-SiO_2 batches. Particle size and distribution have been determined by analysis of TEM images, drying methods and heat treatment have been applied.

Catalyst	TEM Au NPs (size)	Drying method	Reduction/Calcination	Au/APS-SiO_2 Batch
Au-Mn/SiO_2	7.65 ± 1.7 nm	60 °C	300 °C/3h + 450 °C/4h	No. 1
Au-Mo/SiO_2	4.07 ± 1.4 nm	60 °C	300 °C/3h + 450 °C/4h	No. 2
Au/APS-SiO_2	3.52 ± 1.2 nm	60 °C	None	No. 3
Au/SiO_2	3.48 ± 0.60 nm	60 °C	300 °C/3h + 450 °C/4h	No. 3
Au/APS-SiO_2	2.48 ± 0.71 nm	60 °C	None	No. 4

Figures 21AB show TEM images of the bifunctional catalysts, Au-Mn/Silica and Au-Mo/Silica, respectively. The theoretical weight loadings of gold are 0.5wt%. Rather large gold nanoparticles with diameters of 7.7 and 4.1 nm are formed on the support after the heat treatment and are likely to have a hemispherical shape. The difference between particle size originates from different Au/APS SiO_2. Based on literature, the gold particles were expected to have a diameter of approximately 2-4 nm [36,89]. Based on earlier characterization by UV-Vis Spectroscopy, it is assumed that particle growth is induced upon heat treatment. Insufficient washing leads to limited removal of chloride ions. It is known that chloride ions induce sintering of supported (gold) nanoparticles upon heat treatment. Therefore, it is likely that the first batch of Au/SiO_2 is not washed sufficiently to ensure the removal of chloride ions [38].

Since the phenomenon of gold nanoparticle growth on (inert) supports is often observed, several studies are carried out with in-situ TEM to investigate the mechanism of particle growth. This particle sintering takes place by a form of Ostwald ripening [38]. Ostwald ripening describes the change i.e., growth of particle structure in both gas/liquid phases and deposited on SiO_2 over time. It is thermodynamically driven, because larger particles are energetically more stable and have relatively fewer surface atoms. Surface atoms are more reactive and thereby less stable. The mechanism of Ostwald ripening is that atoms are transferred from one particle to another, resulting in a smaller particle and a larger one, which increases the particle size distribution. The chloride ions play a pivotal role in Ostwald ripening. Chloride ions can form a complex with gold particles, which results in the stabilization of the ionic gold species. The increased stabilization makes the movement of the gold particles over the support possible, facilitating the monomer transfer from smaller gold particles into a larger one. The size of supported gold nanoparticles is pivotal in the propene epoxidation reaction. In general, larger gold nanoparticles have a smaller specific surface area and less accessible active sites, undesirable for catalysts as all reactions occur at active sites. Secondly, in propene epoxidation, larger gold nanoparticles increase the gold-metal interface that inhibits any spillover of the hydroperoxy species and prevents propene epoxidation [1,19].

Therefore, particle growth is further investigated by synthesizing another batch of extensively washed Au/APS-SiO_2. Figure 21C confirms that very small and dispersed gold nanoparticles (3.52 ± 1.2 nm) are formed via electrostatic adsorption of tetra chloroauric acid trihydrate on APTES-functionalized silica, followed by reduction with NaBH4. Furthermore, there is no significant increase in the particle size (3.48 ± 0.6 nm) upon heat treatment, which is confirmed by TEM-images acquired of Au/SiO_2 (batch 2) and shown in Figure 21D.

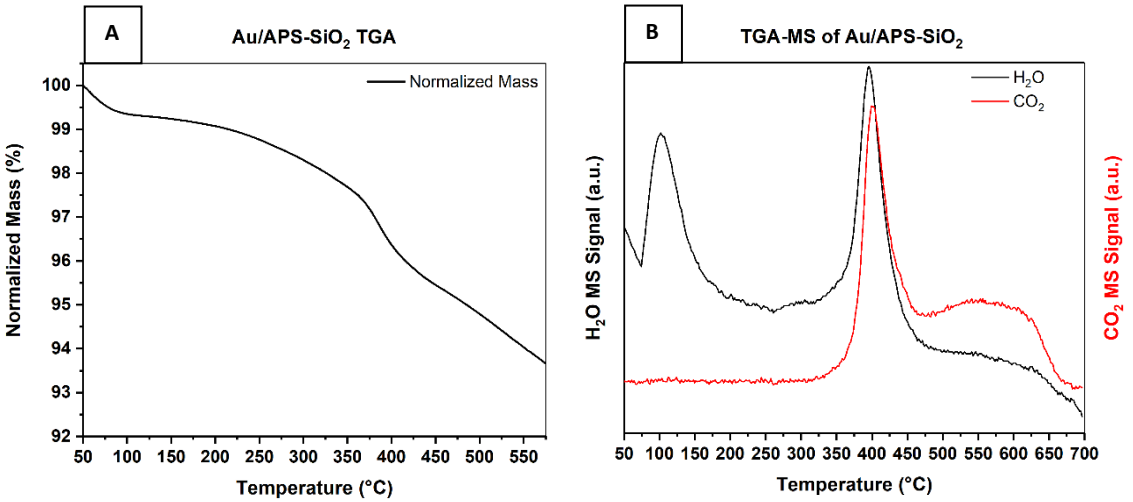

Figure 22: A) TGA measurement of Au/APS-SiO_2 complemented with B) TGA-MS spectra.

After studying the effects of heat treatment on the gold nanoparticles' size, we investigated the removal of organic groups and formation of supported nanoparticles was successful by a TGA measurement. The TGA measurement is shown in Figure 22. The TGA shows a loss in mass of 6.5% over time when gradually increasing the temperature with 10 °C/min. The MS-Spectra of the TGA confirmed the removal of organic groups between 375-450 °C since we observed a peak in the CO_2 and H_2O signal. We attributed these peaks to the complete combustion of the APTES-groups and the removal of these functional groups was successful.

5.1.2. Hydrogen conversion

To study the catalytic performance of the bifunctional catalysts, these bifunctional catalysts were subjected to catalytic tests. The catalytic activity and selectivity were studied in a plug-flow reactor at 200 °C with a gaseous reaction mixture of 10% H_2, O_2, and C_3H_6 in 70% He (30 mL/min, GHSV = 10000h^{-1}). Bifunctional catalysts were composed of two parts, the supported gold nanoparticles responsible for forming hydroperoxy species and metal complexes for the propene epoxidation. Therefore, the performance of the gold nanoparticles was analyzed first and subsequently the propene epoxidation by transition metals.

The importance of the gold nanoparticle size is addressed upon in previous sections. First of all, larger supported gold nanoparticles have a smaller relative surface area compared to smaller gold nanoparticles. Secondly, in the direct propene epoxidation with H_2/O_2 mixtures, larger supported gold nanoparticles are highly undesired because they increase the gold-metal interface and possibly inhibit the hydroperoxy species' spillover to the active metal-sites [1,19]. In Figure 23 the hydrogen conversion of different bifunctional catalysts is shown accompanied by the table that shows the characteristics of the bifunctional catalysts. Despite the average size of the gold nanoparticles (7.65 ± 1.7 nm), a significant amount of hydrogen (30%) is converted.

On the contrary, most H_2 and O_2 molecules are converted into H_2O. The formation of water is explained by a kinetic study [25]. Water is formed by two different mechanisms related to either isolated gold nanoparticles or the possibility of hydroperoxy species decomposition. The bifunctional catalysts have a theoretical 0.5wt% Au and XRD measurements confirm that a high dispersion of both the gold nanoparticles and metals is achieved. Furthermore, the calcined bifunctional catalysts (Au-Fe, Au-Mn, and Au-Re) have an atomic ratio of 1:1 between gold and the metals. Therefore, we likely deal with (some) isolated gold nanoparticles. Isolated, supported gold nanoparticles are capable of producing a large quantity of water [25]. Secondly, a large gold-metal interface results in the decomposition of the in-situ formed hydroperoxy species and water is formed as a reaction intermediate [25].

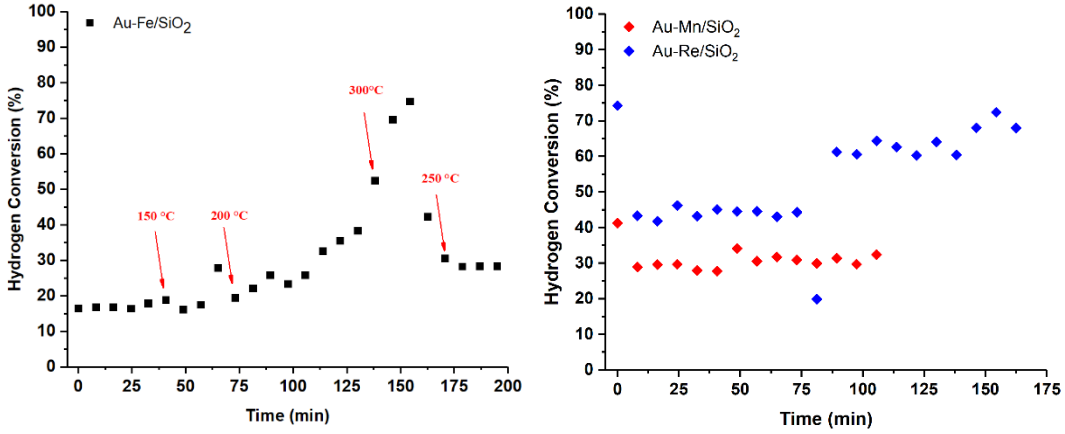

Figure 23: Hydrogen conversion over supported Au particles, In-situ reduced at 250 °C for 90 min under He/H_2 (24:6mL/min), reduced; (300 °C, 20% H_2, 3h), calcined (450 °C, 20% O_2, 4.5h). Reaction conditions: 70% He, 10% H_2, 10% O_2, 10% C_3H_6 (17.5;2.5;2.5;2.5mL); Reaction Temperature: 200 °C, unless stated otherwise, GHSV = 10000h^{-1}.

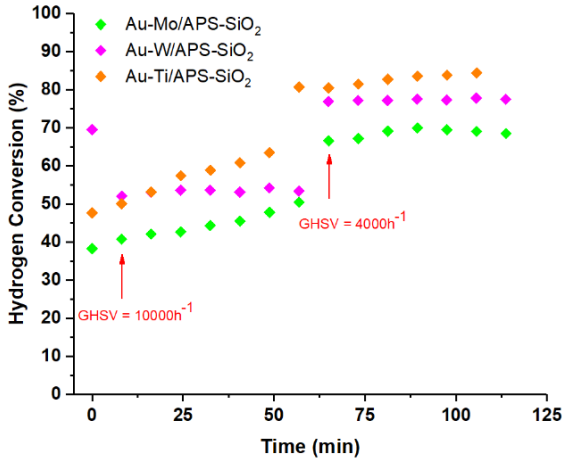

Figure 24: *H_2/O_2 conversion over supported Au particles, Reaction conditions: 70% He, 10% H_2, 10% O_2, 10% C_3H_6; Reaction Temperature: 200 °C, unless stated otherwise. In-situ reduction of 1.5h at 250 °C under He/H_2 (24:6mL/min).*

Table 6: Overview of Theoretical wt%, particle size distribution and heat treatment of supported bifunctional catalysts.

Catalyst	ICP wt% Au	AU NPs	Reduction/Calcination
Au-Mn/SiO_2	0.42	7.65 ± 1.7 nm	300 °C/3h + 450 °C/4h
Au-Re/SiO_2	0.42	7.65 ± 1.7 nm	300 °C/3h + 450 °C/4h
Au-Mo/APS-SiO_2	0.43	4.07 ± 1.4 nm	None
Au-W/APS-SiO_2	0.43	4.07 ± 1.4 nm	None
Au-Ti/APS-SiO_2	0.44	3.52 ± 1.2 nm	None

Figure 24 shows the hydrogen conversions of uncalcined bifunctional catalysts, which have a smaller gold nanoparticle size. The Au-Mo and Au-W have gold nanoparticles with a size of 4.07 ± 1.4 nm and exhibit higher activity for hydrogen conversion than the calcined catalysts and reach hydrogen conversions up to 90-95%. These conversions show the importance of gold nanoparticles' size and relative surface area. Since smaller nanoparticles have a larger fraction of surface atoms than larger sized particles, they are expected to show higher activity since surface atoms are more reactive because of the degree of bonding and extent of orbital sharing. However, there is a second reason why smaller gold nanoparticles show higher activity besides the relatively more surface atoms. In general, the smaller the gold nanoparticles are, the lower their coordination number. Coordination number is defined as the number of ligands or atoms bonded to a central atom. A lower coordination number results in lower adsorption energy because the strain effect by surrounding ligands is limited. Lower adsorption energies result in stronger bonding of the reactants to the catalysts and allow the oxidation reaction to happen more efficiently [53].

Additionally, the catalytic activity depends on the reaction conditions. In general, it is known that the gas hourly space velocity, temperature, and weight loadings affect the conversion of the reactants besides particle size. In Figure 24, an increasing hydrogen conversion is observed over time for every catalyst. One explanation is that a change in the gas hour space velocity can affect the reactant conversion. For example, the hydrogen conversion of the uncalcined bifunctional catalysts is increased by changing the GHSV from 10000 h^{-1} to 4000 h^{-1} at approximately 60 minutes. A lower grade hour space velocity can lead to a more contact time between the reactant and the catalyst, which results in a higher percentual conversion of the hydrogen conversion.

5.1.3. Bifunctional Au-M/APS-SiO_2 catalysts in propene epoxidation.

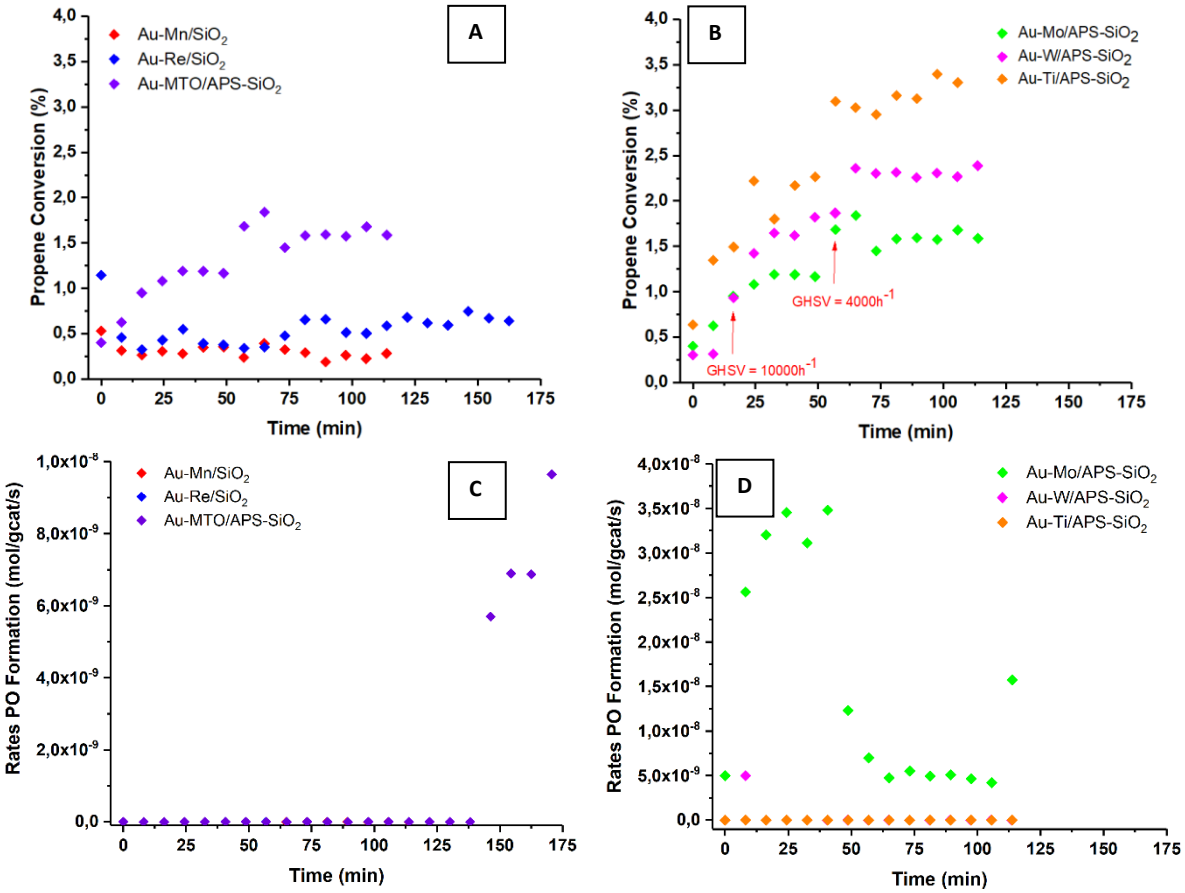

Figure 25: C_3H_6 conversion and rates of PO formation over supported bifunctional catalysts, In-situ reduced at 250 °C for 90 min under He/H_2 (24:6mL/min). Reaction conditions: 70% He, 10% H_2, 10% O_2, 10% C_3H_6 (17.5;2.5;2.5;2.5); Reaction Temperature: 200 °C, unless stated otherwise, GHSV = 10000h^{-1}.

Table 7: Overview of the characteristics of the bifunctional catalysts and propene oxide selectivity, the average size of the gold nanoparticles determined by TEM, theoretical wt% assuming complete adsorption.

Catalyst	ICP wt% Au	AU NPs Size.	Reduction/Calcination Conditions	Theoretical Metal wt%	Propene Oxide %	Metal Precursor
Au-Mn/SiO_2	0.42	7.65 ± 1.7 nm	300 °C/3h + 450 °C/4h	3.33	0	$FeCl_3{}^*6H_2O$
Au-Re/SiO_2	0.42	7.65 ± 1.7 nm	300 °C/3h + 450 °C/4h	1.72	0	$Mn(NO_3)_{2*}4H_2O$
Au-Mo/APS-SiO_2	0.43	4.07 ± 1.4 nm	None	5.00	14.37	$(NH_4)_6Mo_7O_{24}$
Au-W/APS-SiO_2	0.43	4.07 ± 1.4 nm	None	10.0	0.88	$H_{26}N_6O_6O_{40}W_{12}$
Au-Ti/APS-SiO_2	0.44	3.52 ± 1.2 nm	None	5.00	0	$Ti(OBU)_4$
Au-MTO/APS-SiO_2	0.48	2.48 ± 0.72 nm	None	1.00	15.38	CH_3ReO_3

Figure 25A presents the results of the bifunctional catalysts regarding catalytic activity. First of all, propene conversion depends on the amount of active metal sites accessible and the type of metal. Higher weight loadings resemble a higher amount of active sites. This partially explains the differences in propene conversions of uncalcined and calcined catalysts.

Furthermore, a lower GHSV allows more contact time between the reactant and the metal surface. Figure 25B represents the catalytic activity of uncalcined bifunctional Au-M/APS-SiO_2 catalysts and a lower GHSV clearly leads to a higher propene conversion. Smaller gold particles have a smaller interface and are more likely to spill over the formed hydroperoxy intermediate and are less susceptible to water formation, which competitively adsorbs with propene [1,19,26]. However, an accurate evaluation of the catalytic activity is not possible since we deal with different elements (Fe, Re, Mn, Mo, W) and different weight loadings, represented in table 7.

Table 7 also provides an overview of the propene oxide selectivity of all bifunctional catalysts. Firstly, it is clear that iron and manganese are not active for the epoxidation of propene. These late transition metals usually epoxidize alkenes via a redox mechanism, in which is the metal is first of all reduced. The easily accessible lower oxidation states lead to the metal-catalyzed decomposition of the hydroperoxy species [96]. Therefore, propene epoxidation most likely occurs via a Lewis-acid mechanism.

Early transition metals such as vanadium, molybdenum, titanium and rhenium do not show high activity and selectivity towards propene oxide. Because of the initial suspicion of particle growth upon heat treatment, heat treatment was not applied in the preparation for several bifunctional (early TM) catalysts. This results in metal-ligand complexes and ligand effects in oxidation reactions are widely studied [10]. Ligand complexation is a factor that partially explains the lack of propene oxide production. Early transition metals operate via the Lewis acid mechanism to form propene oxide. In general, early transition metals such as vanadium(V), molybdenum(VI) and titanium(IV) have low redox potential, which allows ligand substitution i.e., insertion of the hydrogen peroxide. To carry out the oxidation reaction, the in-situ formed hydrogen peroxide needs easily accessible coordination sites. If ligands still surround the metal, it makes the coordination sites more difficult to access and the insertion of hydrogen peroxide is not possible. The surrounding ligands alter the electronic and steric environment, thereby affecting the coordination of hydrogen peroxide and oxygen insertion into propene [10**].** Epoxidation reactions are accelerated by the introduction of donor ligands [41]. For example, the Au-Ti(OR_4)/SiO_2 catalyst contains butoxide ligands surrounding the titanium(IV) center. Despite the presence of donor ligands, the Au-Ti(OR_4)/SiO_2 catalyst shows no selectivity towards propene oxide. Moreover, Ti- and Au/Ti-supported catalysts have been proven to be active in epoxidation reactions [1,19,63]. Therefore, it is very likely that ligand complexation is not the only factor preventing the successful epoxidation of propene to propene oxide.

A second reason that can explain the lack of activity and selectivity is none or limited intimacy between the gold nanoparticles and metal-complexes on the silica surface. In this situation, the overall reaction relies on the gold nanoparticles and the metals' acidic sites. As stated before, the gold nanoparticles are responsible for forming the hydroperoxy species and the acidic metal sites for the epoxidation of propene to propene oxide. The activity of bifunctional catalysts depends on the ratio of gold/metal sites and the distance between them [42]**.** If the distance between is between the elements is too large, it influences both the activity and selectivity of the reaction, explained by the intimacy criterion by Weisz [28]. For instance, if two gold nanoparticles are in close proximity, the oxidation reaction can only occur on the active sites of gold. The produced hydrogen peroxide spills over to nearby active gold nanoparticles instead of acidic metal sites.

Table 8: Overview of the side-product formation over both calcined and uncalcined bifunctional catalysts. Sel. % are resembling average over all measured data points.

Catalyst	Operating Temperature (°C)	CO2 (sel. %)	CO (sel. %)	Acetal-dehyde (sel. %)	Acrolein (sel. %)	Acetone (sel. %)	Propanal (sel. %)
Au-Fe/SiO2	150-300	2.30	8.20	39.64	12.96	5.57	2.14
Au-Mn/SiO2	200	x	x	17.76	71.18	11.06	x
Au-Re/SiO2	200	x	x	21.25	46.71	6.62	25.42
Au-Mo/APS-SiO2	200	x	18.56	33.93	10.24	0.78	22.13
Au-W/APS-SiO2	200	x	19.00	18.50	6.03	1.06	54.58
Au-Ti/APS-SiO2	200	16.89	5.64	39.72	0.98	5.63	31.13
Au-MTO/APS-SiO2	200	x	x	79.52	1.09	2.64	79.52

Since there is a lack of selectivity from propene towards propene oxide, a low of unwanted products are formed. One of the main "by-products" that is consistently formed by every catalyst is acetaldehyde. Stangland et al. talks about the oxidative cracking of propene [43]. Catalysts used in propene epoxidation are more sensitive to oxidative cracking at higher temperatures independent of any other reaction conditions. The production of acetaldehyde can not simply be prevented by increasing the number of actives sites. Stangland et. al state that low-temperature regions <100 °C are desired for optimal propene oxide selectivity, which is outside the scope of this study.

Secondly, acrolein is a frequent product present in the gas stream formed by a redox mechanism. The redox mechanism has been described in chapter 2.3. The redox mechanism is primarily a mechanism applied by metals that are easily oxidized and reduced, for instance molybdenum and vanadium. Furthermore, acrolein is formed by coordination of propene to the easily oxidized metal, and an oxygen atom from the lattice is attached at the allylic position. In addition, gold nanoparticles have the ability to produce little acrolein themselves**.** Gold nanoparticles can activate molecular oxygen, which is one of the gasses in the gas stream. Negatively charged gold surface sites activate oxygen. The antibonding orbitals of oxygen overlap with the d-orbitals of the surface atoms of the nanoparticles. This creates an electron density that is transferred from the nanoparticles to the antibonding orbital of oxygen [23].

Thirdly, a by-product that is produced besides acrolein and acetaldehyde is propionaldehyde. Once propene oxide is produced as an intermediate, it can react a second time to form acetone and propionaldehyde. Early transition metals are Lewis acids, and the (strong) Lewis acid sites in the catalysts are responsible for converting propene oxide to propionaldehyde [43]. The acidic OH-groups facilitate isomerization of propene oxide to products as propionaldehyde and acetone.

The formation of CO_2 and CO is caused by the complete combustion of molecular oxygen with propene or oxidative cracking at higher temperatures[1,43]. It is frequently observed by well-respected researchers within gold catalysts that hydrogenation can occur in the presence of very small gold nanoparticles since Au nanoparticles <2nm are capable of hydrogenation. However, during the catalytic tests, the production of propane is never noticed.

5.1.4. Intermediate Conclusions.

A series of bifunctional catalysts was synthesized. First, SiO_2 was functionalized by 3-amino(triethoxy)silane, followed by a gold-precursor deposition by strong electrostatic adsorption. Subjecting these catalysts to BF-TEM confirmed that sufficiently small gold nanoparticles with a size between 1-8 nm were synthesized. Furthermore, the introduction of transition-metal complexes by ligand substitution was proven to be successful by the application of UV-Vis Spectroscopy. Transition metals complexes such as Ti(IV), Mo(VI), W(VI) and Re(VII) were used. It was found that the uncalcined bifunctional catalysts containing 0.5wt% Au and a theoretical 5.0wt% Ti achieved the highest propene conversion and thereby highest activity. Despite the high activity of these gold-based bifunctional catalysts, the selectivity to propene oxide in the gas-phase oxidation of propene was neglectable. It was concluded that the ligand complexation and the lack of intimacy between supported AuNPs and the active accessible sites were the primary explanations for low selectivity.

5.2. Gold-titania based catalysts.

As was observed previously, gold-titanium based catalysts were the most active bifunctional catalysts (Au-Ti/APS-SiO_2) i.e., achieved the highest propene conversion. The selectivity towards propene oxide of these gold-titanium based catalysts was unsatisfactory. The reaction products observed are likely due to the rearrangement of propene oxide over the Ti-modified support. Gold-titanium(IV) catalysts are frequently studied in literature, and therefore the decision was made to shift the focus to Ti-containing supports TiO_2 and Ti-SiO_2 to study the effect of mono- and bimetallic gold nanoparticles in propene epoxidation with H_2/O_2 mixtures.

In this chapter, the results obtained of monometallic and bimetallic titania supported catalysts are displayed. Firstly, the mono- and bimetallic catalysts are characterized by XRD, UV-Vis spectroscopy, ICP-AES, and TEM. Secondly, the monometallic catalysts are subjected to catalytic tests. Subsequently, it is tried to synthesize bimetallic nanoparticles supported on titania by sequential deposition-precipitation using Au/TiO_2 as starting catalysts (0.1wt% Au). With bimetallic nanoparticles, we aim to decrease hydrogen conversion and increase efficiency with respect to monometallic Au/TiO_2. All bimetallic nanoparticles of AuAg, AuPd and AuCu that are synthesized and characterized have a theoretical atomic ratio of 20:1, with gold being the predominant element in all bimetallic catalysts synthesized.

5.2.1. Characterization of mono- and bimetallic Catalysts.

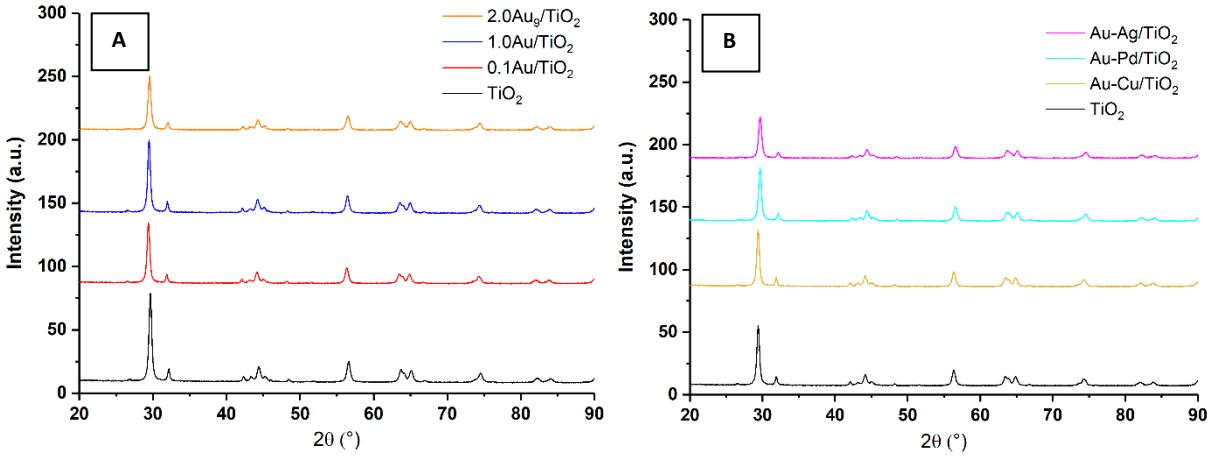

Figure 26: XRD Diffractograms of supported Au on Titania with: A) different weight loadings of gold (0.1wt%, 1.0wt% and 2.0wt%), compared by the XRD patterns of the support; B) Supported bimetallic nanoparticles on titania.

Figure 26AB shows the XRD diffractograms of supported gold nanoparticles on titania. As can be observed from the XRD patterns, no characteristics diffraction peaks occur when gold nanoparticles are deposited on the support. Since there are no additional diffraction peaks, we can assume that the gold nanoparticles' crystalline size is sufficiently small. Low weight loading contributes to the absence of peaks, mostly 0.1% wt Au. The same explanations apply to the synthesized bimetallic nanoparticles, with weight loadings <0.01%. No additional peaks appear when a second metal is introduced to the supported gold nanoparticles. These low weight loadings of both Au and the second metal are necessary since high Au loadings (>1wt% on TiO_2) give rise to unfavorable combustion of hydrogen and results in larger supported AuNPs [68]. On the other hand, too low weight loadings of Au on TiO_2 result in the formation of very small gold nanoparticles and enhance the hydrogenation reaction [63]. Furthermore, the second metals we want to use are well-performing hydrogenation catalysts under the selected reaction conditions of propene epoxidation (200°C). To prevent unwanted hydrogenation of propene to propane, we focus on catalysts with low weight loadings of the second metal i.e. an atomic ratio of 20:1 with gold being the predominant element.

With DR UV-Vis, we were able to verify that the deposition-precipitation method is successfully applied to synthesize Au/TiO_2, since we observe absorption bands at 520nm. Furthermore, the intensity of gold absorption is proportional to the weight loading of each catalyst and thereby the adsorption of higher gold loaded catalysts is the most intense. On the contrary, the $Au9/TiO_2$ catalyst (gold cluster) does not show a characteristic absorption band at 520 nm. Gold clusters have an average particle size of <1 nm and localized surface plasmon resonance is no longer present in UV-Vis spectra. The disappearance of the characteristic LSPR peak can be attributed to the fact that the LSPR of gold lies within the area of interband transitions and diminish the LSPR for gold nanoparticles with a size <2 nm. Moreover, gold clusters have electronic levels similar to bulk gold that do not show any characteristic adsorption band. To conclude, the preparation of supported gold clusters by impregnation is successful and simultaneously we can assume complete adsorption of gold on TiO_2, a characteristic of the impregnation preparation method. The intense absorption peak at 320 nm can be attributed to TiO_2 and its semiconductor properties [101].

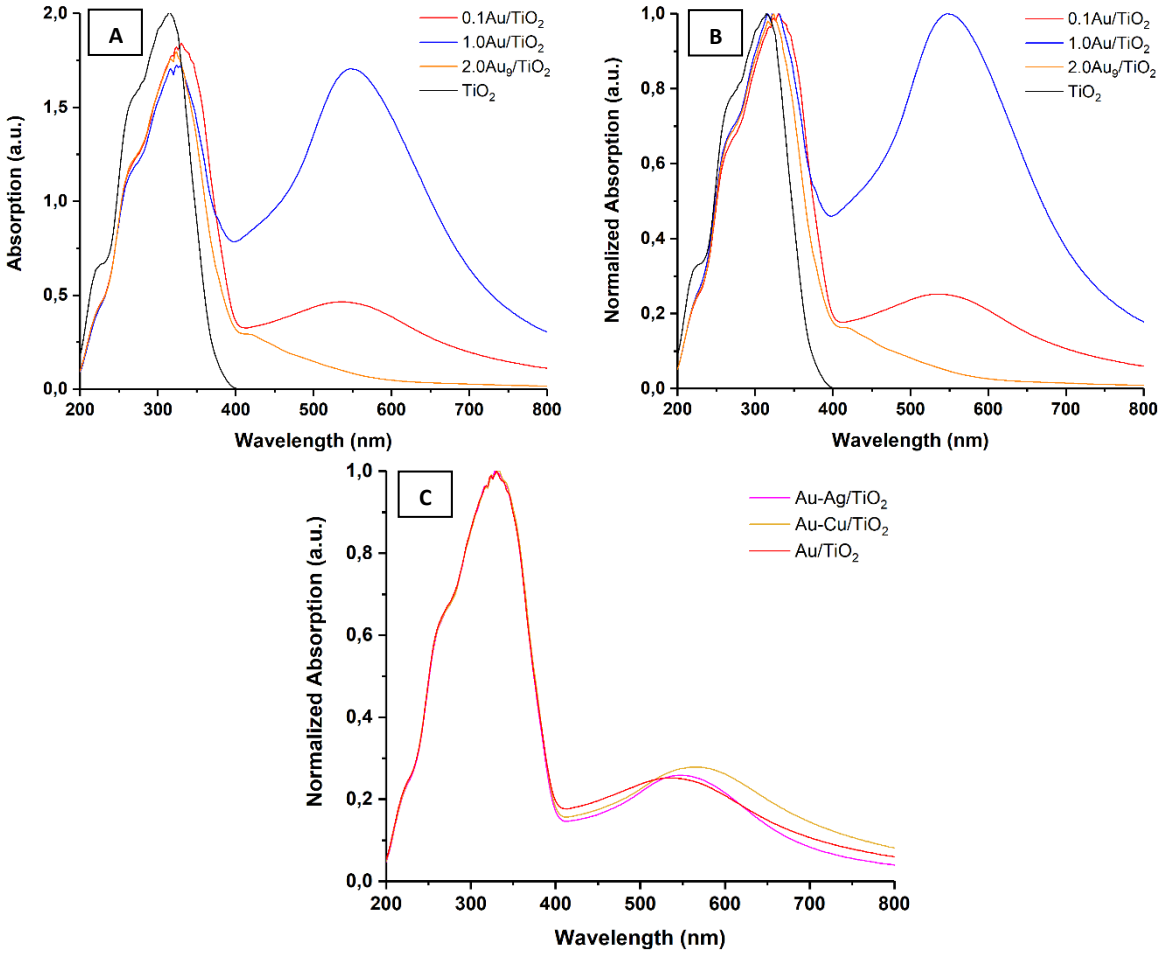

Figure 27: UV-Vis absorption spectra, Kubelka-Munk corrected. A) Absolute adsorption values of gold nanoparticles supported on TiO_2 with various wt%;. B) Normalized absorption values. C) Bimetallic catalysts with a theoretical 20:1 atomic ratio with gold being predominant.

Secondly, UV-Vis spectroscopy provides us with information about the atomic distribution of the supported bimetallic nanoparticles. We expect the formation of bimetallic nanoparticles since it is often reported that gold-silver alloy catalysts are created by deposition-precipitation with either NaOH or urea [80,81]. Figure 27 shows the absorption values of supported gold nanoparticles in comparison with the supported bimetallic catalysts. For example, besides gold, silver, and copper are well known to exhibit localized surface plasmon resonance. Monometallic Ag/TiO_2 or Cu/TiO_2 exhibit LSPR at approximately 410 nm and 560-600 nm. Besides the characteristic peak of gold LSPR, we do not observe any additional distinctive absorption peak clearly originating from Ag LSPR or Cu LSPR. This can be attributed to the very low weight loadings of Ag and Cu (<0.01 wt%) regarding the bimetallic catalysts, which are needed to prevent any propene hydrogenation.

On the other side, it does also apply to the atomic distribution of the bimetallic catalysts. It is often reported that gold-silver alloy catalysts can be created by the deposition-precipitation method with either NaOH or urea [80,81]. If any alloys are formed, we expect a blue shift from the maximum absorbance wavelength for gold-silver catalysts. For the gold-silver catalyst, either no blue and a red shift is observed. Furthermore, surface silver is likely oxidized because of drying, calcination, and storing under air. Oxidized surface silver causes a redshift, which might compensate for the blue shift of alloy gold-silver catalysts [82]. The gold-copper catalysts show a clear red shift of approximately 20nm. Since the Cu LSPR is generally relatively weak, especially for very low weight percentages (<0.01%), linear dependent and found at 560-600nm, the LSPR should not cause a red shift this distinctive. Moreover, The XRD-diffractograms did not show any characteristic peaks for Cu/CuO and thereby, we do not assume the formation of large copper nanoparticles.

The BF-TEM images of both catalysts show small (<5nm) likely hemispherical gold nanoparticles highly dispersed across the support and we can thereby conclude that the deposition-precipitation was successful. Furthermore, most gold nanoparticles are uniform in shape. The gold nanoparticle size of different catalysts was determined by individually counting at least 50 nanoparticles, which was sometimes complicated due to the low weight loadings. The $0.1Au/TiO_2$ catalyst contains supported nanoparticles of approximately 2.5 nm. However, the $1.0Au/TiO_2$ catalyst has a particle size of approximately 3.5 nm with a larger particle size distribution. The variation in particle size between these catalysts is attributed to the preparation method. The reaction time is an essential factor with respect to the particle size of the AuNPs. Zanella R. suggests that progressively increasing the pH over a longer time results in changes in the surface charge density [77]. Finally, BF-TEM is used to investigate the sequential deposition-precipitation method and the influence of introducing a second-metal on the particle size distribution of supported gold nanoparticles. Figure 28C represents the particle size distribution of $Au\text{-}Pd/TiO_2$ and we thereby conclude that the effect on the particle size with the introduction of a second metal is neglectable.

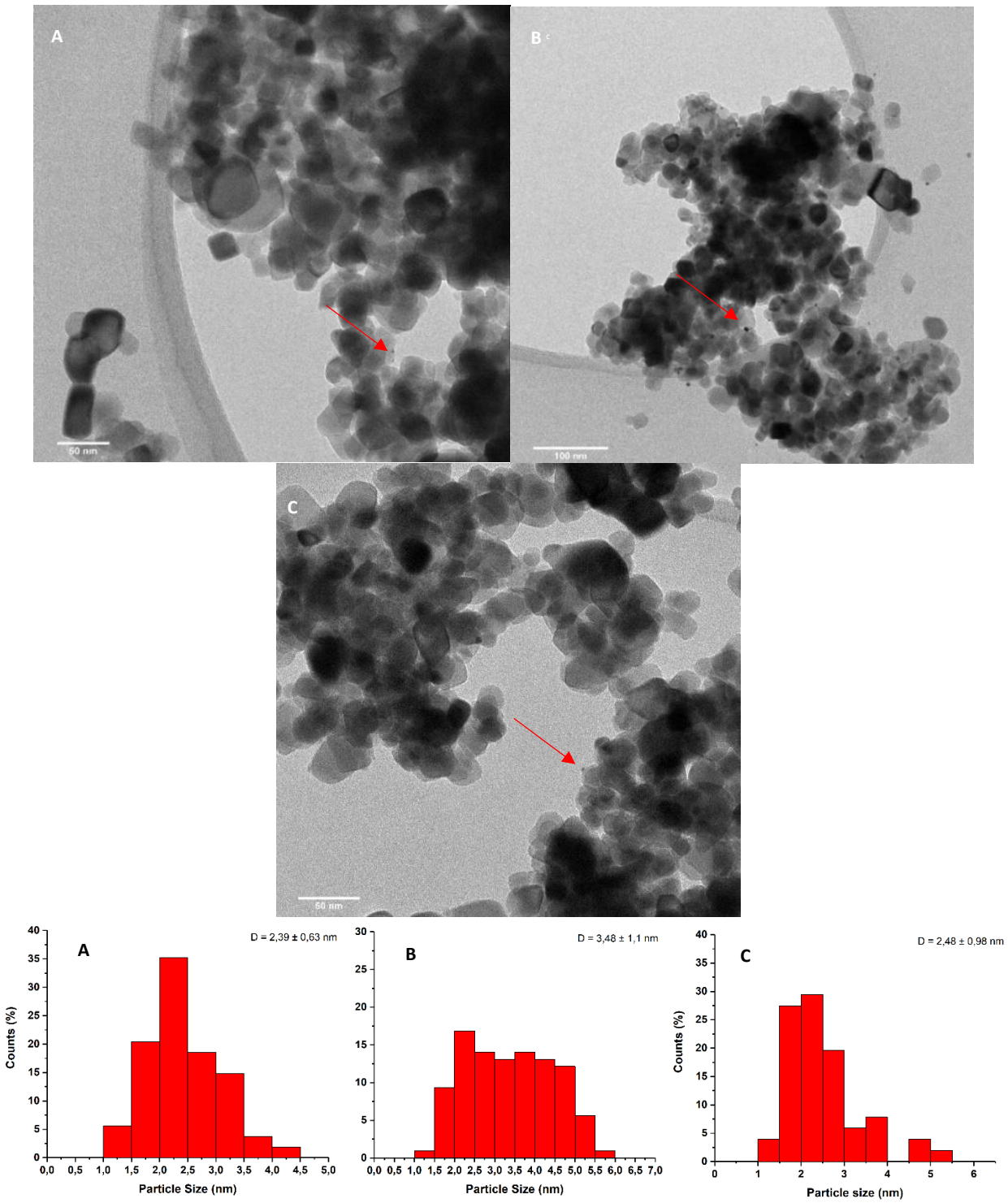

Figure 28: BF-TEM images of supported gold nanoparticles on titania; Figure A) 0.1wt% Au; B) 1.0wt% Au; C) Au-Pd/TiO_2 with corresponding histograms of particle size distribution.

5.2.2. Catalytic tests of monometallic catalysts.

Firstly, the catalytic performance and stability of monometallic catalysts with different weight loadings of Au are evaluated by subjecting these catalysts to catalytic tests regarding propene oxidation to propene oxide. Figure 29 provides an overview of reactant conversion and performance of the catalysts. Since the formation of a hydroperoxyl-intermediate is both the pivotal and rate-determining step, the hydrogen and oxygen conversions are displayed in combination with propene conversion and selectivity towards propene oxide. The conversion of hydrogen and oxygen, which the gold nanoparticles are responsible for, is similar for all catalysts despite the difference in weight loadings. The 0.1Au/TiO_2 catalyst has smaller supported AuNPs than the 1.0Au/TiO_2 catalysts (2.5nm vs. 3.5nm). Smaller gold nanoparticles are preferable in the propene oxidation reaction, since the rate of hydrogen dissociation is higher over small gold nanoparticles. This indirectly affects the rate-determining step, which involves the formation of hydroperoxy species [31].

We can indirectly observe that from Figure 29B, which represents the propene conversion and is significantly higher for the 0.1Au/TiO_2 catalyst than the 1.0Au/TiO_2 catalyst. Furthermore, the higher loaded catalysts (1.0wt%) deactivates more quickly than the lower loaded catalysts (0.10wt%). A higher gold weight loading results in a higher percentage of Au-Ti interfaces (more accessible active sites). Therefore, propene/propene oxide adsorption is most likely higher and results in quick deactivation of the catalyst. A high initial propene conversion and selectivity to propene oxide contribute to the 1.0Au/TiO_2 catalyst's quick deactivation.

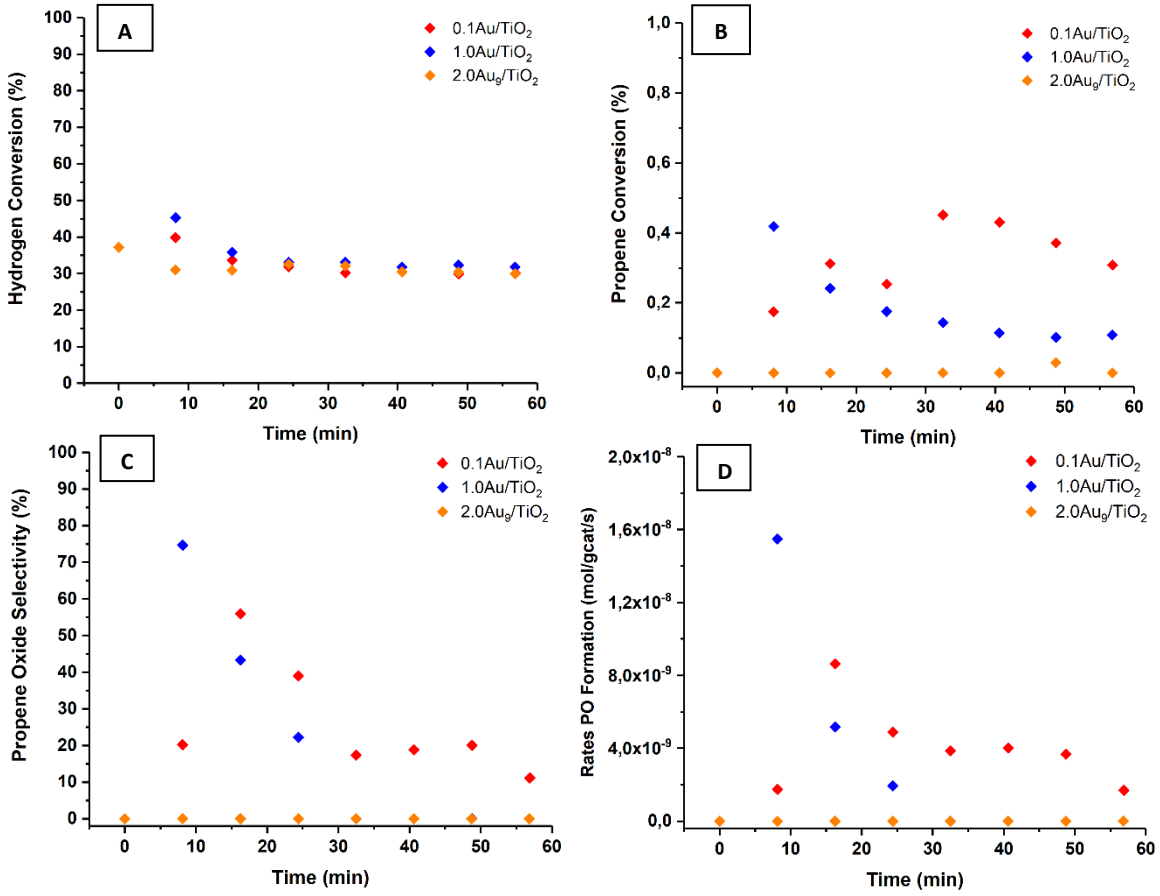

Figure 29: Representation of conversions of reactants at 100°C and a GSHV of 4000 h^{-1} (C_3H_6; H_2, O_2 1 mL/min, He 7 mL/min). A) Hydrogen conversion; B) Propene conversion; C) Propene oxide selectivity over time; D) PO Formation rate. Pretreatment; Calcined at 300°C for 4h (Air), In-situ Reduced at 150°C for 45 minutes (20% H_2, 80% He; 6:24mL/min).

Table 9: Characterisation overview of monometallic Au/TiO_2 catalysts and their catalytic results (after 60 minutes), TEM particle size distribution and ICP-AES to determine weight loadings.

Catalyst	ICP wt% Au	TEM (Size nm)	H2 Conversion (%)	Initial C_3H_6 Conv. (%)	Final C_3H_6 Conv. (%)	Highest PO Sel. (%)	Final PO Sel. (%)
0.1Au/TiO_2	0.097	2.69 ± 0.63	30	0.17	0.31	56	11
1.0Au/TiO_2	x	3.48 ± 1.1	32	0.41	0.11	74	0.0
2.0Au_9/TiO_2	x	0.693 ± 0.21	30	0.0	0.0	0.0	0.0

Initially, the catalytic selectivity was approximately 80% towards propene oxide of the 1wt% Au/TiO_2. Several studies have reported that Au/TiO_2 catalysts are able to achieve >95% propene oxide selectivity at lower temperatures [1,20,26]. At elevated temperatures, >120°C, competing side reactions occurred, such as partial and complete oxidation, leading to acetaldehyde, acrolein, and finally CO2 that resulted in decreased propene oxide selectivity [83]. Our research group has developed a kinetic model combined with experimental data sets for the deactivation of Au/TiO_2 in dependence of temperature and GHSV [83]. Higher temperatures led to quicker deactivation, according to their kinetic model and data sets. Their kinetic model predicted a sixfold decrease in propene oxide production within approximately 40 minutes at 92°C, which corresponds with our observations regarding Au/TiO_2 deactivation.

Secondly, Figure 29C shows a rapid decline in propene oxide selectivity within the time span of 60 minutes. Studies in literature have reported on the deactivation of Au/TiO_2 within 4h, and therefore we are surprised to observe this rate of catalytic deactivation. In general, the deactivation of the Au/TiO_2 catalysts in propene oxidation with H_2/O_2 mixtures has several explanations. Firstly, as addressed in the theory section, Mul. G. et al. found that the catalyst's instability is attributed to the irreversible adsorption of propene and propene oxide that leads to a ring-opening reaction [78]. The desorption of propene oxide is inhibited, which leads to a ring-opening reaction. This decomposition of propene oxide is an acid-catalyzed reaction because the acidic OH-groups on TiO_2 react with propene oxide, resulting in the formation of bidentate propoxy species. Further oxidation of these bidentate propoxy species form carboxylate species that are irreversibly adsorbed and cause blocking of the active Ti-sites [78].

Moreover, Mul. G et al. have found an alternative route, called the acrylate route [78]. The oxygen covered surface of Au allows for the insertion of oxygen to the allylic C-H bond in propene. Subsequently, an allyloxy intermediate is formed. This particular allyloxy intermediate reacts further to acrolein, which is not stable under the conditions studied and ultimately combusted into CO_2. These carbonate species and higher oligomers of PO on the surface of the Au/TiO_2 likely contribute to the deactivation of the catalysts and are in consonance with the theory of bidentate-propoxy species. At last, oligomerization of propene oxide on the catalytic surface is frequently observed. In general, oligomerization, decomposition of propene oxide, and carboxylate species formation all lead to inaccessible, blocked active Ti-sites and further propene oxide production is inhibited.

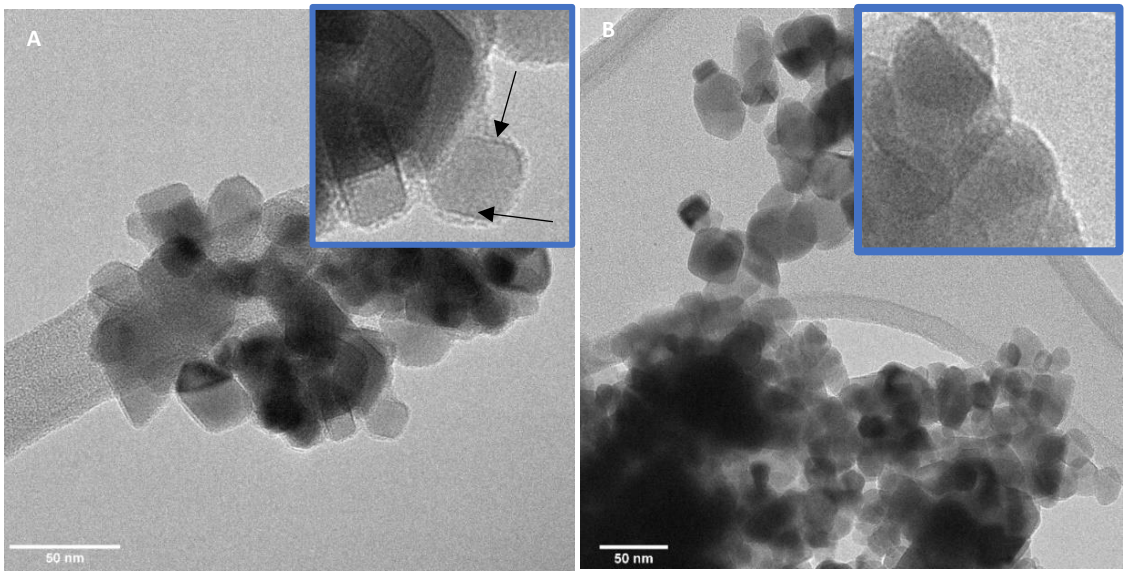

Figure 30: A) BF-TEM images of the spent Au/TiO_2 catalyst with 0.1%wt Au. Black arrows indicate possible coke formation. B) BF-TEM images of fresh Au/TiO_2 catalyst with 0.1wt% Au.

This proposal of deactivation by product oligomerization is strengthened by the BF-TEM images of the 0.1Au/TiO_2 spent catalyst are shown in Figure 30A. On the surface of the TiO_2 support we observed the formation of a solid layer, which we propose is due to the oligomerization of PO or coke. Figure 30B represent the spent catalyst and black arrow indicate the newly formed 'coke' layer, not present on the BF-TEM image of fresh Au/TiO_2. Gold nanoparticle sintering is ruled out based on the TEM-observations represented in Figure 31. Quantitative analysis of these TEM-images is not possible since too little supported gold nanoparticles are visible for the spent catalyst. However, qualitative analysis denies the possibility of sintering. To conclude, the deactivation of the Au/TiO_2 catalysts can primarily be attributed to the oligomerization of propene oxidation reaction products on the surface of the crystalline TiO_2.

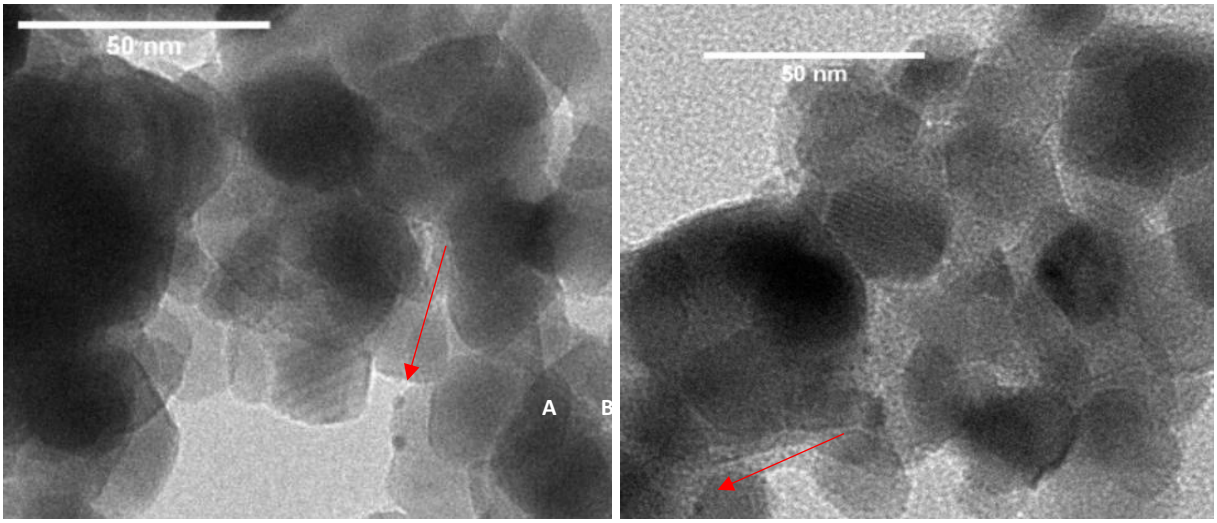

Figure 31: BF-TEM images of fresh and spent catalysts. Figure A) fresh 0.1Au/TiO_2; B) spent 0.1Au/TiO_2. No aggregation of supported gold nanoparticles is observed. Red arrows indicate supported AuNPs.

In order to verify this hypothesis, the spent 0.1Au/TiO_2 is subjected to a TGA measurement. The TGA measurement is shown in Figure 32. Since CO_2 is detected by MS, it proves the presence of adsorbed species on the catalytic surface used in propene epoxidation, similar to coke on Titanium-silicate O_2 catalysts used in propene epoxidation [44]. Figure 32A shows the loss of relative mass of both the fresh and spent catalyst. Where the fresh catalysts shows a loss in mass of 0.9%, the spent catalyst shows a significant mass decrease of 2,6% over time. We attribute this to the adsorption of carboxylate species on the surface of the spent catalyst.

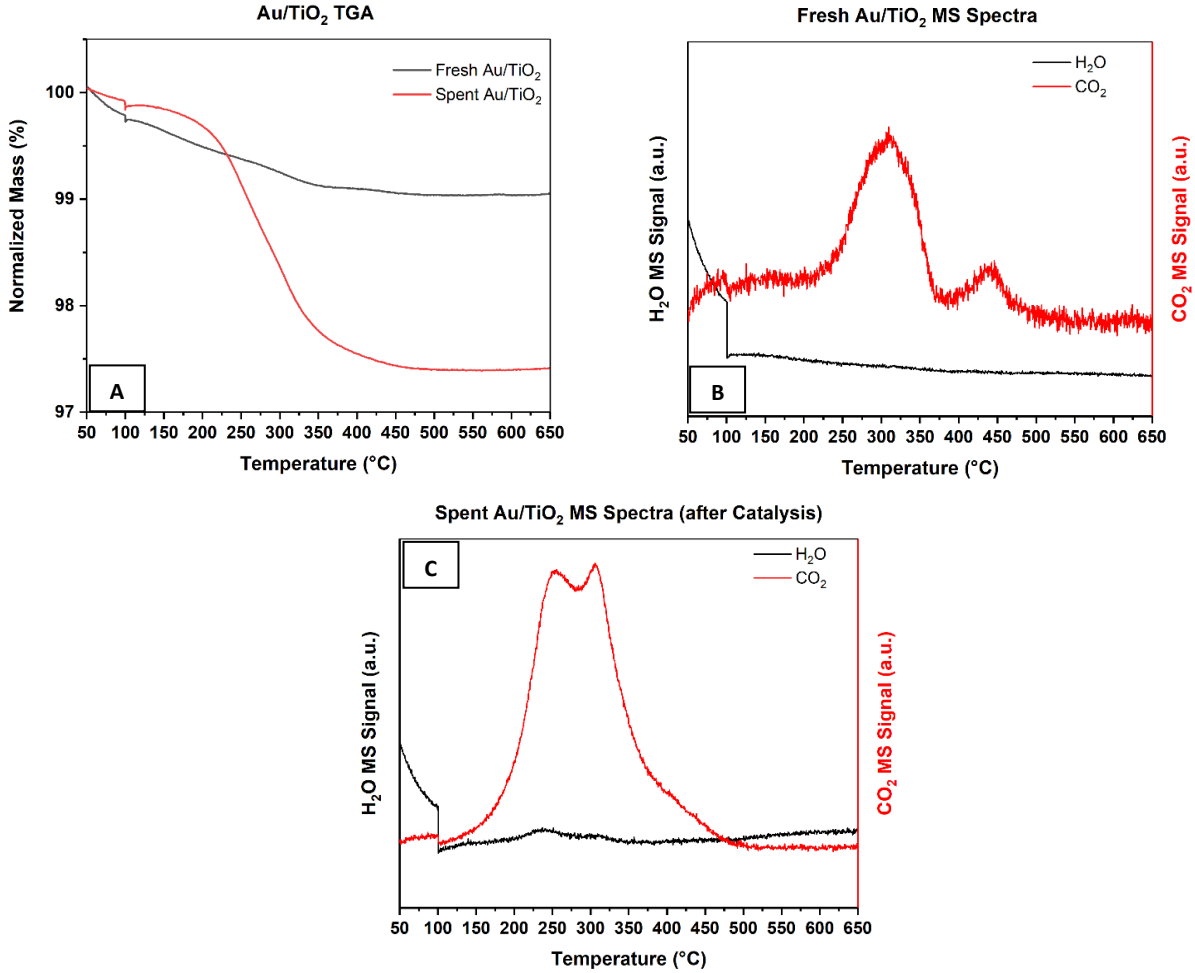

Figure 32: TGA measurement of fresh and spent Au/TiO_2 with a nominal 0.1wt% Au.

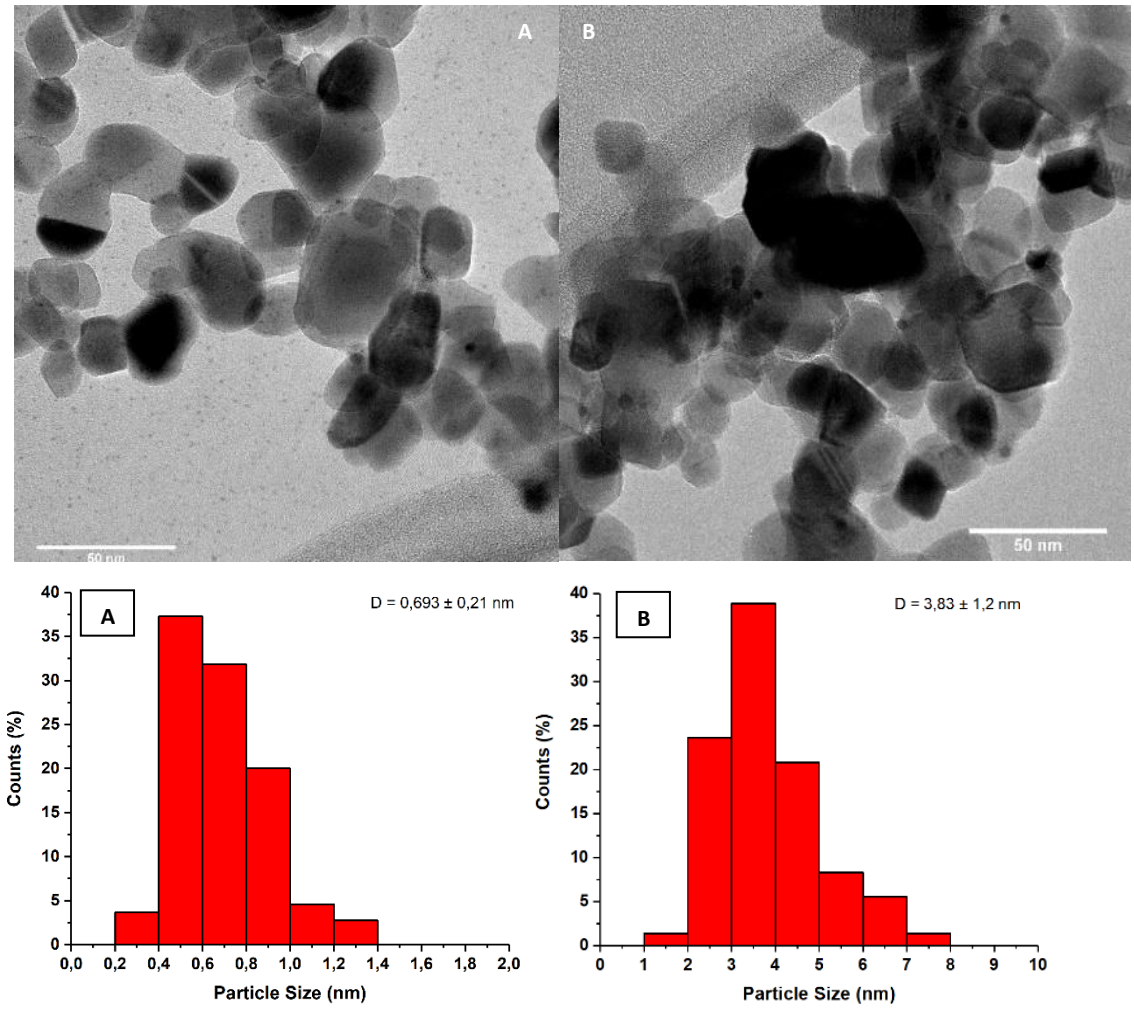

Figure 33: BF-TEM images of fresh 2.0Au_9/TiO_2 (A) and spent 2.0Au_9/TiO_2 (B). Gold clusters are observed before catalytic tests (A), gold nanoparticles after subjection to catalytic tests (B).

When gold clusters $(Au_9(PPh_3)_8(NO_3)_3$ were supported on titania, the catalysts were not active are not active in the propene epoxidation at all. These gold clusters started to sinter to nanoparticles sizes ~5nm at higher temperatures (i.e. 200°C), as observed by the purple color (vs the orange/beige color prior to catalytic tested and the TEM results displayed in Figure 33. The sintering of the gold clusters to larger gold nanoparticles is related to the strength of the metal-support interaction. It is known that supported gold clusters on metal-oxide surfaces combined with elevated temperatures and gaseous mixtures such as hydrogen is contributing to the aggregation of gold clusters [43].

Despite no desired propene oxide was observed, a constant propene conversion and by product formation was observed: mostly acetaldehyde, CO_2 and propanal. Propionaldehyde is formed by over-oxidation of propene-oxide due to strong Lewis acids (i.e. Ti-sites) and acetaldehyde is the results of cracking of propene oxide. CO_2 is the result of complete combustion of propene at elevated temperatures or the conversion of the unstable acrolein formed by partial oxidation [87].

5.2.3. Catalytic tests of bimetallic catalysts.

A series of bimetallic Au-X/TiO_2 catalysts were synthesized by sequential deposition-precipitation. The catalysts prepared are Au-Ag/TiO_2, Au-Pd/TiO_2 and Au-Cu/TiO_2 with a theoretical atomic ratio of $Au_{20}X_1$, with "X" resembling Ag, Pd and Cu. In the previous section, the bimetallic catalysts were characterized by UV-Vis spectroscopy, XRD, TEM and ICP-AES. Subsequently, these catalysts were subjected to catalytic tests to evaluate the catalytic performance and compare their catalytic activity, stability and selectivity with monometallic Au/TiO_2.

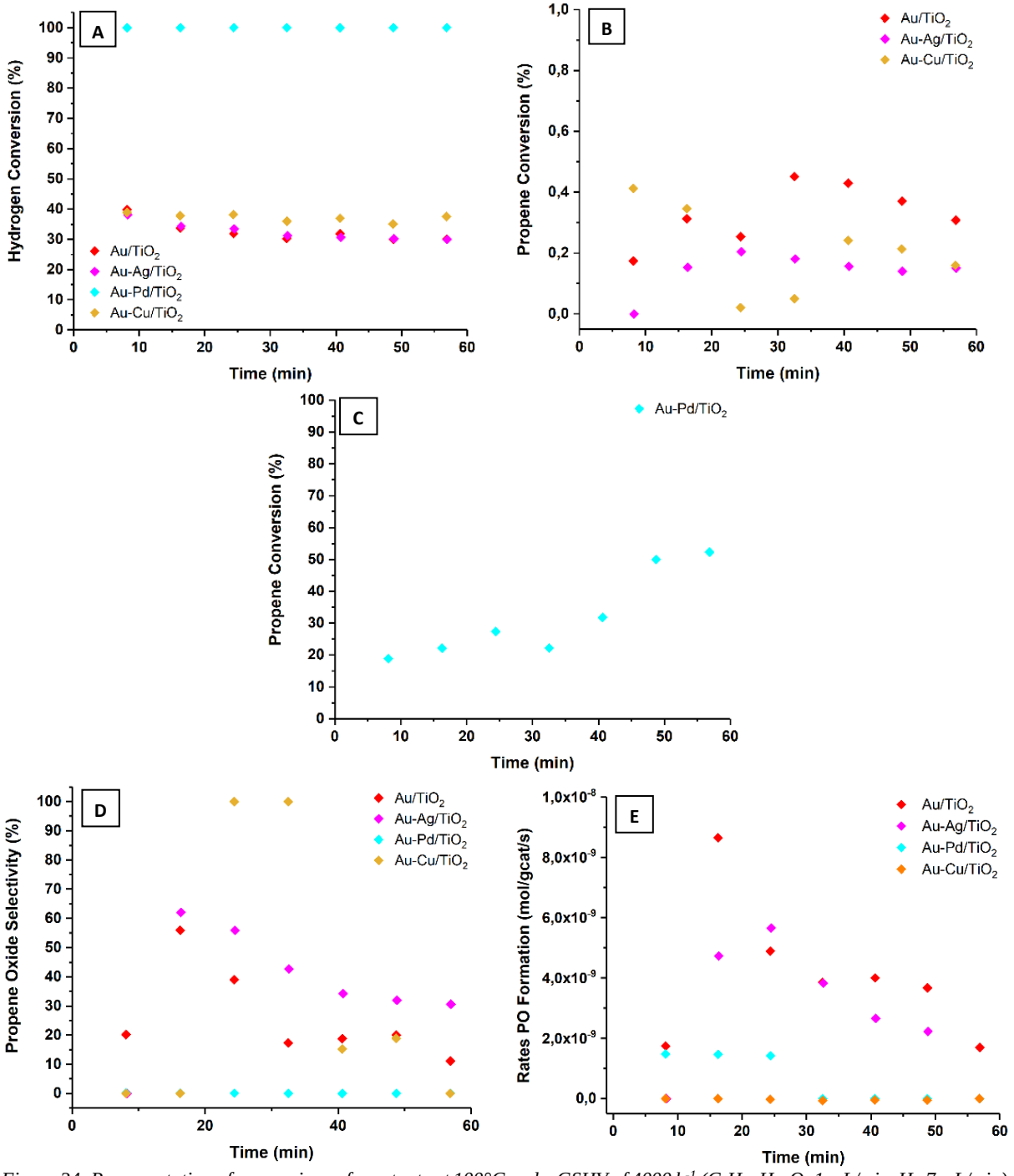

Figure 34: Representation of conversions of reactants at 100°C and a GSHV of 4000 h^{-1} (C_3H_6; H_2, O_2 1 mL/min, He 7 mL/min). A) Hydrogen conversion; B) Propene conversion; C) Propene conversion; D) Propene oxide selectivity over time; E) Rates of PO Formation. Heat treatment; Calcined at 300°C for 4h (Air), In-situ reduced at 150°C for 45 minutes (20% H_2, 80% He; 6:24mL/min).

Table 10: Characterisation overview of monometallic Au/TiO_2 catalysts and their catalytic results (after 60 minutes), TEM particle size distribution and ICP-AES to determine weight loadings.

Catalyst	ICP wt% Au	Theoretical Atomic Ratio	TEM (Size nm)	H2|O2 Conv. (%)	C_3H_6 Conv.(%)	Initial PO Sel. (%)	Final PO Selectivity
Au/TiO_2	0.097	X	2.69 ± 0.63	30	0.31	56	11
Au-Pd/TiO_2	0.097	20:1 Au|Pd	2.48 ± 0.98	100	52	0.0	0.0
*Au-Cu/TiO_2	0.097	20:1 Au|Cu	*n.d.	38	0.16	0.0	0.0
*Au-Ag/TiO_2	0.097	20:1 Au|Ag	*n.d.	30	0.15	62	31

The conversion of reactants over time regarding the monometallic and bimetallic catalysts are represented in Figure 34. At first sight, the hydrogen conversion over Au-Pd/TiO_2 is increased threefold compared to Au/TiO_2 that achieves an average hydrogen conversion of 30-35% over, represented in Figure 34A. Furthermore, the propene conversion increases by 150x with the introduction of palladium. On the contrary, a selectivity of 100% towards propane attributes to the formation of monometallic Pd nanoparticles instead of alloyed AuPd. Zwijnenburg A. et al. observed the undesired hydrogenation of propene to propane over (Au)Pd/TiO_2 catalysts. Their research solidifies our assumption since they observed the formation of separate Pd nanoparticles along with AuNPs with deposition-precipitation [76]. Most likely, the energy adsorption barrier of propene on Pd is much lower in comparison to the Au-Ti interface.

The stability and increasing propene conversion of the Au-Pd/TiO_2 catalyst strengthen the assumption that propene is not adsorbed on the Au-Ti interface but on the Pd nanoparticles' surface. Adsorption of propene would lead to deactivation of the catalysts by oligomerization, the formation of bidentate propoxy or carboxylate species, previously addressed in the monometallic Au/TiO_2 section. Also, the isolated/separate palladium nanoparticles are capable of breaking the O-O catalytically bond of either hydroperoxyl species or hydrogen peroxide. The O-Pd is stronger adsorbed on the Pd surface than O-O bonds, facilitating the breaking of the O-O bond, which leads to the decomposition of H_2O_2 and -OOH. Therefore, the production of hydroperoxyl species over Pd is not possible, and propene oxide production is inhibited [82]. The decomposition of -OOH or H_2O_2 species results in water formation. Our results verify these conclusions since besides the hydrogenation of propene, water is the primary product detected by gas-chromatography.

5.2.4. Intermediate conclusion

Both Au-Ag/TiO_2 and Au-Cu/TiO_2 did not show an increase in catalytic activity compared to Au/TiO_2. In general, the introduction of Ag to the monometallic Au-TiO_2 leads to better oxygen adsorption and electron transfer from Au to O_2, beneficial for the adsorption of electron-dense propene [45]. However, propene conversions of Au-Ag/TiO2 and Au-Cu/TiO_2 did not differ from monometallic Au/TiO_2. This may lead to the assumption that synergetic effects are not present and no alloyed Au-Ag nanoparticles are formed, necessary for the presence of synergetic/electronic effects. Furthermore, the hydrogen conversions were equal among all catalysts, besides Au-Pd/TiO_2. The Au-Ag/TiO_2 catalyst does show a minor increase in propene oxide selectivity, but the introduction of silver to monometallic Au/TiO_2 does not improve the stability of the catalysts. The introduction of Ag, Pd and Cu does not change the characteristics of the support. Therefore, the oligomerization of propene oxide, the formation of carboxylates, or the acid-catalyzed ring-opening reaction that forms bidentate propoxy species is not inhibited [78,83]. Unfortunately, the catalysts are highly unstable, more than expected beforehand and therefore the synergy effects between Ag, Cu and Au cannot be investigated in much detail.

5.3. Gold-titanium(IV)-silica based catalysts.

As the use of TiO_2 as support for bimetallic AuPd, AuCu and AuAg was not successful in determining the effect of the second metal on propene epoxidation, a different support was used. By dispersing titanium(IV) on a silica surface the stability of the Au/Ti-SiO_2 catalysts is enhanced in respect to TiO_2 where the oligomer Ti-OH sites cause oligomerization of PO as a form of deactivation of the catalyst.

In this chapter, we strive to increase the hydrogen efficiency and stability of Au/TiO_2 in the gas-phase propene oxidation with H_2/O_2 mixtures by adding noble metals and by grafting 2.0wt% titanium in SiO_2. We have synthesized a series of bimetallic nanoparticles by a deposition-precipitation with NaOH of various precursors (see experimental section), resulting in either Au-Pd or Au-Cu, supported on Ti-SiO_2 at 0.2wt% Au loading with <0.01wt% Cu. At first, the bimetallic supported nanoparticles are characterized by XRD and BF-TEM. Subsequently, the catalytic stability and activity are evaluated by subjecting these catalysts to catalytic tests.

5.3.1. Characterization of bimetallic catalysts on Ti-SiO_2

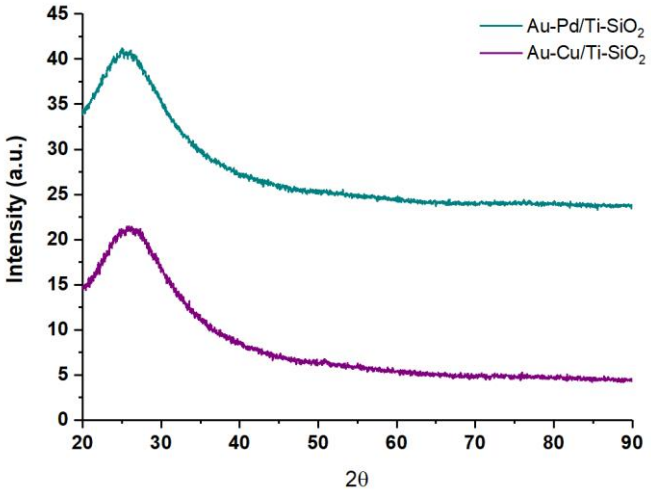

*Figure 35: XRD Diffractograms of supported bimetallic nanoparticles on Ti-SiO_2 after heat treatment (reduction at 300°*C *for 3h, calcination in air for 4h at 450°C).*

XRD measurements were performed to obtain information about the crystalline phases and sizes present of the bimetallic catalysts. First of all, we only observed a broad peak originating from the amorphous silica used (GRACE® SI 1404, silicagel). Secondly, no information was obtained by XRD to identify the gold and copper phases present since either the particle sizes were significantly small or the weight percentages are too low, 0.2wt% Au and <0.02wt% Cu. Finally, the XRD diffractograms confirm the high dispersion of Ti-sites (2wt% titanium) on the surface because no crystalline phases were observed.

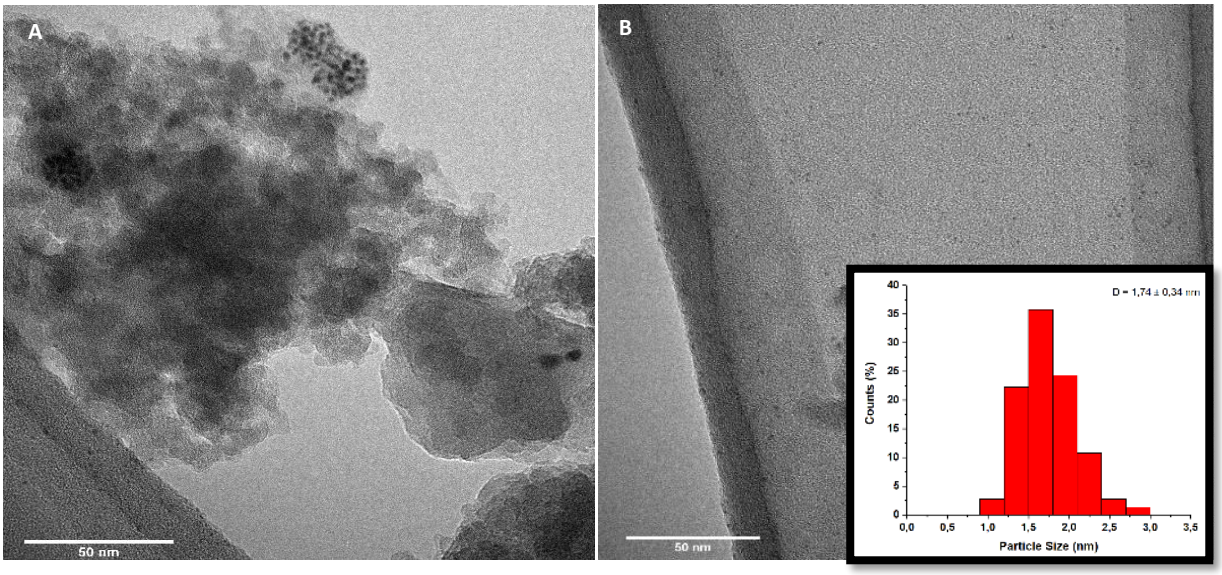

Figure 36: Representative BF-TEM images of Au-Cu/Ti-SiO_2 including a histogram of particle size distribution after heat treatment (reduction at 300°C for 3h, calcination in air for 4h at 450°C).

In order to determine the shape and number average particle size of the bimetallic nanoparticles, information that could not be retrieved from the XRD diffractograms, these catalysts were subjected to a BF-TEM analysis. Representative BF-TEM images are shown of Au-Cu/Ti-SiO_2 in Figure 36AB Figure 36B proves that deposition-precipitation was successful because very small gold nanoparticles are formed on the support (1.74 ± 0.34 nm). On the contrary, it is also noticed that many gold nanoparticles are on the copper grid instead of on the support. Metal-support interactions are crucial in catalytic reactions, so unsupported Au nanoparticles are expected to be quite mobile and unstable. Mobile nanoparticles are expected to be susceptible towards particle sintering upon heat treatment and our reaction conditions in propene epoxidation. Further elaboration on this topic is given once spent Au-Cu/Ti-SiO_2 catalysts are subjected to BF-TEM.

Secondly, Figure 36A shows a marginal dispersion of metal nanoparticles. Initially, we suspected that these were isolated copper nanoparticles. After discovering the lack of supported gold nanoparticles, reduction and calcination at >300 °C initiated particle growth by nanoparticle migration across the support. Since we are unsure about the nature of the nanoparticles, these nanoparticles were not incorporated into the determination of number average particle size. Both XRD and BF-TEM were not sufficient to completely verify the structure of possible bimetallic nanoparticles. Other characterization techniques, such as TEM-EDX and XPS, were not utilized due to a lack of time.

5.3.2. Catalytic Tests of bimetallic catalysts on Ti-SiO_2

Monometallic and bimetallic supported nanoparticles on with titanium-grafted silica are subjected to catalytic tests in order to evaluate the catalytic stability and activity in comparison with Au/TiO_2 catalysts. Hydrogen conversions, propene conversions, and selectivity for propene oxide are displayed in Figure 37 and table 11.

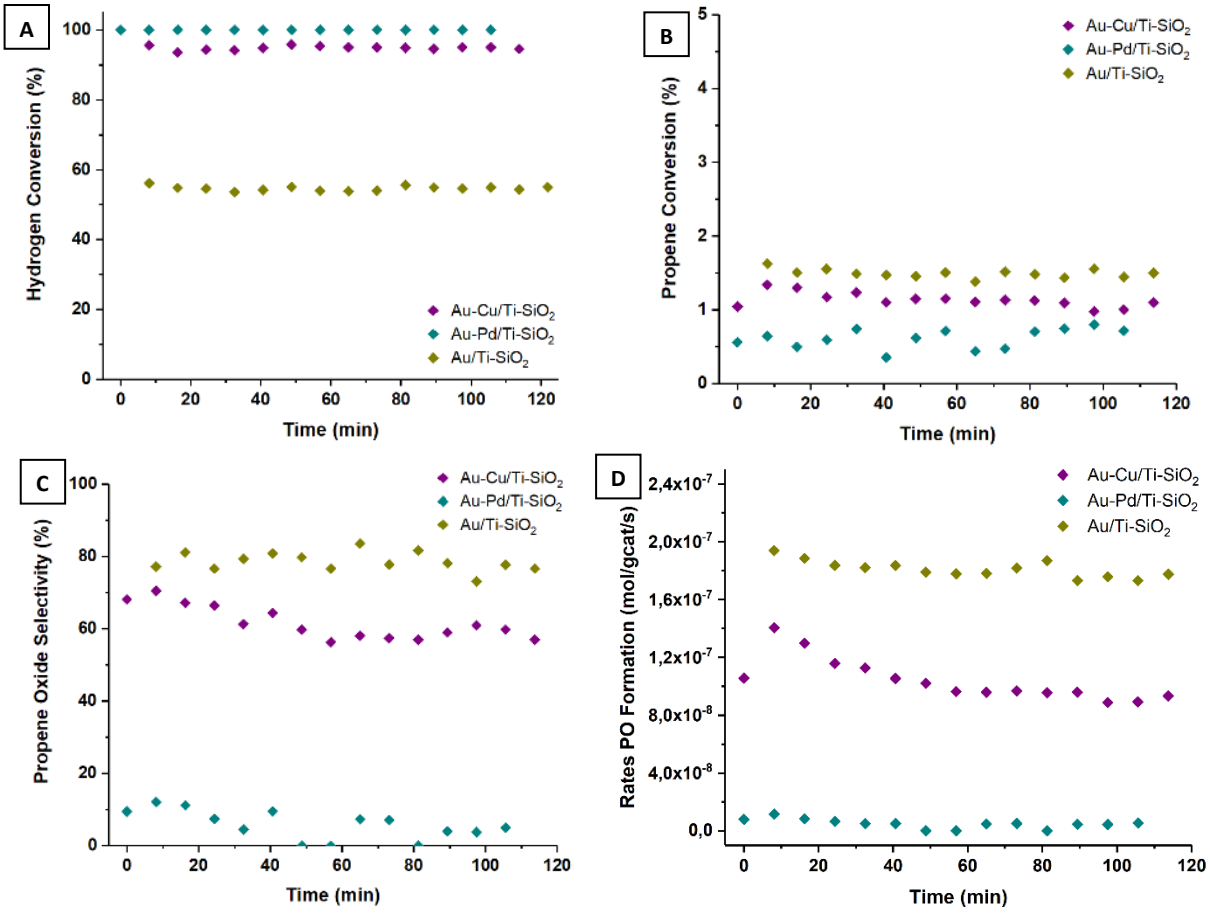

Figure 37: Representation of conversions of reactants at 200°C and a GSHV of 10000 h^{-1} (C_3H_6; H_2, O_2 2,5 mL/min, He 17,5 mL/min). A) Hydrogen conversion; B) Propene conversion; C) Propene oxide selectivity over time. D)Rates of PO Formation. Pretreatment of catalysts; Calcined at 450°C for 4h (Air), Reduced at 300°C for 3h (20% H_2, 80% He). In-situ reduction of 60 minutes at 250 °C under 20% H_2 in He.

*Table 11: Characterization overview of monometallic Au/TiO_2 catalysts and their catalytic results (after 105 minutes), TEM particle size distribution and ICP-AES to determine weight loadings. *No TEM-images were obtained for these catalysts. Therefore, the particle sizes are assumed to be similar, since the preparation methods were equal. 0.2wt%-Au/0.1wt-Ti*

Catalyst	ICP wt% Au	Theoretical Atomic Ratio	TEM (Size nm)	Preparation method	H2|O2 Conv. (%)	C_3H_6 Conv.(%)	PO Sel. (%)
$Au/Ti-SiO_2$	0.20	x	2.70 ± 0.81	DP (NaOH)	55|40	1.6	70
*$Au-Pd/Ti-SiO_2$	0.20	20:1 Au|Pd	1.5-3.0	DP (NaOH)	100|55	0.72	0.0
$Au-Cu/Ti-SiO_2$	0.20	20:1 Au|Cu	1.74 ± 0.34	DP (NaOH)	95|79	1.0	61

As previously discussed, monometallic supported gold nanoparticles on titania show severe catalytic deactivation in the propene oxidation at >100 °C. Grafting titanium on the silica surface in combination with supported gold nanoparticles greatly enhances catalytic stability to propene oxide, shown in Figure 37C. Multiple factors explain the greatly enhanced stability and hydrogen conversion of Au/Ti-SiO_2 with respect to Au/TiO_2. For Au/TiO_2, the adsorption of propene oxide is on Ti-sites is too strong, which inhibits produced propene oxide to desorb from the active sites. By grafting titanium on the silica surface, the formation of Ti-O-Si bonds decreases the amount of adsorption and adsorption strength, which facilitates the desorption of propene oxide [85]. Furthermore, possible coke formation, i.e., oligomerization of propene oxide and carboxylate species formation is restricted since a high dispersion of Ti-sites is achieved. High dispersion of Ti-sites leads to a more considerable distance between potentially desorbing propene oxide and thereby inhibiting oligomerization of propene oxide.

Figure 37A represents the hydrogen conversions of the respective catalysts. Hydrogen conversions of both the monometallic and bimetallic supported Ti-SiO_2 catalysts are considerably improved titania supported catalysts. Earlier, we reported that hydrogen conversions were 30% for titania supported catalysts while Ti-SiO_2 catalysts achieve stable hydrogen conversions over 60% in combination with stable propene conversion and propene oxide production. First of all, the twofold enhanced hydrogen conversions can be attributed to increased gold weight loadings (0.10wt% vs. 0.20wt%). Moreover, Au-Pd/TiO_2 and Au-Cu/TiO_2 exhibit a higher hydrogen conversion than Au/Ti-SiO_2. This is probably due to the formation of either isolated copper/palladium nanoparticles or alloyed structures. Furthermore, the bimetallic nanoparticles have smaller gold nanoparticles deposited on the support than Au/Ti-SiO_2, shown in table 11. Smaller gold nanoparticles have a larger relative surface area and a lower coordination number i.e., lower adsorption energy [53].

The introduction of Pd and Cu leads to a higher dissociative adsorption rate due to the strong interaction and thereby strong chemical binding, which is related to the number of electrons that occupy the d-orbitals. An increase in the rate of dissociative adsorption of hydrogen indirectly affects the rate of formation of hydroperoxy species. The rate of formation of hydroperoxyl is the rate-determining step in propene oxidation. The introduction of copper led to an increase in hydrogen conversion. Despite an increase in hydrogen conversion, we observe a decreasing rate of propene conversion and propene oxide selectivity and formation rate for Au-Pd/Ti-SiO_2 and Au-Cu/Ti-SiO_2 with respect to Au/Ti-SiO_2.

Bimetallic Au-Cu/Ti-SiO_2 exhibited excessive water formation. The formation of water is attributed to two factors, either the inability to spillover generated hydroperoxyl species (i.e., decomposition) or the formation of water by isolated Au or Cu nanoparticles (i.e., oxidation of hydrogen) [25]. The ability to spillover hydroperoxy species is partially dependent on gold nanoparticle size. Initially, we synthesized highly dispersed and small gold nanoparticles (1.74 ± 0.34 nm) on the support, verified by TEM analysis. BF-TEM images presented in Figure 38 of fresh and spent Au-Cu/Ti-SiO2 indicated particle growth by migration due to weak metal-support interactions.

The growth in the gold nanoparticle size leads to an increasing interface between Au-Ti, limiting the ability to spillover formed hydroperoxy species [1,21,26]. This directly affects the catalytic activity i.e. propene conversion. Furthermore, this phenomenon indirectly contributes to water formation. Since water is adsorbed on the Au-Ti interface, the concentration of propene adsorbed is lowered due to competitive adsorption [79,86]. To conclude, the particle growth of gold initiates a chain reaction. The growth of gold nanoparticles limits the ability to spillover formed hydroperoxy species, limiting propene conversion. Water formation contributes to the declining propene conversion due to competitive adsorption between propene. The introduction of Cu to Au/Ti-SiO_2 (Au20:Cu1) led to a decreasing selectivity towards propene oxide despite ultimate hydrogen conversions and thereby negatively affecting the hydrogen efficiency.

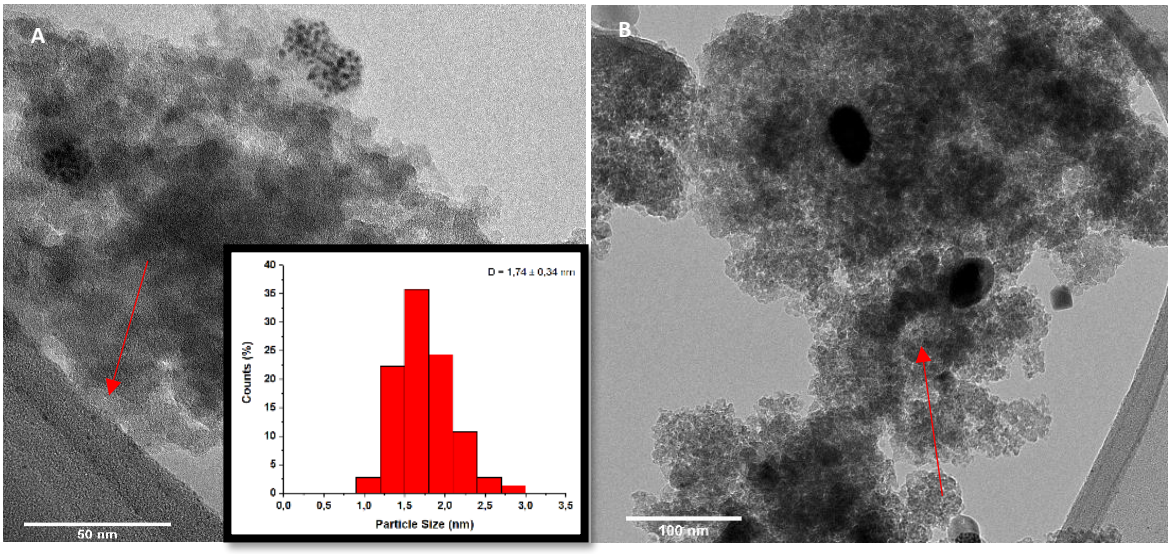

Figure 38: Representative BF-TEM images of Au-Cu/Ti-SiO_2; Fresh Au-Cu/Ti-SiO_2 (A) and Spent Au-Cu/Ti-SiO_2 (B) (reduction at 300°C for 3h, calcination in air for 4h at 450°C). Arrows indicate difference in nanoparticle size, significant growth is observed when analyzing spent catalyst (Too few BF-TEM images available for extensive/quantitative analysis).

Figure 37ABC show that the introduction of Pd to Au/Ti-SiO_2 leads to a higher hydrogen consumption but almost completely diminishes propene oxide production. Instead, only acetone, acrolein, acetaldehyde, and propane are formed. Quantification of the propane amount is difficult since it overlaps partially with the initial propene peak in gas chromatography. The hydrogenation is lower than the previously studied AuPd-TiO_2 catalysts, which strengthens the assumption that bimetallic alloyed AuPd nanoparticles are formed on the Ti-SiO_2 support since isolated supported Pd nanoparticles are known as excellent hydrogenation catalysts. Despite an earlier reported enhanced propene oxide formation rate when Pd was introduced to Au/TS-1, we did not obtain similar results [75].

What is more, in our case, the introduction of Pd led to minimal propene oxide formation and observed the production of frequently encountered by-products in the gas-phase oxidation of propane. For example, acrolein is formed over isolated negatively charged gold nanoparticles, which are able to active oxygen. The antibonding orbitals of oxygen overlap with the d-orbitals of the surface atoms of the nanoparticles. This creates an electron density, which is transferred from the nanoparticles to the antibonding orbital of oxygen [23]. While the mechanism for epoxidation is different, the electron density from the double bond of propene is transferred to the peroxide species' electrophilic oxygen [5]. As is proposed by Stangland, acetone is formed from the rearrangement of propene oxide over Bronsted bases present on the catalytic surface [113]. The AuPd/Ti-SiO_2 catalyst is prepared by

deposition-precipitation with NaOH, so in this case, it is suggested that improper washing leads to NaOH's presence on the catalytic surface.

Table 12: Overview of the side-product formation over bimetallic catalysts supported on Ti-SiO_2. Sel. % are representing an average over all measured data points.

Catalyst	Operating Temperature (°C)	GHSV (ml/g_{cat}/ h)	CO2 (sel. %)	CO (sel. %)	Acetal-dehyde (sel. %)	Acrolein (sel. %)	Acetone (sel. %)	Propanal (sel. %)
Au/Ti-SiO_2	200	10000	0.26	2.2	8.6	11	0.0	1.31
Au-Cu/Ti-SiO_2	200	10000	6.5	0.0	6.5	25	0.0	1.4
Au-Pd/Ti-SiO_2	200	10000	7.0	0.0	19	27	41	0

To conclude, the introduction of noble metals to create alloyed structured bimetallic nanoparticles to increase hydrogen efficiency and the propene oxide formation rate was unsuccessful. It was attributed to either the lack of electronic/synergetic effects because presumably no alloyed (or core-shell structure) bimetallic supported nanoparticles were created.

6. Conclusions

In conclusion, it was investigated if the active Ti-sites in supported Au/Ti-catalysts in propene epoxidation with H_2/O_2 mixtures could be replaced by various transition metals (Ti(IV), Mo(VI), W(VI)). Therefore, a series of catalysts were synthesized comprised of small gold nanoparticles and transition-metal complex on amine-functionalized silica. Initially, severe gold nanoparticle sintering was encountered upon heat treatment due to Ostwald ripening. After slight modifications were made in the synthesis procedure, sufficiently small gold nanoparticles between 3-4nm were synthesized, which was confirmed by subjecting these Au/APS-SiO_2 (0.5wt% Au) catalysts to BF-TEM. Subsequently, it was confirmed by UV-Vis spectroscopy that ligand substitution is a successful method to form bifunctional Au-X/SiO_2 or Au-X/APS-SiO_2 catalysts. In order to evaluate the catalytic performance of these bifunctional catalysts in propene oxidation, they were subjected to $H_2/O_2/C_3H_6$/He mixtures. It was found that the uncalcined bifunctional catalysts containing 0.5wt% Au and a theoretical 5.0wt% Ti achieved the highest propene conversion and thereby highest activity. Despite the catalytic activity of the Au/Ti catalysts, the product distribution of propene oxidation was inferior to catalysts comprised of Mo(VI) or Re(VII). The major products formed are derived from propene oxide. It was assumed that the presence of ligands and the lack of intimacy between the pivotal components of the bifunctional catalysts were the primary explanations for low selectivity towards propene oxide.

Since Ti(IV) was the most active and therefore promising element in propene oxidation, monometallic Au and bimetallic AuPd, AuCu, and AuAg particles were supported on TiO_2. Firstly, a series of Au/TiO_2 catalysts with various weight loadings of Au were synthesized by either deposition-precipitation or impregnation. All catalysts were subjected to BF-TEM and ICP-AES and it was concluded that supported gold nanoparticles had been formed with an average size of 2.5-3.5 nm. Furthermore, all monometallic Au/TiO_2 catalysts were subjected to catalytic tests to investigate the stability of these catalysts. It was observed that the catalysts deactivated within 60 minutes, due to the formation of oligomeric species or coke on the support surface and inhibiting further epoxidation of propene. In order to decrease hydrogen conversion and increase hydrogen efficiency of Au/TiO_2 catalysts, several noble metals such as Pd, Cu and Ag were introduced by sequential deposition-precipitation in a theoretical atomic ratio of 20:1 to monometallic Au/TiO_2. Furthermore, it is likely that separate monometallic nanoparticles are formed, concluded by analyzing BF-TEM images and subjecting these catalysts to UV-Vis spectroscopy. However, the quick deactivation of bimetallic AuX/TiO_2 catalysts in the gas-phase propene oxidation prevented any detailed analysis.

To allow for a detailed analysis of the catalytic performance of both monometallic and bimetallic nanoparticles (AuPd, AuCu), the same series were prepared using a Ti-SiO_2 support, which is known to show no deactivation since highly dispersed Ti-sites prevent oligomerization and coke formation. The synthesized bimetallic nanoparticles were subjected to BF-TEM and we observed that highly dispersed hemispherical gold nanoparticles had formed across the Ti-SiO_2 surface with an average particle size of 2-3 nm. Once subjected to catalytic tests, both the Au/Ti-SiO_2 and Au-Cu/Ti-SiO_2 catalysts showed high stability and selectivity towards propene oxide. The introduction of bimetallic nanoparticles with respect to monometallic supported catalysts negatively affected hydrogen efficiency and absolute propene oxide production and selectivity. For Au-Cu/Ti-SiO_2, it was concluded that excessive water formation led to competitive adsorption between propene and water at the Au-Ti interface. Furthermore, particle growth due to the migration of gold nanoparticles across the support facilitated the formation of large gold nanoparticles, which decreased the catalytic performance. The introduction of Pd to Au-Pd/Ti-SiO_2 did not lead to undesired propene hydrogenation. However, Pd introduction led to the formation of different types of side-products often observed in propene oxidation due to the presence of Bronsted bases (NaOH).

7. Outlook.

This research has extensively studied the viability of bifunctional and bimetallic catalysts for the direct oxidation of propene with H_2/O_2 mixtures to propene oxide. This outlook discusses the possibility of further in-depth research based on the obtained experimental results. First of all, it was shown that the addition of various noble and transition metals results in different catalytic performances regarding activity and selectivity. However, the presence of APS-SiO_2 and its effect on the catalytic performance in respect to SiO_2 supported bifunctional catalysts is not investigated in depth. Therefore, to precisely determine the influence on the catalytic activity and selectivity of the use of amine-functionalized silica-supported bifunctional catalysts, bifunctional catalysts with the same composition should be synthesized on silica and subjected to catalytic tests. Furthermore, different weight loadings are applied in the synthesis of several bifunctional catalysts, which possibly prevents an accurate analysis of the results obtained so far.

Furthermore, we have studied the catalytic performance of bimetallic nanoparticles in the gas-phase oxidation of propene with H_2/O_2 mixtures to propene oxide. First of all, the characterization of X-ray diffraction and UV-VIS spectroscopy was not sufficient to determine the atomic distribution of the bimetallic catalysts with complete certainty. Therefore, XPS or EDX could be applied to identify the surface species, their electronic structure and the geometric interface between the bimetallic elements. Furthermore, by ICP-AES, the precise weight percentages of all bimetallic catalysts should be determined in order to provide a more detailed analysis of the obtained results. Secondly, only a limited amount of elements (Cu and Pd) have been investigated on stable Ti-SiO_2 supports. Therefore, the addition of other noble metals such as rubidium, rhodium, iridium, silver, and platinum and their influence on the catalytic performance in respect to Au/Ti-SiO_2 should be investigated in more detail. Moreover, it is frequently observed that in bimetallic nanoparticles catalysis in propene the atomic ratios between both elements affect the catalytic performance [45,73,75]. Since only the atomic ratio 20:1 is evaluated in this research, a series of bimetallic catalysts with increasing/decreasing atomic ratios can be synthesized to investigate synergistic effects in bimetallic catalysis further.

8. Acknowledgements.

Foremost, I would like to express my sincere gratitude to my daily supervisor Johan de Boed for guiding and supporting me throughout this project at the department of Inorganic Chemistry and Catalysis of Utrecht University. The sharing of your knowledge have not only enabled me to write this report, but also guided me to experimental work and rejuvenated my interest in chemistry. Furthermore, I highly appreciate all the time you spent in acquiring TEM-images and your support in the interpretation of results. Moreover, thank you for all the relaxed conversations we have conducted that definitely reduced the pressure and made my stay at Inorganic Chemistry & Catalysis very pleasant.

Secondly, I would like to thank my first and second examiner, Prof. Dr. Petra De Jongh and Dr. P. Ngene for evaluating my progress and finally grading my efforts. Furthermore, I want to thank Petra Keizer Dr. Baira Donoeva and Dr. Jongkook Hwang in particular, for supervision and your valuable support during synthesis procedures and catalytic testing.

Thirdly, I thank Dennie Wezendonk for XRD-training and Remco Dalebout for showing me how to execute heat treatment reactions. Moreover, I appreciate the immense efforts of technicians, in particular Mr. Jan Willem de Rijk, to provide all required equipment I have used throughout my project.

Last but not least, thank you to all PhD-candidates and master students who have provided help if I encountered any minor problems. The helpful nature and atmosphere at Inorganic Chemistry and Catalysis has made my time rather pleasant.

9: Bibliography

[1]: Nijhuis, T. A., Makkee, M., Moulijn, J. A., & Weckhuysen, B. M. (2006). The production of propene oxide: Catalytic processes and recent developments. *Industrial and Engineering Chemistry Research*, *45*(10), 3447–3459. https://doi.org/10.1021/ie0513090

[2]: Kalich, D.; Wiechern, U.; Linder, J. Propylene Oxide. In Ullman's Encyclopedia of Industrial Chemistry, 5th Edition; Verlag Chemie: Weinheim, Germany, 1993; Vol. A22, p 239.

[3]: *Propylene Oxide Market by Application (Polyether Polyols, Propylene Glycol), Process (Chlorohydrin, Styrene Monomer, TBA Co-Product, Cumene-based, Hydrogen Peroxide), End-use Industry (Automotive, Building & Construction), and Region - Global Forecast to 2022*. (2016). Accessed on 14th of October 2019, MarketsAndMarkets: https://www.marketsandmarkets.com/Market-Reports/propylene-oxide-market-55659975.html

[4]: *Propylene Oxide Market Size, Share, Global Industry Report, 2022* . (2015). Accessed on 14th of October 2019, Grand View Research: https://www.grandviewresearch.com/industry-analysis/propylene-oxide-market

[5]: Oyama, T. S. (2008). *Mechanisms in Homogeneous and Heterogeneous Catalysis*. Elsevier.

[6]: Taylor, B., Lauterbach, J., & Delgass, W. N. (2005). Gas-phase epoxidation of propylene over small gold ensembles on TS-1. *Applied Catalysis A: General*, *291*(1–2), 188–198. https://doi.org/10.1016/j.apcata.2005.02.039

[7]: Ghanta, M., Fahey, D. R., Busch, D. H., & Subramaniam, B. (2013). Comparative economic and environmental assessments of H2O2-based and tertiary butyl hydroperoxide-based propylene oxide technologies. *ACS Sustainable Chemistry and Engineering*, *1*(2), 268–277. https://doi.org/10.1021/sc300121

[8]: Buijink, J. K. F.; van Vlaanderen, J. J. M.; Crocker, M.; Niele, F. G. M. Propylene epoxidation over titanium-on-silica catalysts. The heart of the SMPO process.

[9]: Ishino, M. (2006). Development of new propylene oxide process. *16th Annual Saudi-Japanese Symposium - Catalysts in Petroleum Refining and Petrochemicals, Proceedings*, *2006*, 145–155.

[10]: Jørgensen, K. A. (1989). Transition-Metal-Catalyzed Epoxidations. *Chemical Reviews*, *89*(3), 431–458. https://doi.org/10.1021/cr00093a001

[11]: Epoxidation of olefins with homogeneous catalysts-quo vadis? *Catalysis Science and Technology*, *3*(3), 552–561. https://doi.org/10.1039/c2cy20595e

[12]: Clerici, M. G., & Ingallina, P. (1993). Epoxidation of lower olefins with hydrogen peroxide and titanium silicalite. In *Journal of Catalysis* (Vol. 140, Issue 1, pp. 71–83).

[13]: Synthesis of propylene oxide from propylene and hydrogen peroxide catalyzed by titanium silicalite. *Journal of Catalysis*, *129*(1), 159–167. https://doi.org/10.1016/0021-9517(91)90019-Z

[14]: Li, N., Chen, Y., Shen, Q., Yang, B., Liu, M., Wei, L., Tian, W., & Zhou, J. (2018). TS-1 supported highly dispersed sub-5 nm gold nanoparticles toward direct propylene epoxidation using H2 and O2. *Journal of Solid State Chemistry*, *261*, 92–102. https://doi.org/10.1016/j.jssc.2018.02.016

[15]: Carter, E. A.; Goddard, W. A., III. The surface atomic oxyradical mechanism for Ag-catalyzed olefin epoxidation. J. Catal. 1988, 112 (1), 80-92.

[16]: Geenen, P. V., Boss, H. J., & Pott, G. T. (1982). A study of the vapor-phase epoxidation of propylene and ethylene on silver and silver-gold alloy catalysts. *Journal of Catalysis*, *77*(2), 499–510. https://doi.org/10.1016/0021-9517(82)90190-7

[17]: Cant, N. W., & Hall, W. K. (1971). Catalytic oxidation. IV. Ethylene and propylene oxidation over gold. *Journal of Physical Chemistry*, *75*(19), 2914–2921. https://doi.org/10.1021/j100688a007

[18]: Gorokhovatskii, Ya. B., and Rubanik, M. Ya., Ukr. Khim. Zh. 24, 63 (1958).

[19]: Hayashi, T., Tanaka, K., & Haruta, M. (1998). Selective vapor-phase epoxidation of propylene over Au/TiO2 catalysts in the presence of oxygen and hydrogen. *Journal of Catalysis*, *178*(2), 566–575. https://doi.org/10.1006/jcat.1998.2157

[20]: Haruta, M. (1997). Novel catalysis of gold deposited on metal oxides. *Catalysis Surveys from Japan*, *1*(1), 61–73. https://doi.org/10.1023/A:1019068728295

[21]: Haruta, M. (1997). Size- and support-dependency in the catalysis of gold. Catalysis Today (36), 153-166. https://doi.org/10.1016/S0920-5861(96)00208-8

[22]: Yamazoe, S., Koyasu, K., & Tsukuda, T. (2014). Nonscalable oxidation catalysis of gold clusters. *Accounts of Chemical Research*, *47*(3), 816–824. https://doi.org/10.1021/ar400209a

[23]: Huang, J., Akita, T., Faye, J., Fujitani, T., Takei, T., & Haruta, M. (2009). Propene epoxidation with dioxygen catalyzed by gold clusters. *Angewandte Chemie - International Edition*, *48*(42), 7862–7866. https://doi.org/10.1002/anie.200903011

[24]: Chang, C. R., Wang, Y. G., & Li, J. (2011). Theoretical investigations of the catalytic role of water in propene epoxidation on gold nanoclusters: A hydroperoxyl-mediated pathway. *Nano Research*, *4*(1), 131–142. https://doi.org/10.1007/s12274-010-0083-8

[25]: Chen, J. (2013). *Direct Propene Epoxidation over Gold – Titania Catalysts : Kinetics and Mechanism*.

[26]: Kanungo, S. (2018). *Gold based bifunctional catalysts for one-step oxidation reactions*. Technische Universiteit Eindhoven.

[27]: Monnier, J.R. (2001). The direct epoxidation of higher olefins using molecular oxygen. *Applied Catalysis A: General*, *221*(1–2), 73–91. https://doi.org/10.1016/S0926-860X(01)00799-2

[28]: Weisz, P.B. (2008). Polyfunctional Heterogeneous Catalysis. *Advances in catalysis, 13, 137-190.* https://doi.org/10.1016/S0360-0564(08)60287-4.

[29]: Short, P. L. BASF, Dow Open Novel Propylene Oxide Plant. *Chem. Eng. News* 2009, 87 (11), 21.

[30]: *Global Styrene Market – Industry Analysis and Forecast 2018-2026, by Product Type, By application, By regions. Accessed on the 20th of Augusts 2020, Maximizemarketresearch.* https://www.maximizemarketresearch.com/market-report/global-styrene-market/23532/.

[31]: Nijhuis, T. A., Visser, T., & Weckhuysen, B. M. (2005). Mechanistic study into the direct epoxidation of propene over gold/titania catalysts. *Journal of Physical Chemistry B*, *109*(41), 19309–19319. https://doi.org/10.1021/jp053173p

[32]: Arends, I. W. C. E., & Sheldon, R. A. (2002). Recent developments in selective catalytic epoxidations with H 2 O 2. *Topics in Catalysis*, *19*(1), 133–141. https://doi.org/10.1023/A:1013897703249

[33]: Jacobson, S. E., Frank, M., & Zambri, P. M. (1979). Biphase and Triphase Catalysis. Arsonated Polystyrenes as Catalysts for Epoxidation of Olefins by Aqueous Hydrogen Peroxide. *Journal of the American Chemical Society*, *101*(23), 6946–6950. https://doi.org/10.1021/ja00517a026

[34]: Atwood, D.A. (2016). Sustainable Inorganic Chemistry. Wiley, October 2016.

[35]: van Vliet, M. C. A., Mandelli, D., Arends, I. W. C. E., Schuchardt, U., & Sheldon, R. A. (2001). Alumina: A cheap, active and selective catalyst for epoxidations with (aqueous) hydrogen peroxide. *Green Chemistry*, *3*(5), 243–246. https://doi.org/10.1039/b103952k

[36]: Liu, X., Wang, A., Yang, X., Zhang, T., Mou, C. Y., Su, D. S., & Li, J. (2009). Synthesis of thermally stable and highly active bimetallic Au-Ag nanoparticles on inert supports. *Chemistry of Materials*, *21*(2), 410–418. https://doi.org/10.1021/cm8027725

[37]: G.C. Bond, P.A. Sermon, Gold catalysts for olefin hydrogenation, Gold Bull. 6 (1973) 102– 105

[38]: Meijerink, M. J., De Jong, K. P., & Zečević, J. (2020). Growth of Supported Gold Nanoparticles in Aqueous Phase Studied by in Situ Transmission Electron Microscopy. *Journal of Physical Chemistry C*, *124*(3), 2202–2212. https://doi.org/10.1021/acs.jpcc.9b10237

[39]: El-Brolossy, T. A., Abdallah, T., Mohamed, M. B., Abdallah, S., Easawi, K., Negm, S., & Talaat, H. (2008). Shape and size dependence of the surface plasmon resonance of gold nanoparticles studied by Photoacoustic technique. *European Physical Journal: Special Topics*, *153*(1), 361–364. https://doi.org/10.1140/epjst/e2008-00462-0

[40]: Yan, W., Petkov, V., Mahurin, S. M., Overbury, S. H., & Dai, S. (2005). Powder XRD analysis and catalysis characterization of ultra-small gold nanoparticles deposited on titania-modified SBA-15. *Catalysis Communications*, *6*(6), 404–408. https://doi.org/10.1016/j.catcom.2005.04.004

[41]: Mechanism of the Chromium-Catalyzed Epoxidation of Olefins. Role of Oxochromium(V) Cations. *Journal of the American Chemical Society*, *107*(25), 7606–7617. https://doi.org/10.1021/ja00311a064

[42]: Zecevic, J., Vanbutsele, G., De Jong, K. P., & Martens, J. A. (2015). Nanoscale intimacy in bifunctional catalysts for selective conversion of hydrocarbons. *Nature*, *528*(7581), 245–254. https://doi.org/10.1038/nature16173

[43]: Stangland, E. E., Stavens, K. B., Andres, R. P., & Delgass, W. N. (2000). Characterization of gold-titania catalysts via oxidation of propylene to propylene oxide. *Journal of Catalysis*, *191*(2), 332–347. https://doi.org/10.1006/jcat.1999.2809

[44]: Wang, Q., Wang, L., Chen, J., Wu, Y., & Mi, Z. (2007). Deactivation and regeneration of titanium silicalite catalyst for epoxidation of propylene. *Journal of Molecular Catalysis A: Chemical*, *273*(1–2), 73–80. https://doi.org/10.1016/j.molcata.2007.03.068

[45]: Feng, X., Yang, J., Duan, X., Cao, Y., Chen, B., Chen, W., Lin, D., Qian, G., Chen, D., Yang, C., & Zhou, X. (2018). Enhanced Catalytic Performance for Propene Epoxidation with H 2 and O 2 over Bimetallic Au-Ag/Uncalcined Titanium Silicate-1 Catalysts [Research-article]. *ACS Catalysis*, *8*(9), 7799–7808. https://doi.org/10.1021/acscatal.8b01324

[46]: Landon, P., Collier, P. J., Carley, A. F., Chadwick, D., Papworth, A. J., Burrows, A., Kiely, C. J., & Hutchings, G. J. (2003). Direct synthesis of hydrogen peroxide from H2 and O2 using Pd and Au catalysts. *Physical Chemistry Chemical Physics*, *5*(9), 1917–1923. https://doi.org/10.1039/b211338b

[47]**:** Lefferts, L., & Hanefeld, U. (Eds.) (2018). *Catalysis: An Integrated Textbook for Students*. (1st ed.) Wiley-VCH Verlag.

[48]: Deraz, N. M. (2018). The comparative jurisprudence of catalysts preparation methods: II. Deposition-precipitation and adsorption methods. *J Ind Environ Chem*, *2*(2), 1–3. http://www.alliedacademies.org/journal-industrial-environmental-chemistry/

[49]: Louis, C. (2016). Chemical preparation of supported bimetallic catalysts. Gold-based bimetallic, a case study. *Catalysts*, *6*(8). https://doi.org/10.3390/catal6080110

[50]: Sharma, G., Kumar, A., Sharma, S., Naushad, M., Prakash Dwivedi, R., ALOthman, Z. A., & Mola, G. T. (2019). Novel development of nanoparticles to bimetallic nanoparticles and their composites: A review. *Journal of King Saud University - Science*, *31*(2), 257–269. https://doi.org/10.1016/j.jksus.2017.06.012

[51]: An, K., & Somorjai, G. A. (2015). Nanocatalysis I: Synthesis of Metal and Bimetallic Nanoparticles and Porous Oxides and Their Catalytic Reaction Studies. *Catalysis Letters*, *145*(1), 233–248. https://doi.org/10.1007/s10562-014-1399-x

[52]: Kitchin, J. R., Nørskov, J. K., Barteau, M. A., & Chen, J. G. (2004). Role of strain and ligand effects in the modification of the electronic and chemical Properties of bimetallic surfaces. *Physical Review Letters*, *93*(15), 4–7. https://doi.org/10.1103/PhysRevLett.93.156801

[53]: Lopez, N., Janssens, T. V. W., Clausen, B. S., Xu, Y., Mavrikakis, M., Bligaard, T., & Nørskov, J. K. (2004). On the origin of the catalytic activity of gold nanoparticles for low-temperature CO oxidation. *Journal of Catalysis*, *223*(1), 232–235. https://doi.org/10.1016/j.jcat.2004.01.001

[54]: Hutchings, G. J., Catlow, C. R. A., Hardacre, C., Davidson, M. G., & Hutchings, G. J. (2016). *Catalysis making the world a better place : satellite meeting Subject Areas : Author for correspondence :* 1–8.

[55]: Catalyst Market Size, Share & Trends Analysis Report By Raw Material (Chemical Compounds, Zeolites, Metals), By Product (Heterogeneous, Homogeneous), By Application, By Region, And Segment Forecasts, 2020 – 2027. Accessed on 20th of August 2020. https://www.grandviewresearch.com/industry-analysis/catalyst-market

[56]: *S.M. George, Introduction: Heterogeneous Catalysis, American Chemical Society, Chemical Reviews 95(3):475-476, 1995.*

[57]: *Erica Farnetti, Roberta Di Monte and Jan Kaspar, Inorganic and Bio-Inorganic Chemistry- Vol. II, Homogeneous and Heterogeneous Catalysis.*

[58]: L. Prati and M. Rossi, Chemoselective catalytic oxidation of polyols with dioxygen on gold supported catalysts, Studies in Surface Science and Catalysis, vol. 110, pp. 509–515, 1997. https://doi.org/10.1016/S0167-2991(97)81012-9

[59]: Comotti, M., Weidenthaler, C., Li, W. C., & Schüth, F. (2007). Comparison of gold supported catalysts obtained by using different allotropic forms of titanium dioxide. *Topics in Catalysis*, *44*(1–2), 275–284. https://doi.org/10.1007/s11244-007-0300-1

[60]: Saoud, K.M. Carbon Monoxide Oxidation on Nanoparticle Catalysts and Gas Phase Reactions of Small Molecules and Volatile Organics with Metal Cations. Ph.D, Thesis, Virginia Commonwealth University, Richmond, VA, USA, 2005.

[61]: Haruta, M., Tsubota, S., Kobayashi, T., Kageyama, H., Genet, M. J., & Delmon, B. (1993). Low-temperature oxidation of CO over gold supported on TiO2, α-Fe2O3, and Co3O4. In *Journal of Catalysis* (Vol. 144, Issue 1, pp. 175–192). https://doi.org/10.1006/jcat.1993.1322

[62]: Ousmane, M., Liotta, L. F., Pantaleo, G., Venezia, A. M., Di Carlo, G., Aouine, M., Retailleau, L., & Giroir-Fendler, A. (2011). Supported Au catalysts for propene total oxidation: Study of support morphology and gold particle size effects. *Catalysis Today*, *176*(1), 7–13. https://doi.org/10.1016/j.cattod.2011.07.009

[63]: Uphade, B. S., Yamada, Y., Akita, T., Nakamura, T., & Haruta, M. (2001). Synthesis and characterization of Ti-MCM-41 and vapor-phase epoxidation of propylene using H2 and O2 over Au/Ti-MCM-41. *Applied Catalysis A: General*, *215*(1–2), 137–148. https://doi.org/10.1016/S0926-860X(01)00527-0

[64]: Csankó, K., Sipos, P., & Pálinkó, I. (2012). Monometallic supported gold catalysts in Organic transformations: Ring making and ring breaking. *Catalysts*, *2*(1), 101–120. https://doi.org/10.3390/catal2010101

[65]: Matin, S. F. (2018). Editorial Comment. In *Journal of Urology* (Vol. 199, Issue 4). https://doi.org/10.1016/j.juro.2017.10.064

[66]: Aboukaïs, A., Aouad, S., El-Ayadi, H., Skaf, M., Labaki, M., Cousin, R., & Abi-Aad, E. (2013). Catalytic oxidation of propylene, toluene, carbon monoxide, and carbon black over Au/CeO2 solids: Comparing the impregnation and the deposition-precipitation methods. *The Scientific World Journal*, *2013*. https://doi.org/10.1155/2013/824979

[67]: Veith, G. M., Lupini, A. R., Rashkeev, S., Pennycook, S. J., Mullins, D. R., Schwartz, V., Bridges, C. A., & Dudney, N. J. (2009). Thermal stability and catalytic activity of gold nanoparticles supported on silica. *Journal of Catalysis*, *262*(1), 92–101. https://doi.org/10.1016/j.jcat.2008.12.005

[68]: Mul, G., Zwijnenburg, A., Van der Linden, B., Makkee, M., & Moulijn, J. A. (2001). Stability and selectivity of Au/TiO2 and Au/TiO2/SiO2 catalysts in propene epoxidation: An in situ FT-IR study. *Journal of Catalysis*, *201*(1), 128–137. https://doi.org/10.1006/jcat.2001.3239

[69]: Kozuch, S., & Martin, J. M. L. (2012). "Turning over" definitions in catalytic cycles. *ACS Catalysis*, *2*(12), 2787–2794. https://doi.org/10.1021/cs3005264

[70]: *Gold Nanoparticle Properties | Cytodiagnostics Inc*. (2020). https://www.cytodiagnostics.com/pages/gold-nanoparticle-properties. Accessed on 9th of August 2020.

[71]: Lucci, F. R., Darby, M. T., Mattera, M. F. G., Ivimey, C. J., Therrien, A. J., Michaelides, A., Stamatakis, M., & Sykes, E. C. H. (2016). Controlling Hydrogen Activation, Spillover, and Desorption with Pd-Au Single-Atom Alloys. *Journal of Physical Chemistry Letters*, *7*(3), 480–485. https://doi.org/10.1021/acs.jpclett.5b02400

[72]: Ham, H. C., Stephens, J. A., Hwang, G. S., Han, J., Nam, S. W., & Lim, T. H. (2011). Pd ensemble effects on oxygen hydrogenation in AuPd alloys: A combined density functional theory and Monte Carlo study. *Catalysis Today*, *165*(1), 138–144. https://doi.org/10.1016/j.cattod.2011.02.006

[73]: Aguilar-Tapia, A., Zanella, R., Calers, C., Louis, C., & Delannoy, L. (2015). Synergistic effects of Ir-Au/TiO2 catalysts in the total oxidation of propene: Influence of the activation conditions. *Physical Chemistry Chemical Physics*, *17*(42), 28022–28032. https://doi.org/10.1039/c5cp00590f

[74]: Hosseini, M., Barakat, T., Cousin, R., Aboukaïs, A., Su, B. L., De Weireld, G., & Siffert, S. (2012). Catalytic performance of core-shell and alloy Pd-Au nanoparticles for total oxidation of VOC: The effect of metal deposition. *Applied Catalysis B: Environmental*, *111–112*, 218–224. https://doi.org/10.1016/j.apcatb.2011.10.002

[75]: Li, Z., Gao, L., Zhu, X., Ma, W., Feng, X., & Zhong, Q. (2019). Synergistic Enhancement over Au-Pd/TS-1 Bimetallic Catalysts for Propylene Epoxidation with H2 and O2. *ChemCatChem*, *11*(20), 5116–5123. https://doi.org/10.1002/cctc.201900845

[76]: Zwijnenburg, A., Saleh, M., Makkee, M., & Moulijn, J. A. (2002). Direct gas-phase epoxidation of propene over bimetallic Au catalysts. *Catalysis Today*, *72*(1–2), 59–62. https://doi.org/10.1016/S0920-5861(01)00478-3

[77]: Zanella, R., Delannoy, L., & Louis, C. (2005). Mechanism of deposition of gold precursors onto TiO2 during the preparation by cation adsorption and deposition-precipitation with NaOH and urea. *Applied Catalysis A: General*, *291*(1–2), 62–72. https://doi.org/10.1016/j.apcata.2005.02.045

[78]: Ruiz, A., van der Linden, B., Makkee, M., & Mul, G. (2009). Acrylate and propoxy-groups: Contributors to deactivation of Au/TiO2 in the epoxidation of propene. *Journal of Catalysis*, *266*(2), 286–290. https://doi.org/10.1016/j.jcat.2009.06.019

[79]: Nijhuis, T. A., & Weckhuysen, B. M. (2005). The role of water in the epoxidation over gold-titania catalysts. *Chemical Communications*, *48*, 6002–6004. https://doi.org/10.1039/b512611h

[80]: Sandoval, A., Aguilar, A., Louis, C., Traverse, A., & Zanella, R. (2011). Bimetallic Au-Ag/TiO2 catalyst prepared by deposition- precipitation: High activity and stability in CO oxidation. *Journal of Catalysis*, *281*(1), 40–49. https://doi.org/10.1016/j.jcat.2011.04.003

[81]: Stucchi, M., Jouve, A., Villa, A., Nagy, G., Németh, M., Evangelisti, C., Zanella, R., & Prati, L. (2019). Gold-Silver Catalysts: Ruling Factors for Establishing Synergism. *ChemCatChem*, *11*(16), 4043–4053. https://doi.org/10.1002/cctc.201900591

[82]: Ji, J., Lu, Z., Lei, Y., & Turner, C. H. (2018). Theoretical studies on the direct propylene epoxidation using gold-based catalysts: A mini-review. *Catalysts*, *8*(10). https://doi.org/10.3390/catal8100421

[83]: Min, B. K., & Friend, C. M. (2007). Heterogeneous gold-based catalysis for green chemistry: Low-temperature CO oxidation and propene oxidation. *Chemical Reviews*, *107*(6), 2709–2724. https://doi.org/10.1021/cr050954d

[84]: Nijhuis, T. A., Gardner, T. Q., & Weckhuysen, B. M. (2005). Modeling of kinetics and deactivation in the direct epoxidation of propene over gold-titania catalysts. *Journal of Catalysis*, *236*(1), 153–163. https://doi.org/10.1016/j.jcat.2005.09.027

[85]: Sun, F., & Zhong, S. (2006). Study on chemisorption, catalytic behavior, and stability of supported Au catalyst for the propylene epoxidation reaction. *Journal of Natural Gas Chemistry*, *15*(1), 45–51. https://doi.org/10.1016/S1003-9953(06)60006-6

[86]: Chen, J., Halin, S. J. A., Pidko, E. A., Verhoeven, M. W. G. M. T., Ferrandez, D. M. P., Hensen, E. J. M., Schouten, J. C., & Nijhuis, T. A. (2013). Enhancement of Catalyst Performance in the Direct Propene Epoxidation: A Study into Gold-Titanium Synergy. *ChemCatChem*, *5*(2), 467–478. https://doi.org/10.1002/cctc.201200572

[87]: Wallace, W. T., Min, B. K., & Goodman, D. W. (2005). The nucleation, growth, and stability of oxide-supported metal clusters. *Topics in Catalysis*, *34*(1–4), 17–30. https://doi.org/10.1007/s11244-005-3786-4

[88]: Masoud, N., Partsch, T., de Jong, K. P., & de Jongh, P. E. (2019). Thermal stability of oxide-supported gold nanoparticles. *Gold Bulletin*, *52*(2), 105–114. https://doi.org/10.1007/s13404-019-00259-9

[89]: Masoud, N., Delannoy, L., Schaink, H., Van Der Eerden, A., De Rijk, J. W., Silva, T. A. G., Banerjee, D., Meeldijk, J. D., De Jong, K. P., Louis, C., & De Jongh, P. E. (2017). Superior Stability of Au/SiO2 Compared to Au/TiO2 Catalysts for the Selective Hydrogenation of Butadiene. *ACS Catalysis*, *7*(9), 5594–5603. https://doi.org/10.1021/acscatal.7b01424

[90]: Donoeva, B., Masoud, N., & De Jongh, P. E. (2017). Carbon Support Surface Effects in the Gold-Catalyzed Oxidation of 5-Hydroxymethylfurfural. *ACS Catalysis*, *7*(7), 4581–4591. https://doi.org/10.1021/acscatal.7b00829

[91]: Nexant, (2009). Propylene Oxide Process Technology (including comparison of Sumitomo ' s Cumene Based / HPPO , PO / Styrene Monomer , PO / MTBE and Chlorohydrin / CHP Routes), Production Costs (COP), Capacity , Regional Supply / Demand Propylene Oxide Report Abstract. *Program*, *January*.

[92]: Schmidt, F., Bernhard, M., Morell, H., & Pascaly, M. (2014). The HPPO process - A novel route to propylene oxide. *DGMK Tagungsbericht*, *2014*(3), 243–244.

[93]: Huang, J., Takei, T., Akita, T., Ohashi, H., & Haruta, M. (2010). Gold clusters supported on alkaline treated TS-1 for highly efficient propene epoxidation with O2 and H2. *Applied Catalysis B: Environmental*, *95*(3–4), 430–438. https://doi.org/10.1016/j.apcatb.2010.01.023

[94] Bunaciu, A. A., Udriştioiu, E. gabriela, & Aboul-Enein, H. Y. (2015). X-Ray Diffraction: Instrumentation and Applications. *Critical Reviews in Analytical Chemistry*, *45*(4), 289–299. https://doi.org/10.1080/10408347.2014.949616

[95]: Lyal'ko, I. S., Kaplichnyi, V. N., Shulyak, E. A., Gurin, V. S., Shapovalov, E. A., Savukov, V. T., & Stoyanov, P. A. (1981). Em-125 Transmission Electron Microscope. *Bulletin of the Academy of Sciences of the U.S.S.R. Physical Series*, *47*(6), 13–15.

[96]: Sheldon, R. A., & Van Doorn, J. A. (1973). Metal-catalyzed epoxidation of olefins with organic hydroperoxides. I. A comparison of various metal catalysts. *Journal of Catalysis*, *31*(3), 427–437. https://doi.org/10.1016/0021-

9517(73)90314-X

[97]: Heilig, M. L. (1994). United States Patent Office. *ACM SIGGRAPH Computer Graphics*, *28*(2), 131–134. https://doi.org/10.1145/178951.178972

[98]: Niemantsverdriet, J. W. (2007). Appendix: Metal Surfaces and Chemisorption. *Spectroscopy in Catalysis*, 297–320. https://doi.org/10.1002/9783527611348.app1

[99]: Maschmeyer T., Sankar F.R.G. & Thomas J.M. (1995). Heterogeneous catalysts obtained by grafting metallocene complexes onto mesoporous silica. Nature, 378, 159-162.

[100]: Block, B. P., & Bailar, J. C. (1951). The Reaction of Gold (III) with Some Bidentate Coördinating Groups. *Journal of the American Chemical Society*, *73*(10), 4722–4725. https://doi.org/10.1021/ja01154a071

[101]: Evonik Industries, "AEROXIDE, AERODISP and AEROPERL Titanium Dioxide as Photocatalyst Technical Information," tech. rep., 2015

[102]: Nijhuis, T. A., Huizinga, B. J., Makkee, M., & Moulijn, J. A. (1999). Direct epoxidation of propene using gold dispersed on TS-1 and other titanium-containing supports. *Industrial and Engineering Chemistry Research*, *38*(3), 884–891. https://doi.org/10.1021/ie980494x

[103]: Trent, D.L. (2001). Kirk-Othmer Encyclopedia of Chemical Technology. https://doi.org/10.1002/0471238961.1618151620180514.a01.pub2

[104]: G.F. Thiele, E. Roland. (1997), Propylene epoxidation with hydrogen peroxide and titanium silicalite catalyst: Activity, deactivation and regeneration of the catalyst. Industrial and Engineering Chemistry Research 52(3):1168-1178. https://doi.org/10.1016/S1381-1169(96)00266-X

[105]: Azeb, G., Haben, H., Jolayemi, I., Majdoleen, E.-B., & Precious, I. (2017). *Production of Propylene Oxide via HPPO Technology- Volume I. I.* https://preciousime.files.wordpress.com/2017/12/g5-part51.pdf

[106]: V. Russo, R. Tesser, E. Santacesaria and M. Di Serio, "Chemical and Technical Aspects of Propene Oxide Production via Hydrogen Peroxide (HPPO Process)," Industrial and Engineering Chemistry Research, pp. 1168-1178, 2013.

[107]: Chen L.Y., Chuah G.K., Jaenicke S. (1998). Propylene epoxidation with hydrogen peroxide catalyzed by molecular sieves containing framework titanium. Journal of Molecular Catalysis 132(2-3): 281-292. https://doi.org/10.1016/S1381-1169(97)00276-8

[108]: Kuo-Tseng Li, Chia-Chieh Lin (2004): Propylene epoxidation over Ti/MCM-41 catalysts prepared by chemical vapor deposition. Catalysis Today 97(4): 257-261.

[109]: Wu, Y., Liu, Q., Su, X., & Mi, Z. (2008). Effect of solvents on propylene epoxidation over TS-1 catalyst. *Frontiers of Chemistry in China*, *3*(1), 112–117. https://doi.org/10.1007/s11458-008-0007-2

[110]: Zhang, X., Huang, C., Wang, M., Huang, P., He, X., & Wei, Z. (2018). Transient localized surface plasmon induced by femtosecond interband excitation in gold nanoparticles. *Scientific Reports*, *8*(1), 1–7. https://doi.org/10.1038/s41598-018-28909-6

[111]: Quinet, E., Piccolo, L., Morfin, F., Avenier, P., Diehl, F., Caps, V., & Rousset, J. L. (2009). On the mechanism of hydrogen-promoted gold-catalyzed CO oxidation. *Journal of Catalysis*, *268*(2), 384–389. https://doi.org/10.1016/j.jcat.2009.09.019

[112]: Ford, D. C., Nilekar, A. U., Xu, Y., & Mavrikakis, M. (2010). Partial and complete reduction of O2 by hydrogen on transition metal surfaces. *Surface Science*, *604*(19–20), 1565–1575. https://doi.org/10.1016/j.susc.2010.05.026

[113]: Stangland E.E., Taylor, B., Andres, R.P., Delgass, W.N., (2005). Direct vapor phase propylene epoxidation over deposition-precipitation gold-titania catalysts in the presence of H_2/O_2: Effects of support, neutralizing agent, and pretreatment. Journal of Physical Chem. 109: 2321.

[114]: *M. Sankar, N. Dimitratos, P. J. Miedziak, P. P. Wells, J. Kiely, and G. J. Hutchings, "Designing bimetallic catalysts for a green and sustainable future," Chem. Soc. Rev., vol. 41, pp. 8099–8139, 2012.*

[115]: Chen, J., Beaufort, M. D. L., Gyurik, L., Dorresteijn, J., Otte, M., & Gebbink, R. J. M. K. (2019). Highly efficient epoxidation of vegetable oils catalyzed by a manganese complex with hydrogen peroxide and acetic acid. *Royal Society of Chemistry*, 2436–2447. https://doi.org/10.1039/c8gc03857k

[116]: Mitchell, P. C. H. (2009). Speciation of molybdenum compounds in water Ultraviolet spectra and REACH read across. *Report for the International Molybdenum Association REACH Molybdenum Consortium*, 1–28.